Skeletal muscle and cerebral palsy: Morphological consequences on muscle mechanics

by

Ryan N. Konno

B.Sc. (Hons), University of British Columbia, 2020

Thesis Submitted in Partial Fulfillment of the
Requirements for the Degree of
Master of Science

in the
Department of Mathematics
Faculty of Science

SIMON FRASER UNIVERSITY
Summer 2022

Declaration of Committee

Name:	**Ryan N. Konno**
Degree:	**Master of Science**
Thesis title:	**Skeletal muscle and cerebral palsy: Morphological consequences on muscle mechanics**
Committee:	**Chair:** Weiran Sun Associate Professor, Mathematics
	Nilima Nigam Supervisor Professor, Mathematics
	James M. Wakeling Committee Member Professor, Biomedical Physiology and Kinesiology
	Paul Tupper Examiner Professor, Mathematics

Abstract

Skeletal muscle is a complex three dimensional material; it differs from many other materials in its ability to activate and produce force, and is fundamental in locomotion. Its intricate structure crosses many length scales making it difficult to develop mathematical models that capture microscopic scale contributions to overall mechanics. In this thesis, we develop a homogenized model for the skeletal muscle microstructure, which is implemented in a finite strain nonlinear continuum elasticity model for muscle and solved using a finite element method. This model allows us to investigate consequences of the microstructure on overall mechanics. Further, we explore the influence of a neurological disorder, cerebral palsy, on skeletal muscle. Cerebral palsy muscle undergoes many changes making causation between the morphology of muscle and overall mechanics difficult to determine experimentally. Utilizing a computational approach, we isolate effects from individual variations in cerebral palsy muscle properties on three dimensional muscle behaviour.

Keywords: Skeletal Muscle; Biomechanics; Finite Element Method; Cerebral Palsy; Continuum Mechanics; Mathematical Modelling

Acknowledgements

First, I would like to thank Emma for her constant support throughout this degree. She has always inspired me to work towards my goals and has made me a better person.

I would also like to acknowledge my parents and grandparents, who have always helped and guided me. They have always supported me in achieving my goals.

I would like to acknowledge my supervisors, Nilima Nigam and James Wakeling, for their help and support throughout my many years working at SFU. Their advice and encouragement was always appreciated and make this a successful experience. The work in this thesis would not be possible without their help. They have provided me with invaluable advice not only on research, but my career and future.

I am grateful for my labmates in the Neuromuscular Mechanics Laboratory for their support and guidance during our many scientific and non-scientific discussions. The lab has been a very welcoming environment, and a great place to study over the past few years. I would like to mention Javier Almonacid, Sebastian Dominguez (whom I particularly have to thank for his guidance on the finite element codes and for introducing me to "large-deformation horror"), Evan Chen, Kthim Imeri, Adrian Lai, Kshitj Patil, Jaylene Pratt, Stephanie Ross, David Ryan, and Cassidy Tam. Additionally, I would like to thank all of the other students I have met during my time at SFU, while we were working on assignments or TAing classes. They have made this a great place to study.

I would particularly like to acknowledge and thank Stephanie Ross for her guidance on my projects, our many discussions involving academics, and advice for my future career. I would also like to thank Bart Bolsterlee for his supervision over the past years, as he has always provided me with guidance both related to our projects together and career advice.

Finally, I would like to thank Nilima Nigam and James Wakeling again for their financial support, which allowed to pursue this degree.

Table of Contents

List of Tables

List of Figures

Chapter 1

Introduction

Skeletal muscle is a very complex and highly heterogeneous structure that is used in the body for locomotion and standing. It differs from many other biological and non-biological materials in its ability to activate and produce force. These active forces introduce an added level of complexity and are important to consider along with the passive mechanical forces. In addition to these unique active forces, skeletal muscle has a very heterogeneous structure and composition that contribute to both the active and passive mechanics. Within muscle fibres, there are contractile units, which produce force; meanwhile, the fibres are embedded in a complex matrix of collagen fibres that provide structure, and substantially contributes to the passive mechanics of muscle. This very complex structure of muscle can also vary in the face of muscular disorders, diseases, disuse, and aging; hence, it is crucial to understand the aggregate passive and active response of muscle and its dependence on this complex structure. This will be the one of the main goals of this thesis.

To fully understand muscle mechanics, three dimensional mathematical models of muscle can be used, and there has been substantial development in these models over recent years (see eg. [14, 192]). In this work, we want to be able to capture the influence of deformation, tissue heterogeneity, and muscle architecture on the overall muscle mechanics, so we utilize a continuum model previously developed in Rahemi et al. [129] and Wakeling et al. [192]. This model is highly adaptable, and has been used to investigate many fundamental properties of skeletal muscle [129, 130, 144, 192, 148, 143]. The goal of this thesis is to modify the three dimensional continuum model to apply to skeletal muscle affected by *cerebral palsy* (CP), a neurological disorder. This requires capturing the contributions of the microscopic components of skeletal muscle on the macroscopic scale, modifying the model to capture the influence of CP, and investigating the active and passive mechanics of muscle affected by CP. This work can help to develop causation between the many changes that may occur to muscle and the overall muscle response. The findings can then be used by clinical and experimental researchers working on therapies and methods for treating CP, as it provides insight into the components of skeletal muscle that will be the most influential in whole muscle mechanics.

In the following sections we go through the basic anatomy of the muscle (Section 1.1), background on skeletal muscle mechanics from a mathematical perspective (Section 1.2), and subsequently a description of muscle mechanics from a physiological perspective (Section 1.3). After this background on muscle mechanics is given, a description of muscle pathology is provided with a focus on the influence of CP on muscle mechanics (Section 1.4). Finally, in Section 1.5 an outline of the remainder of the thesis will be given.

1.1 Anatomy of Muscle

The structure of muscle crosses many length scales (Figure 1.1). At the smallest level, there are the sarcomeres which are on the scale of μm and are responsible for the active force produced by the muscle. Sarcomeres are on average about 2.2 μm in length [27] and are connected in series via Z-disks (Figure 1.2). The proteins responsible for muscle contraction are the actin and myosin proteins. The thin actin filaments interdigitate through thicker mysoin proteins connected via the myosin heads or cross bridges (see eg. [187]). The muscle fibre cells contain many sarcomeres connected in parallel and in series. These fibres are then typically grouped (functionally) into motor units, which are defined as a group of muscle fibres innervated by the same neuron cell. These neuron cells send an electrical impulse to stimulate activation of the sarcomeres, which then contract to generate force. Some muscles, for example the medial gastronemius muscle in the calf, can contain up to a million muscle fibres [187].

Within the muscle fibres, chemical reactions occur in which ATP is hydrolyzed, and this energy is subsequently used, by the sarcomeres, for force generation. In particular, the energy is used by actin and myosin proteins to contract the sarcomeres, which shortens the muscle fibre. The theory behind the molecular mechanism that lead to force generation is called sliding filament theory [75, 74, 76], where the actin filaments slide past the mysosin filaments. The myosin filament plays a key role in determining if the muscle fibre will be able to produce force at a given shortening velocity. While there is a range of fibre types, typically the fibres are classified into fast and slow fibres. Structurally, this corresponds to different myosin proteins and their ability to hydrolyze ATP [9, 120], but functionally, this means that fast fibres will be able to produce forces at larger velocities, while slower fibres may not [78, 141]. In addition to the actin and myosin proteins, there are also large titin proteins attaching the myosin to the Z-disks. These proteins produce a passive force when lengthened, which prevent the sarcomere from lengthening beyond a reasonable range. Titin also has implications for active force produced through force enhancement, in which the muscle produces larger forces when activated and subsequently lengthened opposed to lengthening followed by activation (for more details see eg. [71, 69, 109]).

Surrounding the muscle fibres is the extracellular matrix (ECM), which is a highly complex network of collagen fibres [60]. The ECM consists of three distinct layers: the

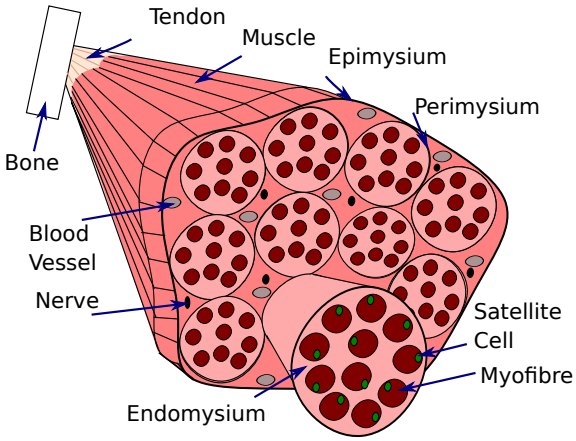

Figure 1.1: The structure of muscle. The myofibres contain the contractile unites of muscle: the sarcomeres. These myofibres are embedded in the deepest layer of the extracellular matrix (ECM) called the endomysium, which group bundles of myofibres into muscle fascicles. The next layer of the ECM, the perimysium, surrounds the muscle fascicles. The outer layer of the ECM, called the epimysium, surrounds the entire muscle belly. In addition to these components of muscle, there are also nerve cells, satellite cells, blood vessels, etc., which are important, physiologically, for muscle function.

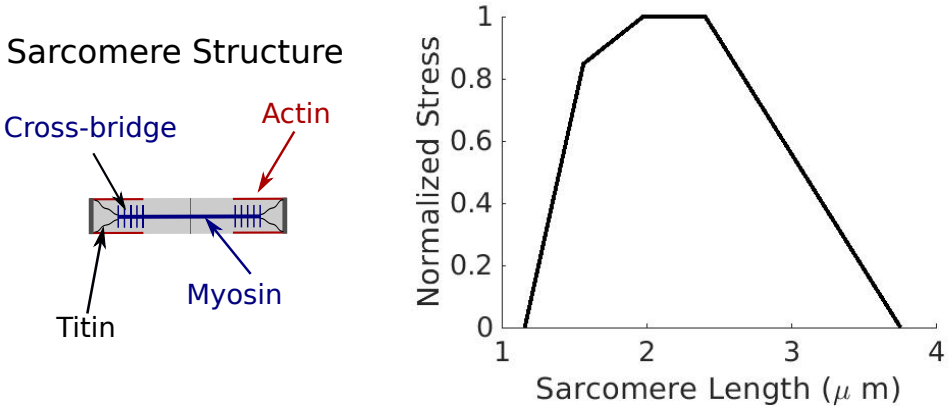

Figure 1.2: Structure (left) and force-length relationship (right) of the sarcomere. The force produced by the sarcomere is dependent on the length of the sarcomere; in particular, on the amount of overlap between the actin and myosin. This is typically modelled using a piece-wise linear function.

endomysium, which encompasses the muscle fibres; the perimysium which is the middle layer encompassing the muscle fascicles (groups of muscle fibres); and the epimysium, which is the outermost layer encasing the muscle [60, 126]. Each of these layers provide a distinct contribution to the structure and function of muscle as they each contain different collagen types and organizations [60]. The endomysium, being next to the muscle fibres has an important role of interacting with the muscle fibres and transmitting force to neighbouring muscle cells and the rest of the ECM [60]. Studies on feline muscle have shown that there

is a nonlinear stress-stretch relationship, as well as a distinct collagen fibre organization at this level resulting in a anisotropic material response [180, 127]. On the perimysial layer of the ECM, there is an orientation to the collagen fibres, which run at an angle to the muscle fibres [128]; however, there is much less known on this layer of the ECM as measurements are difficult [61]. The epimysium is much more accessible than the other layers of connective tissue, and measurements can be performed *in vivo* [54]. Depending on the specific function of the given muscle, the structure, amount, and composition may be varied [126, 125]. The ECM has an intricate structure and is fundamental in muscle mechanics; however, typically for healthy muscle it consists of less than 10 % of the muscle volume [93, 13]. The remainder of the muscle volume consists of cellular components: muscle fibres, nerve cells, satellite cells, adipose tissue etc. Altogether, these components of muscle make up the muscle volume and have their own contribution to muscle mechanics.

On the whole muscle scale, it is important to consider the materials that allow muscle to transfer force to the skeletal system: the *aponeurosis* and the *tendon* [135]. The muscle in combination with the aponeurosis and tendon is referred to as the *muscle-tendon unit*. The aponeurosis and tendon are particularly important for energy storage, and subsequent force transmission [135]. The aponeurosis is a very thin layer of connective tissue (≈ 0.25 to $0.75mm$ [156]), into which the muscle fibres insert. It is made of collagen fibres and similarly to the ECM has an orientation making the material anisotropic, particularly as it reaches the end of the muscle and connects to the tendon [7, 205]. The tendon extends the aponeurosis to the insertion point on the bone; it is also made up of collagen fibres, so it has an anisotropic material response due to the collagen fibre orientation [154].

While some muscle consists of muscle fibres aligned straight along the desired line of force production, this is not the case for most muscles [89]. The fibres are often orientated at an angle to the line of action of the muscle, which is called the pennation angle. This pennation angle is functionally significant to force production and contraction velocity, and is typically in the range 0° to 35° [197, 45]. This orientation of the fibres results in many different muscle architectures, which can be characterized into parallel fibred, pennate, and multipennate muscles (Figure 1.3). The simplest is the parallel fibred in which the fibres are oriented parallel to the line of action of the muscle. The pennate muscles consist of all the fibres oriented along the pennation angle. The multipennate muscle have an central or deep aponeurosis that runs through the middle of the muscle belly, which have muscle fibres inserting from multiple sides; these types of muscles have many pennation angles. This results in a more complex architecture that is seen in muscles with more complex functions, such as the deltoid muscles [118]. The main purpose of the complex architectures is that it allows for the muscle to better perform in specific roles, such as different ranges of muscle shortening velocities [187]. More detail on the functional significance of these architectures will be provided in Section 1.3. In this thesis, we will typically work with an idealized block

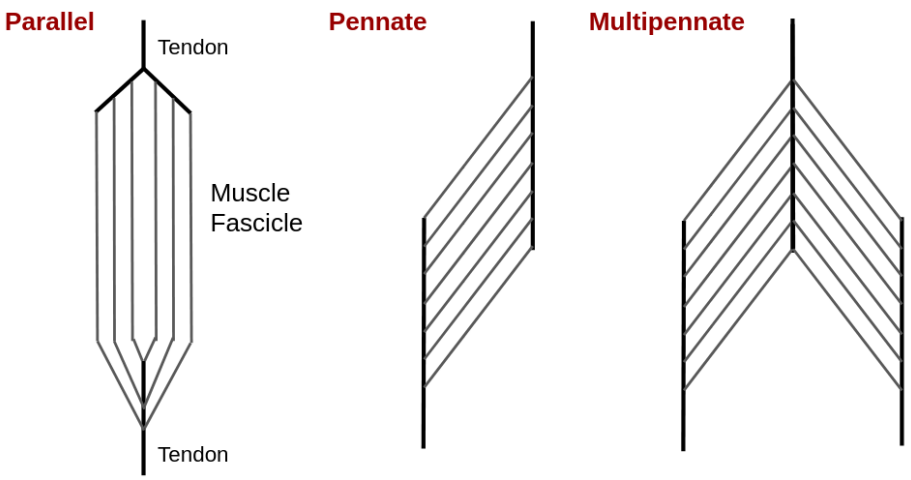

Figure 1.3: Types of muscle architectures: parallel (A), pennate (B), and multipennate (C).

of muscle, aside from the final chapter where we consider more complex pennate muscle geometries.

1.2 Muscle mechanics: a mathematical viewpoint

A complete understanding of skeletal muscle is not possible without the use of mathematical models, due to its complex nature and its many components. Real muscle is difficult to manipulate, and there are many changes that can occur in muscle that prevent measurements of the effect from a change in a property of muscle; however, the development of mathematical models allow for manipulation of individual quantities such as the amount of ECM or the volume of muscle. This is important not only in typically developed muscle, but also in muscle affected by disorders, such as cerebral palsy (CP), where many changes occur to the muscle structure that alter the overall mechanics. These changes are difficult to isolate experimentally, and this prompts the use of mathematical models of muscle. Although models are idealized and make many approximations, they allow for researchers to determine causation between changes occurring to muscle and the overall muscle mechanics.

1.2.1 One dimensional muscle modelling

One dimensional skeletal muscle modelling began with work by A.V. Hill [72], in which he investigated the effect of muscle shortening velocity on force and heat produced. Further work in one dimensional modelling involved using sliding filament theory to explain the force-length relationship previously obtained for muscle [63, 131]. These works led to the development of the Hill type model [203]. This is a one dimensional model for muscle, but provides many insights into the working of muscle. The model is very computationally efficient and allows for its implementation in analysis of muscle mechanics, activation, and

energetics [152, 88]. Additionally, it can also be used in larger scale models of the musculoskeletal system (eg. [40, 41]) and in understanding the influence of muscular diseases (eg. [198, 184]). The model splits the total force produced by muscle into active and passive components. It also includes both length and velocity dependent effects in the model (see Figure 1.4). In particular, the total force produced by a muscle is given by

$$F_{\text{muscle}}(\lambda, \dot{\lambda})) = F_0(F_{\text{pass}}(\lambda) + a(t)F_{\text{act}}(\lambda, \dot{\lambda})), \tag{1.1}$$

where $a(t) \in [0, 1]$ gives the level of activation, λ is the stretch in the muscle, and $\dot{\lambda}$ is the stretch rate of the muscle. Here $F_{\text{pass}}(\lambda)$ and $F_{\text{act}}(\lambda, \dot{\lambda})$ are normalized to the maximum force produced by the muscle during contraction, F_0. The force from the activation is typically modelled as a multiplicative split between the length and velocity dependent effects

$$F_{\text{act}}(\lambda, \dot{\lambda})) = F_{len}(\lambda)F_{vel}(\dot{\lambda}). \tag{1.2}$$

While these types of models have been successful in many applications, typically at larger activation and steady strain rate, it has been observed that the Hill model only accounts for about 50% of the forces in time varying *in vivo* situations with low activation and time varying strain rates [41]. This demonstrates that a more complex model is required to completely capture skeletal muscle tissue. The bulging, architectural effects, and tissue heterogeneity that occur in muscle are not encoded in Hill-type muscle models and require higher dimensional models [133].

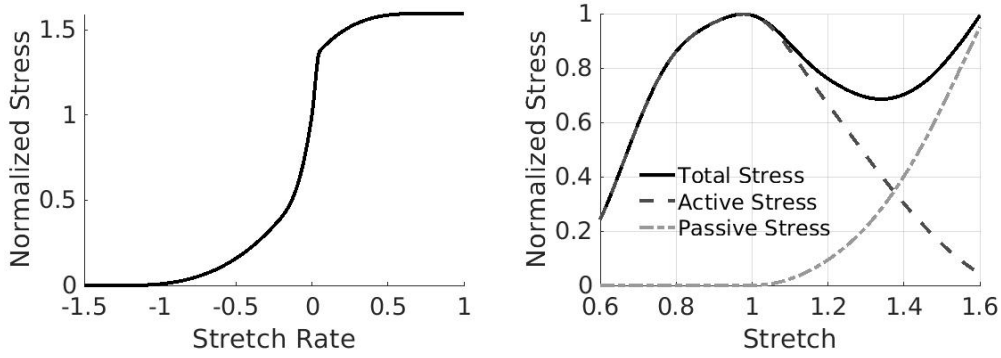

Figure 1.4: Intrinsic muscle force-velocity and force-length relationships.

1.2.2 Three dimensional muscle modelling

To better understand the entire mechanics of skeletal muscle, including muscle bulging, tissue heterogeneity, and architectural effects, three dimensional models were developed (eg. [15, 115, 202, 18, 129]). As the finite deformation of muscle is highly complex and a key factor in muscle mechanics [136], the three dimensional models allow for us to develop an

understanding of the bulging and deformations that may occur to muscle. The nonuniformity of the tissue properties is difficult to capture in a 1D model, and it is impossible to capture the influence of the distribution of materials inside muscle, such as fat [130], or the specific structure of the material, such as the non uniform orientations of collagen fibres [14]. The architecture of muscle is important in determining the muscle function; however, with one dimensional models, it is difficult to fully understand the influence of the architecture on bulging or fibre angles [192]. There are many different types of three dimensional models that have been developed to capture different aspects of skeletal muscle mechanics, and these will be outlined in the remainder of this section.

Hyperelastic continuum models

The most common type of three dimensional models are the hyperelastic continuum models of skeletal muscle. First, we can briefly provide some background on the theory of elasticity. In the linear setting, we have that the stress in a material, $\boldsymbol{\sigma}$, can be written in terms of a fourth order constitutive tensor, $\mathbb{C}$, as

$$\boldsymbol{\sigma} = \mathbb{C} : \boldsymbol{\epsilon}. \tag{1.3}$$

Here $\boldsymbol{\epsilon}$ is the strain in the material and $\mathbf{A} : \mathbf{B} := \text{tr}(\mathbf{A}\mathbf{B}^\top)$. This is known as Hooke's Law and is used in the presence of infinitesimal strains; however, skeletal muscle experiences finite strains, and so a more complex theory is required. Finite strain requires considering a nonlinear relationship between the stress in the material and the strain experienced. To do this we use a hyperelastic formulation, so we can write the stress in terms of a derivative of a *strain-energy potential*, W, as

$$\boldsymbol{\sigma} = 2\mathbf{E}^\top \frac{\partial W(\mathbf{E})}{\partial \mathbf{E}}, \tag{1.4}$$

where $\mathbf{E}$ is a finite strain tensor. This formulation will be described in detail in Chapter 2. The strain-energy potential function is typically a nonlinear function in terms of the invariants of the strain tensor $\mathbf{E}$. To determine the deformation of muscle, the finite strain nonlinear continuum elasticity model is used in the equation of motion given by

$$\nabla \cdot \boldsymbol{\sigma} + \mathbf{b} = \rho\, \ddot{\mathbf{u}}, \tag{1.5}$$

where $\mathbf{b}$ is the forces on the body, ρ is the density of the material, and $\ddot{\mathbf{u}}$ is the second derivative of the displacement with respect to time. These models are often solved using a finite element method.

The hyperelastic continuum models are typically whole muscle models in which the the material is treated as transversely isotropic [195]. The anisotropy is implemented as a one dimensional fibres running along the length of the muscle, similarly to muscle fibres (eg.

[15, 192]). The material is transversely isotropic and the models utilize a nonlinear finite strain hyperelatic material model. These models are often implemented in a quasi-static setting with no time dependence; therefore, the governing equations are developed assuming a balance of stresses without any effects from mass or time (eg. [115, 202, 192]). The quasi-static approximation is reasonable when the time scale of the elastic waves is much faster than the activation-type response, or when the mechanics are occurring slow enough that the system remains nearly in equilibrium, so any of the velocity dependent effects typically observed in muscle are negligible. One example of this in muscle mechanics would be an isometric contraction, and in this case the quasi-static models have been shown to be a good approximation [15, 115, 192]. Comparing to Equation 1.5, the quasi-static version is given by

$$\nabla \cdot \boldsymbol{\sigma} + \mathbf{b} = 0. \tag{1.6}$$

The exact formulation will vary slightly between models, and writing the active response from muscle can be done in terms of the stress or the strain in the material, which have been found to produce a different overall material response [58]. Most of the models follow a three-field formulation involving the displacement, pressure, and dilation, developed by [160]. Oomens et al. [115] utilizes a PDE to govern the active response of the muscle, whereas other models (since they are quasi-static) only utilize a linear ramping activation [192]. More detail can be added to these types of models by including a fibre-mesh model to help understand how force transmission through muscle [202]. While many of these models have been utilized with a simplified geometry of muscle, recently these models have been solved on MRI derived geometries that can provide more a more accurate mesh [81, 192]. While this is important for determining the effects of strain and deformation in muscle, Wakeling et al. [192] find that when looking at the energy associated with muscle contraction the simpler block geometries typically used sufficiently capture the energy associated with contraction.

These models have been used to look at the influence of activation on muscle deformation, and vice versa. [35] and [81] investigated the effects of muscle contraction on aponeurosis strains. [81] varied the aponeurosis properties based on experimental data to understand how they affect the aponeurosis strain, which has been shown to be important to muscle function [7]. These type of models are particularly useful in understanding how stress and strain develops during contraction and passive movements. [148] investigated the effects of compression on strain and stress produced by muscle tissue. Additionally, many models are used to investigate strain throughout the muscle during the contraction and during passive lengthening [115, 192, 19].

Dynamic effects

The aforementioned continuum models of muscle focus on quasi-static deformation, and do not include any velocity dependent effects; however, the velocity dependent creep and relaxation have been found to be important in muscle mechanics [72]. Viscoelastic models of muscle have been developed to capture these effects [185, 196]. [185] developed a viscoelastic model to look at the time-dependent properties of muscle in the passive setting. More recently, [2] developed a passive viscoelastic model using experimental data for cyclic lengthening tests. These models do not, however, look at the active mechanics of muscle tissue using a viscoelastic model. Other dynamic effects that need to be considered are the effects of mass [147, 144, 145]. Muscle deformation is inherently dynamic; however, implementing a dynamic formulation of the model is difficult and computationally intensive using a continuum formulation. The remainder of the work in this thesis will not consider the dynamic effects of muscle, and we will work with a hyperelastic quasi-static formulation of muscle.

Other muscle models

There are other three dimensional models of skeletal muscle that do not utilize the standard continuum mechanics approach. These models are particularly useful as they are able to capture more of the architecture and bulging of muscle, but to do not require the intensive computations that are used to solve the continuum models. The computationally intensive continuum models make them difficult to implement in larger musculoskeletal models such as OpenSim [40] that involve many muscles. [57] has developed a fibre based model, which has a lower computation cost than the typical continuum models. This is for the purposes of implementing in more complex simulations with multiple muscles. The difference between this model and the three dimensional continuum models is that they approximate the muscle as a one dimensional fibres that obeys the properties of continuum mechanics. This essentially results in a model that improves upon the classical Hill model, but does not include all the physical details observed in the full three dimensional models.

Micro-mechanical factors in three dimensional models

The aforementioned models take a continuum approach to the macroscopic characterization of muscle, which utilize phenomenological data for the material parameters. While this works well in many cases, it can be beneficial to take a principled approach that encompasses effects from some of the micromechanical properties of muscle. Micromechanical models of muscle tissue have been developed that do not use a continuum formulation [18]. In this case, Böl et al. [18] develop the muscle model using truss elements, whose properties are based of the microscopic data from muscle tissue. Other models incorporate multiscale aspects of electrophysiology into their model through a combination of ODE systems for

the electrophysiology and the nonlinear continuum equations on the macroscopic scale [68, 140, 138, 139]. Additionally, there are continuum models that investigate the influence of the microstructure, but do not capture whole muscle deformation [157, 186]. Sharafi and Blemker [157] built a model with intention of understanding if the assumptions made on the macroscopic scale were accurate based on the mechanics at the fibre bundle and fascicle level. Other micromechanical models, while not directly computing the overall force produced by the muscle, are able to develop a better understanding of how force is transmitted within the muscle to the tendon through shear forces [158], as well as the influence of neuromuscular diseases [186].

To capture the microstructure on the macroscopic level approximations need to be made; otherwise, it would not be computationally feasible given the complex structure of muscle. This can be done through the use of homogenized muscle models [172, 171, 14]. The homogenization methods used in these studies typically involve combining the effects of the ECM and the cellular fibre effects. These types of models have been found to produce similar results as the phenomenological continuum models, but allow for a better understanding of the effects from specific micromechanical components. In Chapter 3, a homogenized muscle model will be developed and implemented for the muscle model in [192].

Applications to impaired or diseased muscle tissue

Skeletal muscle models have also been developed to specifically address the mechanics of impaired muscle tissue, such as that affected by disease, disuse, or aging. For example, the chemomechanical model developed by [174] can capture the influence of muscular dystrophy. The three dimensional models can also be useful in understanding the effects of a disease or disorder on the fibre level, by varying material properties [186]. As mentioned in Section 1.4.2, adipose (fat) tissue can infiltrate the muscle and cause changes to its composition. Rahemi et al. [130] investigated the effects of adipose tissue distribution and models for incorporating adipose tissue on the force produce by muscle using a continuum model for whole muscle. In these cases, the three dimensional nature of the model is important as it allows for the investigation of adipose tissue distributions throughout the muscle. Now that a variety of muscle models have been described, a description of muscle mechanics from a physiological viewpoint will be given in the next section (Section 1.3).

1.3 Muscle mechanics: a physiological viewpoint

From a physiological and biomechanical perspective, muscle is often considered to be the force generator responsible for locomotion; however, muscle may have many other functional roles. Mechanically, skeletal muscle may act as motors, brakes, springs, or struts [43]. As a brake, muscle will be able to slow movement by storing energy in the muscle and tendon. In insect flight, muscle could act as a spring which will produce an oscillatory forces at high

frequencies [182]. The function of a strut is typically to help transfer force, and is used by many animals in locomotion such as swimming fish [155] or running turkeys [137]. Each of these different functions of muscle are highly dependant on the structure and composition of muscle. Two main properties of muscle that will determine the function of muscle are the contraction speed at which muscle can produce force and the force a muscle can produce at a give length. These properties will depend on many things including architecture, activation, fibre types, and material composition [89]. The remainder of this section will go over the factors that will influence muscle function in relation to the force a muscle produces at a given length or velocity.

1.3.1 Whole muscle level contributions to muscle mechanics

Here we go over the mechanics at the whole muscle level, as there are many factors here that are influential in muscle mechanics. First, we go over the role of muscle architecture and the various functions of muscles, along with the role of the pennation angle in muscle function. Further, we discuss the importance of the aponeurosis on muscle function. Finally, we go over the importance of considering muscle as a three dimensional material with volume and mass.

Architecture and the muscle-tendon unit

Muscle architecture has a large bearing on how muscle will function in a given organism. As previously described in Section 1.1, we see that there are three main types of muscle architectures, and that there is one main feature that distinguishes the paralleled fibered muscle and the pennate muscle, and that is the orientation of the fibres. While the pennation angle redirects the force from the line of action of the muscle, typically the reduction of force from this angle is small since the angle is often less than 25° in humans [197]. In most models of muscle, the force produced by muscle is proportional to the physiological cross sectional area ($PCSA$), which accounts for the orientation of the fibres. While the exact calculation can vary between studies, one common way to calculate $PCSA$ is [89]

$$PCSA = \frac{m_{\text{muscle}}}{\rho_{\text{muscle}}\, l_{\text{fibre}}}. \tag{1.7}$$

Here m_{muscle} is the mass of the muscle, ρ_{muscle} is muscle density, and l_{fibre} is the length of the fibre. The $PCSA$ multiplied by the cosine of the pennation angle, θ, is proportional to the muscle force

$$PCSA \times \cos(\theta) \propto \text{Muscle Force}. \tag{1.8}$$

This means that if we assume at most $\theta = 25$ degrees, there would be at most a 10% reduction in force in the direction of the fibres, which is relatively small. The main benefit

for pennation angle is its use in muscle gearing, as muscle pennation angle will change throughout the course of muscle contraction Typically, the pennation angle will increase as muscle activates, this results in a phenomena called gearing [193]. As the angle increases, the muscle fibres are shortening at a slower rate than the whole muscle belly. The force produced by the fibres would then be larger than if it were to be shortening at the same rate of the entire muscle belly (see Figure 1.4). This is because the muscle fibres are still operating on a region of the force-length curve in which they are producing larger forces. However, for a muscle with larger pennation angle, there are also shorter fibre lengths, which result in less range in length of the muscle fibres and also the muscle. There is a trade off between increasing the force, by increasing the number of fibres in parallel, and muscle's range of motion. Depending on the function of muscle one or the other may be desired. The amount of gearing required will depend on the specific muscle function, but the pennation angle is critical in allowing muscle to perform a wide range of functions while decreasing the size and mass of the muscle.

In addition to the influence of the muscle architecture itself the materials through which muscle force is transmitted to the bone are important. The majority of the muscle fibres in the muscle belly will insert into the aponeurosis for pennate muscle [116], so it is important for the aponeurosis to be able to further transmit force to the tendon. The mechanical behaviour of the aponeurosis is important to muscle function because it needs to be compliant, so that it can bulge and deform with muscle, as well as stiff enough to transmit force. This is achieved through the organization of the collagen fibres in the aponeurosis, so that as muscle bulges during contraction, transverse to the muscle's line of action, it will increase in stiffness in the longitudinal direction [7, 5]; this will allow it to better transmit force [7]. The aponeurosis in turn can limit the muscle's ability to bulge and deform [81], which has consequences for muscle force production [136]. The force that is transmitted from the aponeurosis must also be tranmitted through the tendon, which is important in musculoskeletal mechanics as an energy storage mechanism [135]. While the tendon plays an important role in skeletal muscle function, the remainder of this thesis will focus on the muscle and aponeurosis complex, and so we will not provide an in depth review of the function of tendon. For more detail on the function of the tendon, see eg. [134, 135].

Muscle volume and mass

Early studies in skeletal muscle mechanics (see eg. [203]) work with experimental data obtained through fibres and fibres bundles, and the models are often formulated in one dimension. More recent work has found that there are many more effects to consider in muscle; particularly, the ECM properties and any effects from muscle volume and mass. Typically during contraction the volume of the muscle is assumed to be nearly constant [1, 12] or changes by very small amounts [20]; however, during long sustained contractions or exercise the muscle volume has been observed to increase by up to 10 % [199]. If the volume of

blood is included in the calculation of the muscle volume, then the volume would also change significantly during contraction. This restriction on volume change acts as a constraint on skeletal muscle function resulting in the development of intramuscular pressures, which may act as a main factor in force generation [161, 164, 162]. In addition to pressure acting as a constraint due to near constant volume, there is a constraint on the total volume of the muscle due to its position in the body, so muscle will typically want to have a smaller volume to reduce the energy required for accelerating the inertial mass of the muscle. The benefit of larger muscle volumes is that there will be more muscle fibres, which will allow for the muscle to do more work (at the cost of increased muscle mass).

One aspect of muscle that is often not considered is the influence of muscle mass. Work by [147] has found that muscle needs to do more work to overcome the influence of inertia induced by increased muscle mass. Adding internal mass to skeletal muscle results in reduced work and power output by the muscle [144, 145]. Meanwhile, larger muscles have been found to have a lower mass specific work [143]. This indicates that the size of muscle will alter its mechanics, and so will likely alter the structure of muscle. Studies have found that within a group of animals similarly related the structure will change depending on the size of the muscle [42] and that as muscle size is increased the relative fibre length will decrease [3, 48]. Hence, muscle volume and mass need to be considered when analyzing muscle mechanics.

Another important macroscopic characteristic of muscle is its three dimensional nature. As it contracts to produce force and shorten muscle must bulge. This deformation will change the direction and magnitude of the force produced by the fibres and the speed of contraction [136]. The muscle bulging will change orientation of the fibres throughout the process of contraction resulting in forces not all acting along the muscle's line of action [94]. The benefit is that this allows muscle to shorten and produce force at shorter muscle lengths. It has been shown that preventing bulging of the muscle material in one direction will reduce the contractile force of the muscle along the line of action [149]. This was further corroborated in [148] where it was shown that for smaller pennation angles, a load on the muscle transverse to the line of action resulted in less energy being transmitted by the muscle. The bulging in muscle is also helpful in the gearing of muscle, where the velocity of the fibre shortening is less than the velocity of the entire muscle shortening [193]. The bulging allows the pennation angle of muscle to change to allow for the lower fibre velocity, and, hence, increase force produced by the fibres [136, 132, 191].

1.3.2 Cellular level contributions on muscle mechanics

It is difficult to fully understand how the microscopic components of muscle contribute to the overall muscle force due to difficulties in experimental measurements. It is known that there are two main microscopic contributors to the mechanics of skeletal muscle: the ECM and the contractile units. First, we can discuss what is known at this point on the functional significance of the ECM. As mentioned in Section 1.1, the ECM consists of three main

layers (endomysium, perimysium, and epimysium), and each of these layers have different mechanical properties through variation in structure and collagen types [126, 61]. The main contributions of the ECM to muscle mechanics is passively during tension. The ECM is a stiff and complex structure, so it will tend to resist any deformation. As muscle is lengthened, for example, the stress in the ECM increases and it will store energy. The energy will then be used depending on the function of the muscle (eg. spring, brake) [43]. Another way that the ECM will contribute to muscle mechanics is during active force production through its ability to transmit force from the fibres to the aponeurosis, and consequently, the tendon and skeletal system. There are two main contributing layers that could directly influence the force transmission: the endomysial and the perimysial layers. This is because the endomysium surrounds the fibres and the perimysium surrounds the fascicles (groups of fibres), so they are near and attach to the contracting fibres. It is likely, however, due the mechanical properties of each of the layers that the endomysium is responsible for a larger amount of this force transmission. The reason is that the endomysial layer is much stiffer compared to the perimysial layer, and so it will be more likely to transmit force (see [126]). In skeletal muscle it is not uncommon to have fibres that terminate within the muscle [116], so there needs to be a mechanism for the force transmission from these fibres. The possible modes of this force transmission are either through shear or tensile forces. Sharafi and Blemker [158] used modelling techniques to investigate the modes of force transmission through the ECM, and found that on the endomysial layer, transmission through shear forces is more effective than through tensile forces. The ECM is a fundamental contributor to mechanics; however, it is the contractile properties of muscle that allow it to function in many of its roles.

The second contributor, that we consider, on the microscopic scale to muscle mechanics are the contractile units or sarcomeres. These units are responsible for the active force produced by the muscle and consist of two main force contributions: the active force produced actin-mysosin complex and the passive forces from the titin protein. We can first discuss the actin-myosin force production, which can be explained using cross-bridge theory [75, 74, 76]. In this theory force production depends on a cyclical mechanism, which uses the hydrolysis of ATP, and leads to the cross-bridges pulling on the actin to produce force. This force that the sarcomeres produce depends on the length and velocity of contracting sarcomeres. The relationship between force developed by the sarcomere and its length (which corresponds to amount of overlap between the actin and myosin) is piecewise linear. There is an optimal length at which the sarcomeres will produce force, but at longer or shorter lengths there will be less overlap or the actin and myosin proteins will reach the Z-disks between sarcomeres (Figure 1.2). The other factor, contraction velocity of the sarcomere, will decrease the force as the contraction velocity is increased. At some given contraction velocity, the sarcomere will no longer be able to produce force and this is called the maximum shorten velocity or maximum strain rate. These results can be explained via the Huxley model [75]; at larger

speeds there is a decreased probability of cross-bridges forming as the actin and myosin slide past each other (resulting in decreased force from activation) and there will also be a decreased probability of the cross-bridges that have attached detaching (resulting in forces in the opposite direction of contraction). The specific relationship will depend on the type of myosin protein in the sarcomere. For muscles that typically operate at larger velocities to move quickly, but may not need to produce large forces, the sarcomeres will consist of more myosin proteins with a larger maximum shortening velocity. Beyond the active force produced by the muscle, the actin-mysosin component does not have a large contribution to the passive response of muscle. The passive response from the sarcomeres is mainly due to the titin protein.

Titin, the giant muscle protein, is considered to be the main contributor to passive force within a muscle fibre [97, 87, 70]. The passive force from the titin has been found to correspond inversely to size or isoform type, where the larger titin proteins result in a decreased passive force from the sarcomeres during lengthening [123]. However, on the whole muscle scale it is often argued that this contribution is small compared to the influence of the ECM, due to its stiff collagenous structure [60, 105, 91]. This is because large stress responses from the titin protein are only seen at larger stretches, which are typically not realized in physiologically relevant muscle lengths (see eg. [53]). The main influence of the titin molecules turns out to be in a phenomena called force-enhancement [70], but this will not be investigated in this thesis (for more details on theories and effects of force enhancement, see eg. [70, 69, 109, 144]).

Throughout this section, we have gone over the basics of muscle mechanics. In particular, we have gone over the variations in muscle properties that may alter the forces produced by muscle at a given length and velocity. On the macroscopic scale the overall muscle architecture is a key indication of the muscle function; however, there are subtle properties within the muscle fibres that will influence its function. The ECM is a critical component of muscle giving the muscle its structural stiffness, while the individual proteins in the sarcomeres will vary to influence the velocities at which the muscle will produce force. Other materials have less of an effect but are still relevant in the mechanics. For example, muscular fat, which is typically increased in muscle affected by disease, aging, or disuse, can decrease the passive stiffness of muscle, as well as decrease the amount of space in the muscle available for muscle contraction [130]. Muscle properties cross many length scales, but on each scale the specific construction will alter muscle function. While in this section we have discussed the components of muscle that can influence mechanics, many biological processes, including aging and disease, can lead to changes to this structure and manipulate the mechanics. These will be discussed in the next section under the context of the neurological disorder CP.

1.4 Muscle pathology: cerebral palsy

While the mechanics of skeletal muscle have been described above, they can be altered in the presence of muscular disorders. One such disorder is CP, which results from an upper motor neuron lesion and can significantly alter both activation patterns and structure of skeletal muscle [142]. Most of the modern research on the influence of CP began in 1979 with research by Castle [29]. Much of the early research went into understanding the changes that can occur during CP. First fibre types and diameters were investigated through histological cross-sections of dissected CP muscle obtained through surgery [29, 77]. However, currently, there are improved experimental techniques, including MRI and ultrasound, to see the changes occurring to skeletal muscle *in vivo*. Despite improved techniques, it is still very difficult experimentally to understand the influence of CP on muscle mechanics. One main reason is that the effects of CP vary both between subjects, but also within subjects between different muscle groups [91]. One example is the increased stiffness of fibre bundles in the upper leg muscles observed by Smith et al. [167], whereas no change in fibre bundle stiffness was observed in calf muscles by Mathewson et al. [98]. Typically, results will vary between upper and lower limb muscle groups [91].

This section will be organized as follows. First, the effects of CP on activation of skeletal muscle will be discussed (Section 1.4.1); although, this will be done briefly as the rest of this thesis will mainly focus on the passive mechanics of CP affected muscle with the exception of Chapter 5. Next, in Section 1.4.2, the morphology of skeletal muscle under the influence of CP will be discussed, including changes to the ECM, sarcomeres, and overall structure.

1.4.1 Spasticity and contracture

One main consequence of CP muscle is spasticity, which is the involuntary velocity dependent activation of muscle during lengthening. This is a purely involuntary reflex that results in stiffer muscle and a decreased range of motion, and has been investigated in many studies (eg. [50, 8, 122]). The reason spasticity is important in muscle mechanics is that muscle properties can vary due to changes in neural stimulation [119, 150]. Research is still investigating the activation patterns during spasticity; however, they have been shown to vary between muscle groups within a subject [8]. This may help to explain the wide variation in morphology, as will be discussed in the next section. Since the exact initial insult to the central nervous system may vary between subjects, this means that the changes to the activation patterns will vary between subjects depending on the exact location of the insult [104]. A similar effect is observed in stroke patients, which can result in spasticity occurring and changes to muscle morphology, similarly to CP [153].

To understand the influence of the spacticity in response to a stretch, models have been developed. One such example is the work by Fee et al. [50], in which a swinging pendulum test, which models the lower part of the leg as a pendulum (see eg. [52]), was used on identical

triplets (two with CP and one TD). They found that including a velocity dependent term in the model was required to capture the CP muscle response, but not the TD muscle. This indicates that the spasticity occurring during CP is a velocity dependent response. While spasticity has been shown to be important, there are many techniques and methods available for assessing the degree of spasticity. It can typically be done using a stretch-reflex test [122, 23, 85], but also through more advanced techniques such as wearables [103]. These tests give measure of spasticity on the Modified Ashworth Scale [16], which can be used to rank the severity of the condition.

Once spasticity is assessed there are a number of treatment options including non drug therapies, such as physical therapy and hydrotherapy [49]; drug therapies including Botulinum toxin A [64]; and surgical interventions, which often involves tendon lengthening for growing children [169]. The choice in treatment can vary depending on severity, and a flowchart to guide the order of CP treatments is suggested in [49]. These treatments are still debated today, and so more details on the underlying mechanics of muscle may help to direct future clinical procedures and reduce the number of invasive and irreversible procedures needed. The muscle affected by CP often has a larger passive stiffness than normal muscle. As a result of the increased passive stiffness and muscle weakness, contracture develops, which is the chronic shortening of muscle. This increase in passive stiffness can be observed using shear wave elastography [86, 84], and muscle weakness has been widely investigated using EMG techniques and modelling of the muscle tissue [47, 184, 189]. However, further investigation needs to go into the changes to the material properties that can occur during CP, and to determine the components that have a large contribution to the mechanics of the muscle.

1.4.2 Influence of cerebral palsy on skeletal muscle morphology

The influence of CP on skeletal muscle varies both within and between subjects; however, there are many changes to muscle morphology that are commonly observed [11, 179, 91]: fibrosis, decrease in ECM stiffness, increased fat accumulation, and decreased muscle volume. Along with these factors, changes to other muscle muscle properties commonly reported are decreased fibre size, decreased fascicle diameter, reduced satellite cell number, and decreased serial sarcomere number. While the aforementioned components generally vary as mentioned above, the results are often conflicting between studies. For example, even the more common changes such as increased stiffness from the ECM component [179, 11], through fibrosis in combination with decreased stiffness from the ECM structure, do not always occur (eg. [98]). The rest of this section will go into the common changes that occur to skeletal muscle during CP; these results are also summarized in the reviews [11, 179, 91, 73].

The ECM, as mentioned above, is often considered as one of the primary load bearing structures in skeletal muscle; hence, understanding how it may be altered in CP affected muscle can be critical to understanding the changes in muscle mechanics. Often measure-

ments of collagen content are reported as an indicator of the amount of ECM, since it is difficult to physically measure the volume fraction. It is typically reported that there is an increase in the collagen content [22, 167, 98]. While the collagen content may increase during CP, this may not always correspond to an increased stiffness. It has been reported that there are changes to the structure of the ECM, which may result in a different stiffness value of the ECM [179]. In studies with *mdx* mice, fibrosis has not necessarily resulted in an increase in muscle stiffness [165, 25]. Collagen content is likely not a good indicator of ECM stiffness, and, instead, the organization of the collagen fibres within the ECM should be considered [25]. Despite these conclusions with *mdx* mice, it is not obvious that these same relationships will occur in CP muscle, but it is likely that similar trends may occur. CP may not always influence each layer of ECM equally, it has been observed that in CP muscle the perimysial layer was three times larger in thickness compared to TD muscle [38]. Structurally, it is difficult to understand how this variation in the different layers influences overall function. Studies mainly investigate the overall influence of the ECM. In passive experiments with CP muscle biopsies have been performed on CP muscle during tendon lengthening surgery (eg. [167]). Smith et al. [167] found that there was a significant change in the stress-stretch relationship of the fibre bundles, but not the fibres. This indicates that there must be an influence from the ECM on the muscle force. Other studies, from within the same lab group, have found that there is no effect in fibre bundles and that the difference is from within fibres [98]. The data is highly contradictory, and this emphasizes both the complex nature of CP and the difficulty in experimentally measuring the influence of microstructural properties on whole muscle mechanics.

Another key component of muscle that changes in CP affected muscle is the sarcomere length [167, 98, 91, 179, 99]. The sarcomere length in skeletal muscle is often lengthened [179], and this will impact both its passive and active contributions to muscle mechanics. The influence on passive mechanics is due to the lengthening of the titin molecules in the sarcomeres. The titin, as previously discussed, is the main contributor to the passive mechanics from the sarcomere; however, it does not necessarily have a large contributions on the whole muscle scale within the typical range of skeletal muscle lengths [91, 60]. Lieber and Friden [91] argue that any influence of the titin will not have a significant contribution to the overall mechanics, but during CP and as the muscle is stretched, there may be larger influences from titin. At normal stretches, this is likely the case, but in CP affected muscle the sarcomeres can be double the length of sarcomeres in TD muscle [167]. With these longer lengths, it is possible that sarcomeres have a larger passive force. While the effect on passive mechanics is difficult to guess, it is likely that the sarcomere length will be more influential in the active mechanics of muscle. If we consider the sarcomere force-length relationship in Figure 1.2, then if the sarcomere is lengthened by potentially double the length (as observed in [167]) then there will be around an 80% decrease in the force produced by the sarcomere. It is likely that in skeletal muscle the force produced will be very low relative to the passive

forces experienced at a give stretch. A possibility is that the sarcomere properties are altered in CP muscle, but there is no evidence to support this and so for the remainder of this thesis we assume that there is no change in the sarcomere properties to accompany the change in length. Sarcomere length is a critical component in muscle force production, and so changes during CP will likely have a substantial contribution to muscle mechanics.

A nearly constant finding throughout studies on the gross morphology of CP affected muscle is the decrease in muscle volume relative to TD muscle [11]. MRI studies investigating muscle geometry have found that the average volume in CP muscle is decreased by approximately 20-35% in CP muscle [111, 45, 112, 96], depending on muscle location. These data on muscle volume are important because volume is related to the force a muscle can produce, as PCSA is often approximated by volume divided by fascicle length [89]. The deformation in the muscle volume occurs both lengthwise, through a decrease in the muscle length, but also through a decreased cross-sectional area [96, 10]. There is also typically a decrease in fascicle length observed in CP muscle [96, 101, 107], and so the decrease in volume may not necessarily result in a reduced force. In more recent MRI studies the PCSA was calculated, and it was found that the PCSA was reduced in CP muscle compared to TD muscle [45]. The decreased PCSA, calculated using the median fibre length, implies that CP muscle should produce less force.

While the effect of muscle volume and PCSA is related to the amount of force muscle can produce, the muscle may not have the same material properties as typically developed muscle. Studies have looked at the correlation between muscle size and PCSA, and the force produced by muscle, and found that the the muscle volume does not account for the expected force reduction [66]. As described previously, the ECM properties could vary. The muscle material could also be altered by increased fat infiltration. It has been shown using MRI scans that there is an increase amount of fat [110] and changes to the distribution of fat [46, 110]. Longitudinal studies also looked into fat and found that there is an increase in fatty tissue in CP affected muscle [114]. Modelling work has found that the change in fat content can have an impact on the amount of force produced by muscle [130], but this has not been investigated within the context of CP affected muscle.

Other changes to CP muscle commonly reported are fascicle length, fascicle diameter, fibre length, and serial sarcomere number. In the modelling done in this thesis, which builds from the principle components of muscle mechanics, including the sarcomere properties and material responses, we focus on the changes outlined previously in this section. While fibre length is important in muscle mechanics, when modelling muscle in a three dimensional setting local changes to the fibre length need to be considered; therefore, we typically work with sarcomere length opposed to the fibre length. The many changes observed in CP muscle are difficult to measure and determine experimentally, and so we need to utilize a model for muscle.

1.5 Outline of thesis and contributions

This thesis is the combination of two published articles on homogenizing the skeletal muscle model and applying it to CP, along with a description of the skeletal muscle model. We investigate muscle material properties and the passive and active mechanics of muscle affected by CP.

As described in Section 1.4, understanding the effect of CP on force production is difficult; hence, in this thesis we develop a mathematical model along with a series of numerical simulations that allow us to achieve a better understanding of the mechanical behaviour of muscle affected by CP. We utilize a homogenization of the base material to capture the changes to the ECM. This includes the effects of fibrosis and changes to the ECM structure. The homogenization and validation of the force outputs will be shown in Chapter 3. The purpose of this model is to capture the effects of the microstucture of muscle on the macroscopic scale. Subsequently in Chapter 4, the model is applied to CP muscle to understand how muscular disorders may alter skeletal muscle mechanics. This section will demonstrate the effect of ECM properties and sarcomere length on the overall passive skeletal muscle mechanics during CP. Then in Chapter 5, fat material properties are incorporated into the model along with more complex architectures with aponeuroses. Finally, force-length simulations are performed to understand the influence of the changes that may occur during CP and how they influence passive stiffness and active muscle force.

1.5.1 Chapter 2: A skeletal muscle model

The chapter provides a summary of the model used throughout the remainder of the thesis, including the numerical methods used to solve it. We describe muscle as a fibre reinforced composite in which the active and passive fibre properties of muscle are embedded in a three dimensional base material, which includes any contributions from the ECM and other cellular materials.

Contributions: The development of the model was done by Sebastian Dominguez, Hadi Rahemi, Nilima Nigam, and James Wakeling [129, 44]. The summary of the model included in the thesis was written by Ryan Konno.

1.5.2 Chapter 3: A homogenized muscle model

This chapter was published in PLoS ONE [82]. Here we develop a homogenized model of the base material of muscle, which includes effects from the ECM and any cellular materials in the muscle. This was implemented in the skeletal muscle model described in Chapter 2. To test the influence of the base material properties on force output and energy distributions, lengthening and activation simulations were performed.

Contributions: Ryan Konno, Nilima Nigam and James Wakeling performed conceptualization, experimental design, and editing of the manuscript. Ryan Konno performed all simulations and drafted and edited the manuscript.

1.5.3 Chapter 4: Passive mechanics in cerebral palsy affected muscle

This chapter was published in Frontiers in Physiology [83]. Here the passive mechanics of skeletal muscle are investigated in the presence of the neurological disorder CP. This involves changes to the base material of muscle and its fibre components. This work provides insights into the passive mechanics of skeletal muscle and can help determine causation between individual changes occurring and the overall force muscle produces.

Contributions: Ryan Konno, Nilima Nigam, Stephanie Ross, and James Wakeling carried out experimental design, analyses of results, and edited the manuscript. Ryan Konno performed all simulations and drafted and edited the manuscript.

1.5.4 Chapter 5: Active mechanics in cerebral palsy affected muscle

This final chapter represents work in progress. Here we investigate the active mechanics of muscle effected by CP. Here we also include the effects from fat/adipose tissue into the model and investigate the various material properties used in the muscle model. Additionally, the muscle model is solved on a mesh derived from MRI geometries.

Contributions: Simulations were performed by Ryan Konno. Bart Bolsterlee, Ryan Konno, Nilima Nigam, and James Wakeling designed the experiments.

Chapter 2

Mathematical model

This chapter introduces the three dimensional continuum mechanical skeletal muscle model used throughout the rest of the thesis. First, in Section 2.1, we go over the basics of continuum mechanics including the physical principles, and strain and stress tensors used. Then we go through the formulation of the model (Section 2.3). Finally, we go over the numerical methods and discretization (Section 2.4) used to solve the model along with a convergence study (Section 2.5).

2.1 Continuum mechanics

Let V_0 be a body in $\mathbb{R}^3$ (called the *reference configuration*) and $\mathbf{x}_0$ a point in V_0. Then we can define a mapping $\varphi(\mathbf{x}) : V_0 \mapsto V$, where V is bounded region in $\mathbb{R}^3$ (Figure 2.1). We can define a point $\mathbf{x} := \varphi(\mathbf{x}_0) \in V$. The displacement of a point $\mathbf{x}_0$ is then given by $\mathbf{u} = \mathbf{x} - \mathbf{x}_0$. Using this displacement we can then define the deformation gradient tensor to be

$$\mathbf{F}(\mathbf{x}_0) := \frac{\partial \varphi(\mathbf{x}_0)}{\partial \mathbf{x}_0} = \mathbf{I} + \nabla_0 \mathbf{u}(\mathbf{x}_0), \quad \mathbf{x}_0 \in V_0. \tag{2.1}$$

Here we use the notation that ∇_0 is the gradient with respect to the initial configuration, while ∇ corresponds to the gradient with respect to the current configuration. To simplify the notation, we also write $\mathbf{F} = \mathbf{F}(\mathbf{x}_0)$.

The dilation of the material can also be defined in terms of the deformation gradient

$$J(\mathbf{x}_0) := \det(\mathbf{F}). \tag{2.2}$$

It is will also be useful in formulating the model to split the material response into a volume preserving, isochoric, component and volume changing, volumetric, component. We set $\bar{\mathbf{F}}$ to be the isochoric component of $\mathbf{F}$ so that

$$\mathbf{F} = (J^{1/3}\mathbf{I})\,\bar{\mathbf{F}}. \tag{2.3}$$

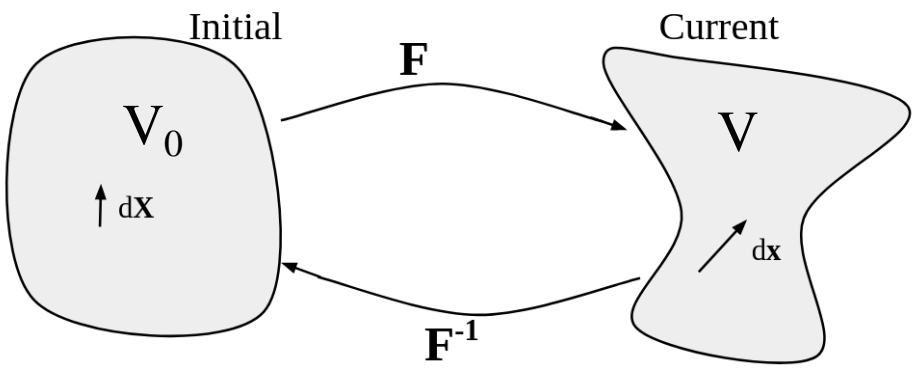

Figure 2.1: Illustration of the action of the deformation gradient $\mathbf{F}$ on a line element $d\mathbf{X}$ in the reference configuration to the current configuration, ie. $\mathbf{F}d\mathbf{X} = d\mathbf{x}$.

To discuss the mechanics of a body we need to introduce stress and strain tensors to describe the deformation of the material. Common strain tensors used are the left and right Caucy-Green Strain tensor $\mathbf{B}$ and $\mathbf{C}$, respectively. They can be defined in terms of the deformation gradient as

$$\mathbf{B} := \mathbf{F}\mathbf{F}^\top, \quad \mathbf{C} := \mathbf{F}^\top\mathbf{F}. \tag{2.4}$$

These tensors can also be expressed in their isochoric and volumetric components

$$\mathbf{C} = (J^{2/3}\mathbf{I})\bar{\mathbf{C}}, \quad \mathbf{B} = (J^{2/3}\mathbf{I})\bar{\mathbf{B}}. \tag{2.5}$$

Cauchy's Theorem gives us that there exists a Cauchy stress tensor, $\boldsymbol{\sigma}$, so that

$$\mathbf{t}(\mathbf{n}) = \boldsymbol{\sigma}\mathbf{n}, \tag{2.6}$$

where $\mathbf{t}$ is the traction on the surface and $\mathbf{n}$ is the unit outward normal in the current configuration. Equation 2.6 is in the current configuration, which is often not ideal for computational purposes. In this work we favor a Lagrangian description of the problem, so that all of our integrals are computed on the reference configuration, V_0. In the reference configuration, we get

$$\mathbf{T} = \mathbf{P}\mathbf{N}, \tag{2.7}$$

where $\mathbf{T}$ is the traction in the reference configuration, $\mathbf{N}$ is the unit outward normal in the reference configuration, and $\mathbf{P}$ is the first Piola-Kirchhoff stress tensor

$$\mathbf{P} := J\boldsymbol{\sigma}\mathbf{F}^{-\top}. \tag{2.8}$$

Using Nanson's formula (see eg. [113]), the relationship between the tractions $\mathbf{T}$ and $\mathbf{t}$ can be obtained as $\mathbf{T}dA = \mathbf{t}da$, where $dA \subset \partial V_0$ and $da \subset \partial V$. Other stress tensors that will also be useful in the formulation and implementation of the skeletal muscle model is the Kirchhoff stress tensor, $\boldsymbol{\tau}$, and the second Piola-Kirchhoff stress tensor, $\mathbf{S}$. These can be defined as

$$\boldsymbol{\tau} := J\boldsymbol{\sigma}, \quad \mathbf{S} := \mathbf{F}^{-1}\boldsymbol{\tau}\mathbf{F}^{-\top}. \tag{2.9}$$

Using $\mathbf{S}$, we can calculate the fourth order elasticity tensor

$$\mathbb{C}(\mathbf{C}) = 2\frac{\partial \mathbf{S}(\mathbf{C})}{\partial \mathbf{C}}. \tag{2.10}$$

These tensors will give us enough information to formulate the basics of elasticity and our mathematical model.

To model muscle tissue, we can rely on its elastic qualities and use a hyperelastic model for muscle. While there are viscoelastic effects observed in skeletal muscle (see Section 1.2), we do not include these in our model. Using a hyperelastic approach, we can formulate the muscle tissue in terms of strain-energy potentials. The strain-energy potential is a measure of potential energy that is a function of the strain in the material. For the model used in this study, we will write the strain-energy potential in terms of the left Cauchy-Green strain tensor, ie. $W(\mathbf{B})$. The relationship between the stress in the material and the strain experienced can be determined through the strain-energy potential using the constitutive law

$$\boldsymbol{\sigma}(\mathbf{B}) = 2J^{-1}\mathbf{B}^{\top}\frac{\partial W(\mathbf{B})}{\partial \mathbf{B}}. \tag{2.11}$$

We can also decompose the strain-energy potentials into isochoric and volumetric components

$$W(\mathbf{B}) = W_{\text{iso}}(\bar{\mathbf{B}}) + W_{\text{vol}}(J). \tag{2.12}$$

The exact form of the strain-energy potential functions, W_{iso} and W_{vol}, depends on the type of material being modelled and will be described in the following section.

2.2 The skeletal muscle model

We now go over the stress response of the skeletal muscle model previously developed in [192, 145, 148, 143]. We model muscle as a fibre reinforced composite material, so we decompose muscle into a three dimensional isotropic component and a one dimensional fibre component, which accounts for the anisotropy. Hence, the strain-energy potential can be decomposed into a fibre component that contains all of the contractile and passive along-

fibre properties, and a base material component that contains the effects from the ECM and other cellular materials. In particular, the isochoric component of the strain-energy will include the effects from the fibre and the base material

$$W_{\text{iso}}(\bar{\mathbf{B}}) = W_{\text{fibre}}(\bar{\lambda}) + W_{\text{base}}(\bar{\mathbf{B}}). \tag{2.13}$$

Here $\bar{\lambda}$ is the stretch in the fibre. Given an initial fibre orientation, $\mathbf{a}_0 \in \mathbb{R}^3$ and deformation gradient, $\mathbf{F}$, at a point $\mathbf{x}_0 \in V_0$, we define $\bar{\lambda} := J^{-1/3}||\mathbf{F}\,\mathbf{a}_0||_2$. Using a similar approach to [129], we take the base material to have an isotropic material response. The exact form of the strain-energy potentials can vary; however, typically we use a Yeoh model [201]

$$W(\mathbf{B}) = \sum_{i=0}^{3} c_i (I_3(\mathbf{B}) - 3)^i, \tag{2.14}$$

where $I_3(\mathbf{B}) = \text{tr}(\mathbf{B})$. The fibre component of the model will be based on the Hill type model and includes the effects from the active and passive properties of the muscle. It can be written as

$$W_{\text{fibre}}(\bar{\lambda}, t) = a(\mathbf{x}, t) W_{\text{act}}(\bar{\lambda}) + W_{\text{pass}}(\bar{\lambda}), \tag{2.15}$$

where $a(\mathbf{x}, t) \in [0, 1]$ is the scalar activation function used to ramp the activation of the muscle fibres.

To determine the constants in the Yeoh model and the form of the active and passive fibre strain energy functions, we need to calculate the stress response from the material. Using Equation 2.11 we can obtain the stress response for the base material, and obtain constants c_i, $i = 1, ...3$, through a nonlinear regression fit to experimental data (Figure 2.2). For the fibre component, can write the material response in terms of the Cauchy stress as

$$\boldsymbol{\sigma}_{\text{fibre}}(\bar{\lambda}, t) = \big(a(\mathbf{x}, t)\sigma_{\text{act}}(\bar{\lambda}) + \sigma_{\text{pass}}(\bar{\lambda})\big)\mathbf{a} \otimes \mathbf{a}, \tag{2.16}$$

where the current fibre orientation, $\mathbf{a}$, can be determined in terms of the initial fibre orientation $\mathbf{a}_0$ through application of the deformation gradient $\mathbf{a} := \mathbf{F}\,\mathbf{a}_0$. $\sigma_{\text{act}}(\bar{\lambda})$ and $\sigma_{\text{pass}}(\bar{\lambda})$ can be obtained from experimental data from [200] (Figure 2.2) [145].

The volumetric strain-energy term, W_{vol}, for the base material acts as a penalty term, which penalizes any changes in volume. For the muscle model used in this thesis, the form of W_{vol} is one typically used for biological materials [32]

$$W_{\text{vol}}(J) = \frac{\kappa}{4}(J^2 - 2\log(J) - 1), \tag{2.17}$$

where κ is the bulk moduli for the tissue and can be obtained through experimental data. The above description of the strain-energy breakdown for muscle can also be used for the

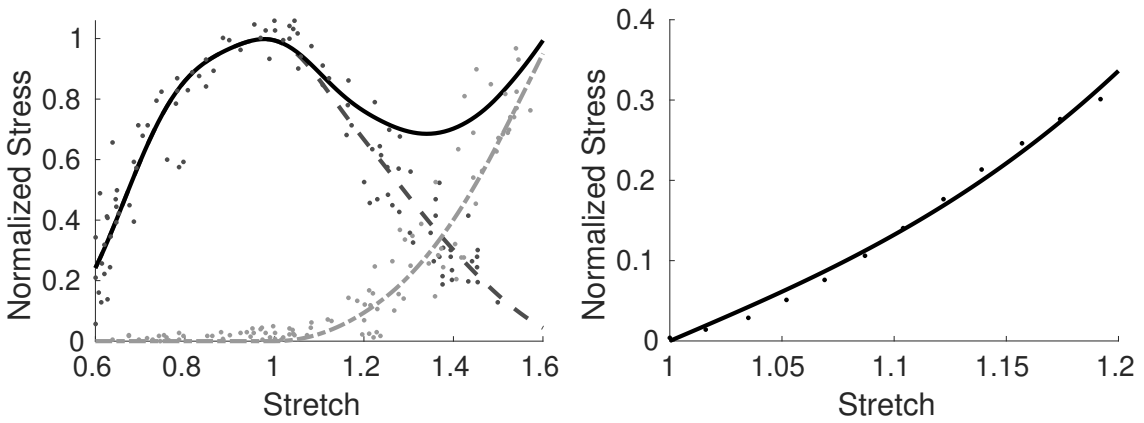

Figure 2.2: Intrinsic muscle fibre properties based on experimental data from [200] (left) and the base material response based on experimental data from the transverse muscle stress-stretch relationship from [108] (right).

other materials in the muscle-tendon unit, such as the aponeurosis or tendon. The only difference is that there will no contribution from the active strain-energy potential, ie. $W_{\text{act}}(\bar{\lambda}) = 0$. In the next section we use a three field formulation to derive the model equations.

2.3 Model formulation

The formulation of our model utilizes a three field formulation in terms of the velocity, pressure, and dilation of the material; in particular, we have unknowns $\mathbf{\Sigma} = \{\mathbf{u}, p, D\} \in \mathbf{X} := \mathbf{H}^1(V) \times L^2(V) \times L^2(V)$. The total potential energy in the system, E_{tot}, is a combination of the internal and external energies. Note that this energy is calculated with respect to the reference configuration, and so there is an undetermined constant that may result in the deformed state having a negative total potential energy. In terms of the strain-energy potentials, and body and traction forces we have

$$E_{tot}(\mathbf{\Sigma}) = \int_{V_0} W_{\text{iso}}(\mathbf{B}) + W_{\text{vol}}(D) + p(D - J(\mathbf{u})) + \mathbf{b} \cdot \mathbf{u}\, dV + \int_{\partial V_0} \mathbf{t}(\mathbf{x}) \cdot \mathbf{u}\, dA. \tag{2.18}$$

We introduce the pressure, p, as a Lagrange multiplier that will enforce the constraint $D - J(\mathbf{u}) = 0$. We now use a variational approach. Assume that we have a stationary minimum point $\mathbf{\Sigma}$, so that

$$E_{tot}(\mathbf{\Sigma}) \leq E_{tot}(\mathbf{\Sigma} + s\delta\mathbf{\Sigma}), \quad \forall s > 0, \tag{2.19}$$

where $\delta\boldsymbol{\Sigma} = (\delta\mathbf{u}, \delta p, \delta D) \in \mathbf{X}$. Through the Principle of Least Action, we have that $D_{\delta\boldsymbol{\Sigma}} E_{tot}(\boldsymbol{\Sigma}, \delta\boldsymbol{\Sigma}) = \frac{d}{ds} E_{tot}(\boldsymbol{\Sigma} + s\delta\boldsymbol{\Sigma})|_{s=0} = 0$. Evaluating the derivative, we get the residual

$$\begin{aligned} R(\boldsymbol{\Sigma}, \delta\boldsymbol{\Sigma}) = \frac{d}{ds} E_{tot}(\boldsymbol{\Sigma})|_{s=0} = \int_{V_0} \left(\frac{\partial W_{\text{iso}}(\mathbf{u})}{\partial \mathbf{u}} + p \frac{\partial J(\mathbf{u})}{\partial \mathbf{u}} + \mathbf{b} \right) \cdot \delta\mathbf{u} \\ + (J(\mathbf{u}) - D)\, \delta p + \left(\frac{dW_{\text{vol}}(J)}{dJ} - p \right) \delta D \, dV \\ + \int_{\partial V_0} \mathbf{t} \cdot \delta\mathbf{u} \, dA. \end{aligned} \tag{2.20}$$

Integrating by parts will give us

$$\begin{aligned} R(\boldsymbol{\Sigma}, \delta\boldsymbol{\Sigma}) = \int_{V_0} (\boldsymbol{\tau}_{\text{iso}} + pJ\mathbf{I}) : \nabla_0 \, \delta\mathbf{u} + \mathbf{b} \cdot \delta\mathbf{u} \\ + (J(\mathbf{u}) - D)\, \delta p + \left(\frac{dW_{\text{vol}}(J)}{dJ} - p \right) \delta D \, dV \\ + \int_{\partial V_0} \mathbf{t} \cdot \delta\mathbf{u} \, dA. \end{aligned} \tag{2.21}$$

For more detail on the derivation of the first term, see [117]. Note that $\boldsymbol{\tau}_{\text{vol}} = pJ\mathbf{I}$.

We can obtain the Euler-Lagrange equations for this by converting back to the current configuration. We get the following system of equations

$$\begin{aligned} \nabla \cdot \boldsymbol{\sigma}(\mathbf{B}) + \mathbf{b} = 0 \text{ in } V, \\ J(\mathbf{u}) = D \text{ in } V, \\ p = \frac{\partial W_{\text{vol}}(D)}{\partial D}. \end{aligned} \tag{2.22}$$

The first equation is the balance of stresses (cf. Equation 1.5) with no time dependent term, since we are working in the quasi-static regime.

2.4 Numerical methods and discretization

The above residual gives a nonlinear problem, which needs to be linearized. We can apply a Newton method to the nonlinear problem. In particular, we can look for a Newton update $d\boldsymbol{\Sigma} := (d\mathbf{u}, dp, dD)$ so that the value at a given Newton iteration is

$$\boldsymbol{\Sigma}_{i+1} = \boldsymbol{\Sigma}_i + d\boldsymbol{\Sigma}_i. \tag{2.23}$$

We can determine the update through the solution of the system of equations

$$\mathcal{D}R(\boldsymbol{\Sigma}_i, \delta\boldsymbol{\Sigma}) \cdot d\boldsymbol{\Sigma}_i = -R(\boldsymbol{\Sigma}_i, \delta\boldsymbol{\Sigma}), \quad \forall \delta\boldsymbol{\Sigma} \in \mathbf{X}. \tag{2.24}$$

Here $\mathcal{D}R(\boldsymbol{\Sigma}_i)$ is the Gateaux derivative

$$\mathcal{D}R(\boldsymbol{\Sigma}_i, \delta\boldsymbol{\Sigma}) = \lim_{\varepsilon \to 0} \frac{R(\boldsymbol{\Sigma}_i + \varepsilon d\boldsymbol{\Sigma}_i, \delta\boldsymbol{\Sigma}) - R(\boldsymbol{\Sigma}_i, \delta\boldsymbol{\Sigma})}{\varepsilon}. \tag{2.25}$$

Computing the derivative gives

$$\mathcal{D}R(\boldsymbol{\Sigma}_i, \delta\boldsymbol{\Sigma}) = \begin{bmatrix} (J\mathbb{C}_i : \nabla_0 d\mathbf{u}_i, \nabla_0 \delta\mathbf{u}) & (D_i \nabla_0 \cdot d\mathbf{u}_i, \delta p) & 0 \\ \quad + (\boldsymbol{\tau}_i \nabla_0 d\mathbf{u}_i, \nabla_0 \delta\mathbf{u}) & & \\ (D_i\, dp_i, \nabla_0 \cdot \delta\mathbf{u}) & 0 & -(dp_i, \delta D) \\ 0 & -(dD_i, \delta p) & (W''_{\text{vol}}(D_i)\, dD_i, \delta D) \end{bmatrix}.$$

Here $(\mathbf{x}, \mathbf{y}) = \int_{V_0} \mathbf{x} \cdot \mathbf{y}\, dV$, $\mathbb{C}_i = \mathbb{C}_{\text{iso},i} + \mathbb{C}_{\text{vol},i}$, and $\boldsymbol{\tau}_i = \boldsymbol{\tau}_{\text{iso},i} + \boldsymbol{\tau}_{\text{vol},i}$.

We use a finite element method to discretize the linear system (Equation 2.24). Given a triangulation $\mathcal{T}$ of the reference volume V_0 of hexahedral elements H_i with diameter h_i. We can define the mesh size as $h := \max_i\{h_i : H_i \in \mathcal{T}\}$. The finite element spaces are chosen to be continuous polynomials for the velocity and discontinuous polynomials in the pressure and dilation. We can consider the space of polynomials P_k so that we have the following finite element spaces for $\mathbf{H}^1_{\partial V}(V_0)$ and $L_2(V_0)$ as

$$\begin{aligned} P_k &:= \{q \in L^2(V_0) : q|_H \in P_k(T),\ \forall H \in \mathcal{T}\}, \\ \mathbf{Q}_{k+1} &:= \{\mathbf{w} \in \mathbf{C}(V_0) : \mathbf{v}|_H \in \mathbf{P}_{k+1}(H),\ \forall H \in \mathcal{T}\}, \end{aligned} \tag{2.26}$$

where $\mathbf{P}_k(V_0)$ is the vector version of $P_k(V_0)$.

Out discretized solution at Newton iteration i is then given by $\boldsymbol{\Sigma}_{i,h} \in \mathbf{X}_h := \mathbf{Q}_{k+1} \times P_k \times P_k$ and similarly the update is $d\boldsymbol{\Sigma}_{i,h} \in \mathbf{X}_h$. The discretized linear system is then given

$$\mathcal{D}R(\boldsymbol{\Sigma}_{i,h}, \delta\boldsymbol{\Sigma}_h) \cdot d\boldsymbol{\Sigma}_{i,h} = -R(\boldsymbol{\Sigma}_{i,h}), \quad \forall \delta\boldsymbol{\Sigma}_h \in \mathbf{X}_h. \tag{2.27}$$

We can solve the linear system is solved using a Conjugate-Gradient method along with a SSOR preconditioner [117]. Since we are trying to minimize the residual with the Newton method, we use the stopping criteria

$$||R(\boldsymbol{\Sigma}_{i,h})||_{L^2(V)} < \tau, \tag{2.28}$$

for some given tolerance τ.

2.5 Convergence

In this section the convergence of the above numerical method is demonstrated. This is done using a simplified block geometry with dimensions 20cm × 5cm × 5cm. The block will be orientated with its length running along the x-axis and the centroid of the block at the

origin. The fibres will be orientated parallel to the x-axis. To investigate the convergence of the method, we perform force-length tests, where we pull the muscle to a strain of 5%, and then activate the muscle quasi-statically using a linear ramp

$$a(t) = \frac{t_{act,end} - t}{t_{act,end} - t_{act,start}}, \tag{2.29}$$

where $t_{act,start} = 0.1s$ and $t_{act,end} = 0.2s$. The pulling of the muscle will consist of applying a zero Dirichlet conditions on the $-x$ face and applying a nonzero positive Dirichlet condition to the other face, which extends the muscle. The rest of the boundary will have a zero traction boundary conditions.

For the convergence properties in the primal variables, we refer the reader to Dominguez [44], where the convergence study was performed for the finite element method used here. The resulting rates of convergence were 1.9223 in the $\mathbf{H}^1$-norm for the displacement, $\mathbf{u}$, and 1.1299 in the L^2-norm for the pressure, p, and dilation, D. These are as expected based on the finite elements used and the convexity of the domain [44]. For a linear problem, we would expect to see quadratic convergence, but due to the nonlinear nature of the problem we are solving here, this is not achieved.

Here we look at the convergence results for some of the model outcomes that will be relevant in later chapters; in particular, we will look at the stretch throughout the muscle belly, $\bar{\lambda}$, and the force computed on the ends of the muscle, $\mathcal{F}$. The stretch will be calculated as

$$\bar{\lambda}(\mathbf{x}) = ||\bar{\mathbf{a}}(\mathbf{x})||_2. \tag{2.30}$$

The force will be calculated as an integral over the $+x$ face

$$\boldsymbol{\mathcal{F}} = \frac{1}{2}\int_V \left(\boldsymbol{\tau} + \boldsymbol{\tau}^\top\right)\mathbf{F}^{-\top}\mathbf{N}\, dV \approx \boldsymbol{\mathcal{F}}_h = \frac{1}{2}\sum_{i=1}^{N}(\boldsymbol{\tau} + \boldsymbol{\tau}^\top)\mathbf{F}^{-\top}\mathbf{N}\, J\, q_i, \tag{2.31}$$

where q_i is the quadrature weight at a given point and N is the number of quadrature points. We look at the magnitude of this force $\mathcal{F}_h = ||\boldsymbol{\mathcal{F}}_h||_2$. For the convergence test, we use $\mathbf{Q}_2 \times P_1 \times P_1$ elements for each level of refinement, and the exact solution is obtained on a highly refined mesh with $\mathbf{Q}_3 \times P_2 \times P_2$ elements. The error is computed after one timestep of activation.

The results are shown in Table 2.1. We see approximately quadratic convergence in the stretch (≈ 2.392), while the force is converging slowly at a rate of ≈ 0.66. Due to the post-processing required for computation of the stretch and force, these rates of convergence are reasonable. Additionally, we are not taking a L^2-norm in force, and so we would not expect the quadratic convergence. Additional error comes from the interpolation from the fine to the coarse mesh. For the force, the rate is lower than the other variables due to

the additional calculations. The force is calculated on the surface of the mesh, but the values are computed on at the quadrature points (which are not on the face), so there is an extrapolation required that introduces additional error.

h	$\|\|\bar{\lambda}_h - \bar{\lambda}_{exact}\|\|_{L^2}$	$\frac{e_h}{e_{h/2}}$	$\|\|\mathcal{F}_h - \mathcal{F}_{exact}\|\|$	$\frac{e_h}{e_{h/2}}$
0.052	1.223×10^{-4}		4.151×10^{-2}	
0.026	2.667×10^{-5}	4.5998	3.079×10^{-2}	1.34
0.013	4.446×10^{-6}	5.9972	1.641×10^{-2}	1.87

Table 2.1: Convergence study of the numerical methods described in Section 2.4 for $\mathbf{Q}_2 \times P_1 \times P_1$ elements. The errors here are calculated in the L^2-norm for stretch, while the error in $\mathcal{F}_h$ is give as the relative error between the successive refinements. $e_h/e_{h/2}$ is the ratio in errors between successive refinements.

Chapter 3

Modelling extracellular matrix and cellular contributions to whole muscle mechanics

3.1 Abstract

Skeletal muscle tissue has a highly complex and heterogeneous structure comprising several physical length scales. In the simplest model of muscle tissue, it can be represented as a one dimensional nonlinear spring in the direction of muscle fibres. However, at the finest level, muscle tissue includes a complex network of collagen fibres, actin and myosin proteins, and other cellular materials. This study shall derive an intermediate physical model which encapsulates the major contributions of the muscle components to the elastic response apart from activation-related along-fibre responses. The micro-mechanical factors in skeletal muscle tissue (eg. connective tissue, fluid, and fibres) can be homogenized into one material aggregate that will capture the behaviour of the combination of material components. In order to do this, the corresponding volume fractions for each type of material need to be determined by comparing the stress-strain relationship for a volume containing each material. This results in a model that accounts for the micro-mechanical features found in muscle and can therefore be used to analyze effects of neuro-muscular diseases such as cerebral palsy or muscular dystrophies. The purpose of this study is to construct a model of muscle tissue that, through choosing the correct material parameters based on experimental data, will accurately capture the mechanical behaviour of whole muscle. This model is then used to look at the impacts of the bulk modulus and material parameters on muscle deformation and strain energy-density distributions.

3.2 Introduction

Skeletal muscle is a complex heterogeneous structure, and a three dimensional continuum model is required to capture its complete mechanics. One dimensional models have been

developed, often to describe whole body movement or inter-muscular dynamics (eg. [203]). However, when examining the mechanics or force production of the muscle these models are not sufficient to understand the complex effects from the heterogeneity or architecture of muscle [89]. In fact, three dimensions are required to fully capture the bulging and deformation seen in skeletal muscle [133]. Therefore, to capture the complex aspects of muscle tissue, these models are typically built using the theory of continuum mechanics and solved using a finite element method [129, 146, 15, 115, 202, 195].

Muscle is composed of many components making it a highly heterogeneous structure, and these aspects are typically investigated in micro-mechanical [157, 186, 31, 140, 18] and homogenization [172, 171, 14] models. The tissue heterogeneity effects are often related to micro-structure [60, 128], and these effects cannot be implemented using a single-scale model. The micro-mechanical components of muscle are those that are visible on a microscopic level and contribute to the mechanical behaviour of muscle tissue. There are many micro-mechanical components of muscle aside from the contractile fibres alone. In particular, muscle consists of connective tissue, fluid, cellular components, and muscle fibres which make it a highly heterogeneous material. Skeletal muscle consists of muscle fibres surrounded by a layer of connective tissue (endomysium), and groups of fibres are bundled together into muscle fascicles by another layer of connective tissue (perimysium). Bundles of fascicles are what composes the muscle volume and is held together with a third layer of connective tissue (epimysium) [60, 128]. The combination of connective tissue layers forms the extra-cellular matrix (ECM) and is typically less than 10 % of the muscle volume in healthy muscle [13], however the ECM has been shown to have a large impact on the muscle force development [93]. The reason for this is the high degree of structure found in the ECM along with the stiff collagen fibres, which results in a significant contribution to the passive stiffness of the muscle [92, 163, 183, 128, 102, 125, 181].

In order to capture the complex effects of the micro-mechanical factors on a whole muscle level, a principled approach needs to be taken. This procedure will allow for consideration of microscopic properties and their effects on the macroscopic muscle model. The micro-mechanical influences on whole muscle effects have been investigated in many studies (eg. [31, 157, 186, 18, 172, 14]). A study by Ceelen et al. [31] developed a micro-mechanical model of skeletal muscle for an analysis of the effect of deformation induced hypoxic damage. Sharafi and Blemker [157] developed a formulation of the micro-mechanical effects for healthy muscle that could be implemented in a macroscopic model. Work by Rhörle et al. [140] produced a multi-scale framework for a continuum mechanical model, and included the effects from motor unit recruitment and allows for analysis of electro-physiological behaviour. These developments however do not allow for simple application to the macroscopic level, and hence studies combining the material effects into a homogenous macroscopic model

have been performed [14, 172, 171]. By performing these homogenizations, a better understanding of the mechanical properties can be obtained in microscopically altered muscle tissue, such as fibrotic tissue that can result from muscular dystrophies, cerebral palsy, and aging [92, 168].

In this study, a principled approach will be taken to develop an isotropic aggregate material that will give a representation of the micro-mechanical effects that can be modelled on a macroscopic level. This homogenization will take into account two factors: a cellular component including the fibres and other cellular materials, and an ECM component. The cellular materials being considered are both effects from cells external to the muscle fibres (eg. satillite cells, nerve bodies, capilleries), as well as the intracellular effect from the fibres aside from the myofibrils. Parameters can be developed independently, so that volume changing as well as isochoric properties can be modified. Additionally, this model will differ from previous homogenization studies (eg. [14, 172]) by considering a nonlinear Yeoh model [201] for the cellular component. Due to the lack of cellular component data, mechanical properties from the cells in brain grey matter will be chosen given the material is composed of the neuron cell bodies. This gives grey matter a nonlinear isotropic response [79, 124], and since this is a collection of cells and similar to the the model's cellular component, these data will be considered. Any anisotropy typically seen in skeletal muscle will be captured in the one dimensional along-fibre component that takes into account the effects from myofilaments within the muscle fibres, and anisotropy conferred by the ECM. Recent experiments have reported varying muscle volume levels over long contractions [199], and changes in volume have been shown to impact passive muscle tension [164]. The distribution of strain energy-densities has been shown to allow for a deeper understanding of the underlying physics of skeletal muscle mechanics [192]. Therefore, the purpose of this study is to develop a principled model that can be accurately fit to existing experimental data, and can then be used to develop a greater understanding of muscle mechanics in response to altered micro-mechanical properties. In particular, we will look at the impact of the stiffness, volume fraction, and bulk moduli of the individual components in the model through a comparison to experimental data and strain energy-density distribution analysis.

3.3 Model

3.3.1 Continuum Mechanical Formulation

Continuum mechanics is an effective method to model the physics of biological materials, and is typically used in three dimensional skeletal muscle models [15, 129, 146, 172, 14, 140]. To characterize the deformation of a body, Ω_0, to a new deformed state, Ω, we can introduce

the deformation gradient, $\mathbf{F}$. The deformation gradient can be defined as

$$\mathbf{F} = \frac{d\mathbf{x}}{d\mathbf{X}} \tag{3.1}$$

where $d\mathbf{X}$ is a line element in the original reference configuration and $d\mathbf{x}$ is a line element in the deformed current configuration. $\mathbf{F}$ contains the information about how the original configuration is deformed, via rotations or stretches, to get to the current configuration. The dilatation of the material can be denoted as $J = \det(\mathbf{F})$, and remains close to 1.

To characterize the response of a material to deformation, the constitutive laws for the material need to be determined. To do this, stress and strain tensors need to be defined. The model developed here will consider the left Cauchy-Green strain tensor $\mathbf{b} = \mathbf{F}\mathbf{F}^T$ to characterize the strain in the material. Skeletal muscle can be modelled using a nonlinear hyperelastic approach. For a hyperelastic material, the formulation of the constitutive relationships can be performed in terms of a strain-energy function which can be calculated at each material point, $\mathbf{X}$. The strain-energy function can be represented in the reference configuration as $W(\mathbf{X}, \mathbf{b}) \equiv W(\mathbf{b})$. Characterizing the material in terms of the strain-energy allows us to write the constitutive law in terms of the Cauchy Stress Tensor, σ, and the left Cauchy-Green strain tensor,

$$\sigma(\mathbf{b}) = 2J^{-1}\mathbf{b}\frac{\partial W(\mathbf{b})}{\partial \mathbf{b}}. \tag{3.2}$$

In order to determine the constitutive law explicitly, the exact form of $W(\mathbf{b})$ needs to be determined. For skeletal muscle the strain-energy function can be broken into a volumetric and isochoric component.

$$W_{\text{muscle}} = W_{\text{vol}}(J) + W_{\text{iso}}(\bar{\mathbf{b}}) \tag{3.3}$$

where $\bar{\mathbf{b}}$ is the isochoric component of the left Cauchy-Green Strain tensor, and is defined as $\bar{\mathbf{b}} = J^{-2/3}\mathbf{b}$. The strain-energy function for skeletal muscle, $W_{\text{muscle}}(\mathbf{b})$, is composed of the three dimensional base material component, $W_{\text{BM}}(\mathbf{b})$, and an along-fibre component, $W_{\text{fibre}}(\lambda)$, which depends on the local fibre stretch ($\lambda = ||\mathbf{F}\mathbf{a}_0||$) along the direction of the muscle fibres. $\mathbf{a}_0$ denotes the initial fibre direction with unit length at a given point and $||(\cdot)||$ denotes the usual L^2 norm of $(\cdot)$. Therefore, the volumetric and isochoric components are

$$\begin{aligned} W_{\text{iso}} &= W_{\text{fibre}}(\lambda) + W_{\text{BM,iso}}(\bar{\mathbf{b}}), \\ W_{\text{vol}} &= W_{\text{BM,vol}}(J). \end{aligned} \tag{3.4}$$

The continuum mechanical formulation developed here can be implemented into a three dimensional finite element model using a three field formulation with the unknowns being the displacement $\mathbf{u}$, pressure p, and dilation J [160]. The Principle of Stationary Energy can be applied to the problem by taking the first variation of the total energy. This gives a nonlinear problem that can be solved using the finite element library Deal ii [6]. Details on the implementation and finite element method can be found in Domínguez[44] and the Supplementary Material.

3.3.2 A Principled Approach to Muscle Base Material

Formulation of the Base Material

Muscle is often modelled as a fibre reinforced material [129, 15, 115], and so the model developed in this study will consider the muscle as a three dimensional isotropic material with one dimensional fibres running along the length of the muscle belly. The one dimensional along-fibre component is designed to account for any anisotropic effects in the direction of the muscle fibres. In particular, this includes the passive along-fibre effects from within the sarcomeres, such as from the protein titin, and active forces developed between actin and myosins. To analyze the micro-mechanical properties in whole muscle, the isotropic base material can then be constructed by combining the effects from the principle components (ECM and cellular materials). Since the base material has both isochoric and volumetric parts, the a homogenization will need to occur in both of these strain-energy components.

The base material can be formulated by considering a representative volume element (RVE) that encompasses a region, V_{RVE}, in the initial reference configuration. Since the RVE consists of each of the micro-mechanical components of the muscle, a portion of it will consist of ECM, V_{ECM}. The rest of the volume will consist of the cellular component, V_{cell}. Let $|V_{\text{RVE}}|$ denote the volume the region V_{RVE}, then the volume fraction of each material can be defined as

$$\frac{|V_{\text{ECM}}|}{|V_{\text{RVE}}|} = \alpha, \quad \frac{|V_{\text{cell}}|}{|V_{\text{RVE}}|} = 1 - \alpha. \tag{3.5}$$

The volume fractions, α and $1 - \alpha$, are determined in the reference configuration of the RVE, and we assume these volume fractions do not change as the muscle deforms. Since skeletal muscle achieves near incompressibility, this is an accurate approximation to leading order.

The total energy of the RVE, E_{RVE}, can be written in terms of the microscopic strain-energy functions for the ECM and cellular components as

$$\begin{aligned} E_{\mathrm{RVE}}(\mathbf{b}) &= \int_{V_{\mathrm{RVE}}} W_{\mathrm{RVE}}(\mathbf{b})\, dV \\ &= \int_{V_{\mathrm{ECM}}} s_{\mathrm{ECM}} W_{\mathrm{ECM,RVE}}(\mathbf{b})\, dV + \int_{V_{\mathrm{CELL}}} W_{\mathrm{CELL,RVE}}(\mathbf{b})\, dV \end{aligned} \tag{3.6}$$

where s_{ECM} is a structural area parameter that is constant over the RVE and will be discussed in more detail in the next section. Dividing by $|V_{\mathrm{RVE}}|$ gives

$$\begin{aligned} \frac{1}{|V_{\mathrm{RVE}}|}\int_{V_{\mathrm{RVE}}} W_{\mathrm{RVE}}(\mathbf{b})\, dV &= \frac{1}{|V_{\mathrm{RVE}}|}\int_{V_{\mathrm{ECM}}} s_{\mathrm{ECM}} W_{\mathrm{ECM,RVE}}(\mathbf{b})\, dV \\ &\quad + \frac{1}{|V_{\mathrm{RVE}}|}\int_{V_{\mathrm{CELL}}} W_{\mathrm{CELL,RVE}}(\mathbf{b})\, dV \\ &= \alpha\frac{1}{|V_{\mathrm{ECM}}|}\int_{V_{\mathrm{ECM}}} s_{\mathrm{ECM}} W_{\mathrm{ECM,RVE}}(\mathbf{b})\, dV \\ &\quad + (1-\alpha)\frac{1}{|V_{\mathrm{CELL}}|}\int_{V_{\mathrm{CELL}}} W_{\mathrm{CELL,RVE}}(\mathbf{b})\, dV. \end{aligned} \tag{3.7}$$

Given that the RVE is microscopic in size, the following approximations were made

$$\begin{aligned} W(\mathbf{b}) &\approx \frac{1}{|V_{\mathrm{RVE}}|}\int_{V_{\mathrm{RVE}}} W_{\mathrm{RVE}}(\mathbf{b})\, dV \\ W_{\mathrm{ECM}}(\mathbf{b}) &\approx \frac{1}{|V_{\mathrm{ECM}}|}\int_{V_{\mathrm{ECM}}} W_{\mathrm{ECM,RVE}}(\mathbf{b})\, dV \\ W_{\mathrm{CELL}}(\mathbf{b}) &\approx \frac{1}{|V_{\mathrm{CELL}}|}\int_{V_{\mathrm{CELL}}} W_{\mathrm{CELL,RVE}}(\mathbf{b})\, dV \end{aligned} \tag{3.8}$$

where $\mathbf{b}$ denotes the left Cauchy-Green strain tensor at the centroid of the RVE. This is the familiar Voigt approximation used in skeletal muscle homogenization studies [172, 171].

It then follows that the strain-energy function for the macroscopic base material can be written as a linear combination of the strain energies from each component:

$$W_{\mathrm{BM,iso}}(\mathbf{b}) = \alpha s_{\mathrm{ECM}} W_{\mathrm{ECM}}(\mathbf{b}) + (1-\alpha) W_{\mathrm{cell}}(\mathbf{b}). \tag{3.9}$$

Similarly, it is possible to decompose the volumetric strain-energy function into its micromechanical components. The volumetric strain-energy component will be characterized using a strain-energy function typically used for soft biological materials [159], and the aggregate function is given as

$$W_{\mathrm{BM,vol}}(J) = \frac{1}{4}(J^2 - 1 - 2\log(J))[\alpha\kappa_{\mathrm{ECM}} + (1-\alpha)\kappa_{\mathrm{cell}}]. \tag{3.10}$$

The bulk moduli, κ_{ECM} and κ_{cell}, are parameters that will impact the compressibility of the model and can be varied independently for each component.

Micro-mechanical Components

The strain-energy function for the ECM, $W_{\text{ECM}}(\mathbf{b})$, can be determined using experimental data from Gillies et al. [61], which obtained stress-strain curves for decellularized skeletal muscle tissue. These data are used as they are the only mechanical data available for the entire ECM. Other micro-mechanical models consider the response from the isotropic component of the ECM to be of the same order of magnitude [172] as that of the fibres, instead, in this model we consider experimental data for the ECM that have been measured for a decellularized matrix. Additional data for the ECM component will allow for a more accurate representation in the model. Due to difficulty in measuring the decellularized cross-sectional area of the ECM, the stress-strain relationship is typically reported with respect to the cross-sectional area of the muscle tissue. Therefore, to account for this cross-sectional area calculation in the model, the additional coefficient, s_{ECM}, is used.

Material data for the cellular (non-contractile and non-ECM) properties of skeletal muscle are not available. Some studies have been able to measure properties of isolated muscle fibres. However, tensile data are only available for the longitudinal direction of the muscle fibres [17], which may not necessarily represent the response in the transverse direction. Ideally, data for the cellular component of the base material would be tensile data for fibre and other cellular components measured transverse to the fibre orientation. Since these data are not available other data need to be considered, such as the mechanical behavior of brain grey matter or liver tissue. These materials are considered since they are essentially a cellular mass with no collagen fibres and are often modelled as non-linear isotropic materials [26, 79, 80, 124, 36]. Along fibre data have been considered in the homogenization models by Bleiler et al. [14] and Spyrou et al. [172], however, they only considered a linear stress-strain response shown by Smith et al. [168]. Since the liver material has been shown to have some anisotropy, which is likely due to micro-structural effects, grey matter is used for the cellular component.

In order to implement the experimental data for the ECM and cellular components into the model a strain-energy function needs to be used for each of the components. The Yeoh model (Eq. 3.11) gives the energy associated with a deformation in terms of the first invariant of $\overline{\mathbf{b}}$ [201].

$$W(\overline{\mathbf{b}}) = c_1(I_1 - 3) + c_2(I_1 - 3)^2 + c_3(I_1 - 3)^3 \tag{3.11}$$

This provides a computationally simplistic model that can sufficiently capture the isotropic behaviour of these components as demonstrated by r^2 values of 0.998 and 0.999 for the ECM and cellular material, respectively (Fig 3.1 A). Fig 3.1 illustrates the fit of the model for the intrinsic micro-mechanical properties (ECM and cellular components) used in the model along with the experimental whole muscle data from Mohommadkhah et al. [108]. s_{ECM} was set at 200 in Fig 3.1 to account for the aforementioned cross-sectional area calculation effects. This gives a significantly stiffer curve for the ECM compared to both the whole muscle data and the cellular component (Fig 3.1(A)), which is expected.

3.3.3 Implementation of the Along-Fibre Component

The along-fibre component of the model was obtained through fitting to experimental data by Winters et al. [200] and is shown in Fig 3.1(B) in terms of its stress-stretch relationship. The stress response for the passive component of the fibres is given as

$$\sigma_{\text{pass}}(\lambda) = \sigma_0 \begin{cases} 0 & 0 \leq \lambda \leq 1.0 \\ 2.353(\lambda - 1.0)^2 & 1.0 \leq \lambda \leq 1.25 \\ 3.44(\lambda - 1.25)^2 + 1.18(\lambda - 1.25) + 0.147 & 1.25 \leq \lambda \leq 1.5 \\ 0.427(\lambda - 1.5)^2 + 2.90(\lambda - 1.5) + 0.656 & 1.5 \leq \lambda \leq 1.65 \\ 3.023(\lambda - 1.65) + 1.1 & \lambda > 1.65, \end{cases} \tag{3.12}$$

and the active component of the fibres as

$$\sigma_{\text{act}}(\lambda) = \begin{cases} \sigma_0(0.642\sin(1.29\lambda + 0.629) & \\ \quad + 0.325\sin(5.31\lambda - 4.52) & \\ \quad + 0.328\sin(6.74\lambda + 1.69) & \\ \quad + 0.015\sin(19.8\lambda - 7.39) & \text{if } 0.4 \leq \lambda \leq 1.75 \\ \quad + 0.139\sin(8.04\lambda + 2.54) & \\ \quad + 0.0018\sin(32.2\lambda - 6.45) & \\ \quad + 0.012\sin(23.2\lambda - 2.64)) & \\ \\ 0 & \text{otherwise.} \end{cases} \tag{3.13}$$

Here, $\sigma_0 = 2 \times 10^5$ Pa is the maximum isometric stress. The active component in the model is also multiplied by a function $a(t)$ that represents the activation, which increased from 0 to 1 over the course of the contraction. $a(t)$ is linearly ramped in discrete steps t, which we will call "timesteps". At each step we compute the new state $\mathbf{u}$, p, and J of the muscle. The

relationship between the stress and the strain-energy functions is given by

$$\sigma(\lambda) = \lambda \frac{\partial W(\lambda)}{\partial \lambda}. \tag{3.14}$$

The strain-energy function for the along-fibre component can then be formulated as

$$W_{\text{fibre}}(\lambda) = W_{\text{pass}}(\lambda) + a(t) W_{\text{act}}(\lambda). \tag{3.15}$$

All of the parameters used in the model, and their values are summarized in Table 3.1. The base material and along-fibre component were implemented in a quasi-static model described in Wakeling et al. [192].

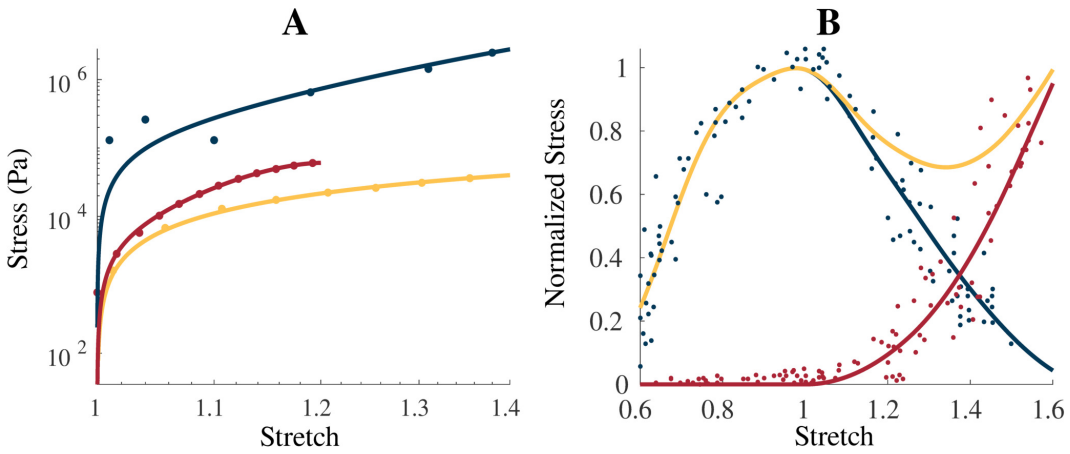

Figure 3.1: Intrinsic model properties. (A) shows the uniaxial stress-stretch relationship for the intrinsic properties of the homogenization: ECM (blue), cellular (yellow), and averaged whole muscle components (red), along with experimental data from Gillies et al. [61] (ECM, blue dot), Jin et al. [79] (brain grey matter, yellow dot), and Mohammadkhah et al. [108] (transverse muscle response, red dot). The averaged whole muscle component was fit to experimental data and is shown for comparison. Total (yellow), passive (red), and active (blue) stress-stretch relationships are shown for the along-fibre response in (B) with the experimental data obtained by Winters et al. [200] and normalized to $\sigma_0 = 2 \times 10^5$ Pa. ECM component was scaled by 200 in (A) to account for cross-sectional area calculations.

3.4 Methods

3.4.1 Stress-Strain Experiments

A block of muscle was constructed as seen in Fig 3.2 (A), which had dimensions 20 cm $\times$ 6 cm $\times$ 4 cm. The fibre properties were implemented along the length of the muscle model in the longitudinal direction (parallel to the x axis). To perform stress-strain tests that will allow for a comparison to experimental whole muscle data, the $-x$ face was constrained from

Parameter	Value/Range of Values
$c_{1,\text{cell}}$	3703
$c_{2,\text{cell}}$	-707.7
$c_{3,\text{cell}}$	123.2
$c_{1,\text{ecm}}$	1988
$c_{2,\text{ecm}}$	4917
$c_{3,\text{ecm}}$	-591.5
α	2 — 20 %
s_{ECM}	150 — 250
κ_{cell}	1×10^6 — 1×10^8 Pa
κ_{ECM}	1×10^6 Pa
σ_0	2×10^5 Pa

Table 3.1: Summary of parameters used in the model. List of the values for the aforementioned parameters used in this model. $c_{\text{i,cell/ecm}}$ are the Yeoh model parameters shown in Equation 3.11 and were obtained using nonlinear regression analysis.

movement in x, y, z directions. A traction was then applied to the $+x$ face of the muscle which extended the muscle in the longitudinal direction.

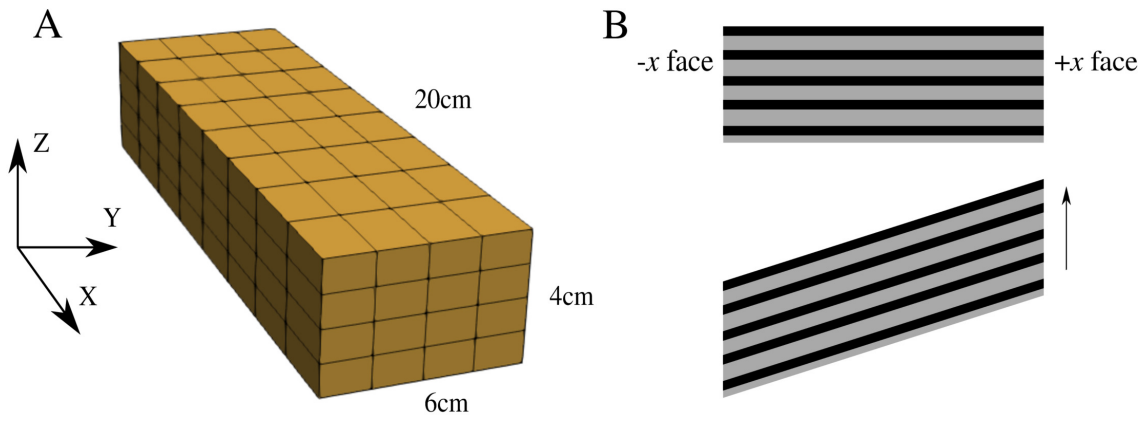

Figure 3.2: Mesh and experiment setup. (A) Mesh of the geometry used for the numerical experiments. The geometry had dimensions 20cm×6cm×4cm and muscle fibre properties are orientated along the x axis. (B) Shear experiment setup. The $-x$ face was constrained in all directions, while the $+x$ face was constrained in the x direction only. The arrow represents direction of applied shear stress.

These tests were performed with varying α in the range 0.02 — 0.20 and s_{ECM} coefficients of 150 and 250. The stiffness coefficients were varied to give results that are comparable to experimental data for muscle. The range from 2 % to 10 % volume fractions of ECM are typically found in healthy muscle [93, 13], and larger volume fractions in the range of 10 % to 20 % are found in fibrotic tissue [93]. By comparing the stress-strain curves of the model to experimental data, the accurate homogenization parameters, s_{ECM} and α, can be

determined.

3.4.2 Shear Experiments

Shear tests were performed to investigate the behaviour of the model in response to more complex deformation modes. A shear stress was applied to the $+x$ face of the model, which was constrained from movement in the x direction. To apply the shear stress to the model, we specify the component of the non-zero traction boundary condition in the y direction and set the x and z component of the traction to 0. Meanwhile, the $-x$ face was constrained in all directions (Fig 3.2 B). The shear stress was applied in three different scenarios to determine the impact of the base material stiffness and anisotropy in the model: (1) the shear stress was applied without activation with $\alpha = 0.05$ and 0.10, (2) the shear stress was applied prior to activation of the model, and (3) the shear stress was applied after activation of the model.

3.4.3 Investigation of Bulk Modulus and Strain-Energy Properties

Muscle is typically considered to be isovolumetric, however, small changes in volume may occur during muscle stretches [20], and also during long fatiguing contractions [199]. Willwacher et al. [199] found that volume changes occured up 9 % in the gastrocnemii during running activities, and so to confine volume changes to this range a value for $\kappa > 1 \times 10^6$ Pa is required. Given the results from previous studies and lack of experimental data for the compressibility of the ECM, the κ_{ECM} was left at 1×10^6 Pa [129]. Skeletal muscle consists of 80 % water [185], which is contained in the cellular component of the muscle and makes it highly incompressible. Therefore, κ_{cell} was varied in the range 1×10^6 to 1×10^8 Pa to look at the effects of the bulk moduli on the stress-strain relationship and strain energy-density distribution. The micro-mechanical components impact the overall stiffness of the base material component, and these effects on the strain-energy distribution were also investigated with $\kappa_{\text{cell}} = 1 \times 10^7$ Pa, $\kappa_{\text{ECM}} = 1 \times 10^6$ Pa, and $s_{\text{ECM}} = 150$. To obtain a better understanding of the physics occurring in the model, the volume fractions of ECM were varied between 2 % and 100 %. The set up for these tests was the same as for the tests for the stress-strain experiments with the addition of an activation phase after the passive lengthening. This involved constraining both the positive and negative x faces of the muscle block after the muscle had been passively lengthened, then increasing the activation in the muscle to 100 %.

3.5 Results

3.5.1 Stress-Strain Results

The model qualitatively demonstrates similar stress-stretch behaviour to available experimental data. These data for skeletal muscle vary depending on the species [177, 108], so it is not useful to compare directly to one particular set of muscle data. The stress values from the model are the applied traction to the $+x$ face of the block, and the stretch values are the whole muscle stretch

$$\lambda_{\text{muscle}} = \frac{l}{l_0}, \tag{3.16}$$

where l_0 and l are the initial length and current length of the muscle belly, respectively. Fig 3.3 shows that for $s_{\text{ECM}} = 150$ and 250 there is a particularly good match at smaller stretch values. Comparable material stiffness to healthy muscle occurs for $\alpha < 0.10$ for $s_{\text{ECM}} = 150$ which is a larger range of volume fractions compared to $s_{\text{ECM}} = 250$ (< 0.05). However, to better capture the nonlinearity seen at larger strains a larger value of $s_{\text{ECM}} = 250$ is required. As the volume fraction of the ECM was increased, there was an increase in stiffness that is expected with fibrotic tissue.

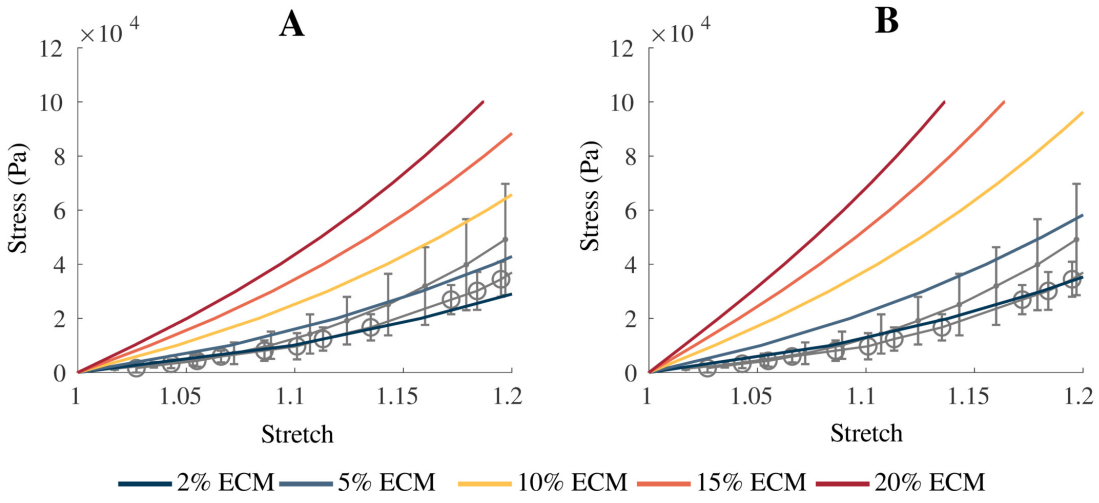

Figure 3.3: Comparison of model results to experimental data. Comparison of model passive stress-stretch curves to experimental data for skeletal muscle. (A) gives the model with a parameter of $s_{\text{ECM}} = 150$, while (B) is the model with a parameter of $s_{\text{ECM}} = 250$. α was varied between 0.02 — 0.20, which corresponds to 2 — 20 % volume fraction of ECM. The grey lines represent experimental data from Takaza et al. [177] (circle) and Mohammadkhah et al. [108] (dot). Error bars represent ± standard deviation when available.

3.5.2 Shear Results

The effects of applying a shear stress to the model was demonstrated in Fig 3.4 with shear strain calcated as

$$\epsilon_{\text{shear}} = \frac{\overline{u}_y}{l_0}, \tag{3.17}$$

where $\overline{u}_y$ is the mean displacement in the y direction of the $+x$ face. At small values of shear strain, there is a linear region in the shear stress-strain relationship and only a small effect from the variation in α (Fig 3.4). This shows there is more influence from the fibres for small shear stresses. At larger strains, the stress response for the model varies with α, and the graph becomes more nonlinear, demonstrating the nonlinearity in the base material (Fig 3.1A). While the model is active, shear stress-strain relationship becomes more linear due to larger fibre forces (Fig 3.4B). In Fig 3.4 (D,E), the three dimensional mesh of the model is shown at 100 % activation. The largest dilations occur in the corners of the model which experience the most stretching during the shear. Fig 3.4 (D) shows the model during a fixed-length contraction after a shear stress has been applied. The deformation and dilation are smaller, compared to Fig 3.4 (E), where the model has been first activated then sheared.

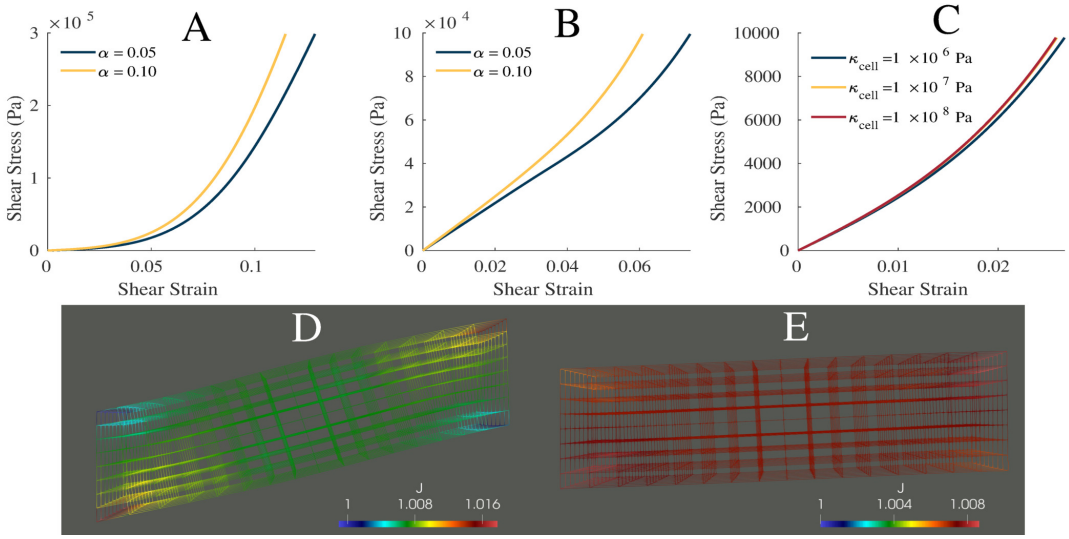

Figure 3.4: Shear properties. Plot of the shear stress-strain relationship for $\alpha = 0.05,\ 0.10$ and $s_{\text{ECM}} = 250$, while the muscle is passive (A) and active (B). (C) Shear stress-strain relationship for bulk moduli of 1×10^6, 1×10^7, and 1×10^8 Pa. Wire mesh of muscle model after shear stress was applied then model was activated (D), and after first activation then application of shear stress (E). (D,E) Color represents the dilation seen in the muscle model. (C) Shear stress-strain relationship for bulk moduli of 1×10^6, 1×10^7, and 1×10^8 Pa.

3.5.3 Volumetric Effects

Variation in the bulk modulus of the cellular component shows small effects on the normal stress-strain (Fig 3.5) and shear stress-strain (Fig 3.4 (C)) relationships. The largest variations in the stress-strain relationships were observed between $\kappa_{\text{cell}} = 1 \times 10^6$ Pa and 1×10^7 Pa whereas smaller variations between the relationships were seen at larger κ_{cell}. Table 3.2 gives the volume changes and normalized stresses on the $+x$ face of the muscle during the normal stress-strain experiment, where the change in volume was calculated as the ratio between the current volume and initial volume. The volume in its new configuration was calculated as

$$Vol = \int_{V_0} \det(\mathbf{F}) dV_0, \tag{3.18}$$

where V_0 is the initial configuration of the muscle. At larger bulk moduli smaller changes in volume were seen at maximal activation, for $\kappa_{\text{cell}} = 1 \times 10^8$ Pa the change in volume was considerably smaller at 0.1 % change in volume compared to the 7.3 % change in volume seen for $\kappa_{\text{cell}} = 1 \times 10^6$ Pa. While the changes in volume varied substantially, the effect on the total muscle force was small (Table 3.2).

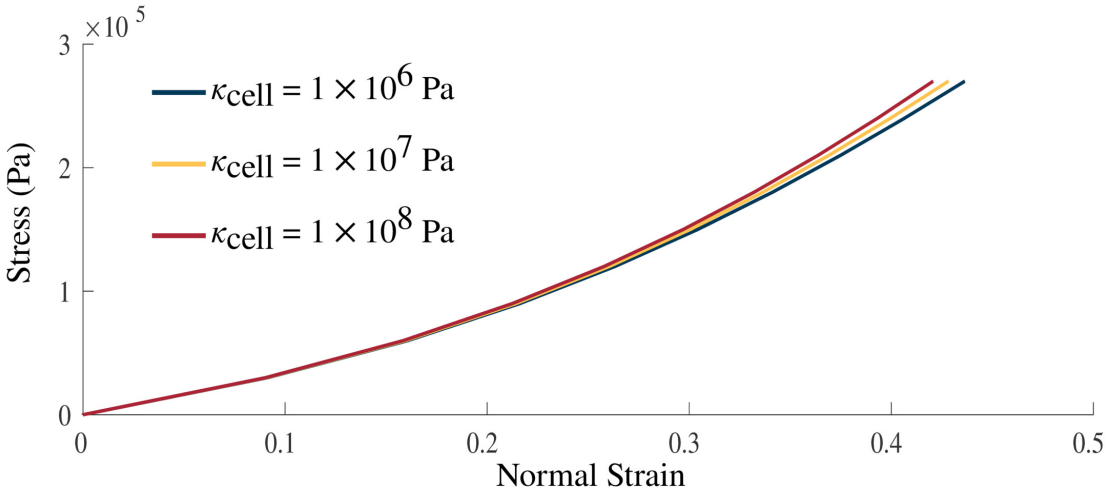

Figure 3.5: Volumetric impact on stress-strain relationship. Stress-strain relationship with $\kappa_{\text{cell}} = 1 \times 10^6, 1 \times 10^7, 1 \times 10^8$ Pa. Stress was applied in the longitudinal direction on the $+x$ face of the muscle model. Increasing values of the bulk moduli result in a stiffer material.

Changes in the κ of the muscle material also had an impact on the strain energy-density distribution of the model. The strain energy-density calculations were performed as in Wakeling et al. [192]. There was very little change to many of the energy components, in particular, the isochoric components of the energies for the passive lengthening periods of the experiments (Fig 3.6). There was only a substantial effect to the strain energy-densities in the volumetric component where the energy decreases with increasing bulk moduli. Large

κ_{cell} (Pa)	Volume Change (%)	Normalized Stress at 100 % Activation
1×10^6	7.3	0.875
1×10^7	0.8	0.907
1×10^8	0.1	0.912

Table 3.2: Total volume change and normalized stress on the $+x$ face of the muscle after passive lengthening to a stress of 1×10^5 Pa and fixed length contraction to an activation of 100%. The stress was normalized to σ_0. These values are measured with homogenization parameters of $\alpha = 0.05$ and $s_{\text{ECM}} = 250$.

effects were seen during activation on the volumetric component with activation increasing the volumetric energy for some values of κ_{cell} (1×10^6 Pa) and decreasing the energy for others ($\kappa_{\text{cell}} = 1 \times 10^7, 1 \times 10^8$ Pa). Overall, the total internal energy remains largely unchanged by the value of κ_{cell}.

3.5.4 Micro-mechanical Impacts on the Strain-Energy Distribution

Fig 3.7 shows the impact of varying the volume fraction of ECM in the ranges 2-100% on the strain energy-density distribution during a passive lengthening test and fixed-end contraction. As the volume fraction of the ECM becomes larger the muscle becomes stiffer, smaller strains are reached and less deformation occurs, which then results in smaller magnitudes of energy potentials. The volumetric component of the energy decreases as the stiffness in the material decreases, while the opposite behaviour occurs for each of the other components in the material. Additionally, similar effects are seen during activation to the results in Fig 3.6, where there is increasing volumetric energy for positive volumetric strain-energies and decreasing volumetric energy for negative volumetric strain-energies. In contrast to variations in the bulk moduli (Fig 3.6), the total internal energy in the model is affected more by variations in the volume fraction of ECM.

3.6 Discussion

3.6.1 Micro-mechanical Properties

The approach taken in this study develops a base material for whole muscle based on the principle micro-mechanical components. This aggregate base material is implemented into a continuum mechanical model developed in previous studies [129, 192]. This homogenized base material showed a good comparison to the experimental data from Takaza et al.[177] and Mohammadkhah et al. [108], with which it was developed. The s_{ECM} parameter was varied to account for uncertainty in the experimental data calculation, however, with improved experimental techniques alteration of s_{ECM} may not be required. As described previously, the larger values of s_{ECM} result in larger nonlinearity in the stress-strain curves for the

muscle tissue. This implies the ECM component of the model is largely responsible (along with the anisotropic component) for the nonlinear effects seen in the model, which agrees with experimental data [168, 60]. Binder-Markey et al. [13] found that the ECM volume fractions for various skeletal muscles were typically less than 10 %, and for some muscles (eg. Semimembranosus) the volume fractions were less than 2 %. Therefore, the volume fractions less than 10 % in Fig 3.3(A) and less than 5 % in Fig 3.3(B) are reasonable ranges when compared to the experimental data for healthy muscle.

While other models have considered an explicit anisotropic ECM [14, 172, 171], in the model developed here these effects are accounted for in the one dimensional along-fibre component. Nevertheless, accurate stress-strain mechanics result from the model (Fig 3.3). A unique component of this model is the use of a nonlinear cellular component derived from brain grey matter. The cellular component of muscle is difficult to measure experimentally, and grey matter provided a good substitute. It demonstrated similar isotropic effects and structure to the cellular component of muscle, and therefore provided good experimental data for the model. Some homogenization methods have considered a linear titin response for the cellular contribution [14, 172], which may not elicit an isotropic response in muscle, or a response derived through a ratio between the fibre and ECM stiffness to ensure they are of the same order of magnitude [172]. Here the model is developed using a different implementation of the cellular component (brain grey matter), and has resulted in realistic behaviour when compared to skeletal muscle (Fig 3.3). Additionally, when a shear stress was applied to the model, the material is able to capture most typical shear behaviour seen in muscle [158, 172]. At small strains there is a linear relationship and little effect from variations in the base material stiffness. At larger strains, there is more nonlinearity in the shear stress-strain relationship and more effect from the base material properties. This demonstrates the nonlinearity in the base material, and is qualitatively similar to the shear results in other muscle models [172]. The order of magnitude of the shear stress is on the same order of magnitude as that of the normal stress, which agrees with the previous findings [158].

3.6.2 Volumetric and Strain-Energy Effects

Skeletal muscles are often viewed as nearly incompressible materials [1], however, volume changes that may occur have often been within the error of the measurement device [20] and recent studies have reported volume changes for long fatiguing contractions [199]. Therefore, the volumetric properties of the model were manipulated to determine the effects of varying the bulk moduli in nearly incompressible materials. Fig 3.5 demonstrates that variations in the bulk moduli have little effect on the overall stress-strain relationship during passive tests, particularly in the physiological range that muscles typically operate over $\lambda_{\text{muscle}} < 1.1$ [95], which agrees with previous results [121, 55]. This demonstrates that when considering the

mechanical behaviour the model there is little dependence on the bulk moduli assuming it is nearly incompressible. [192] suggested that the isochoric and volumetric components of the strain-energy can play a critical role in understanding muscle mechanics on a three dimensional level. When considering the distribution of the strain energy-densities there is an effect from the bulk moduli of the material. The total potential energy in the system, including the energy from activation and external work on the material, is balanced during the quasi-static simulation ran in this study. As the material became more incompressible, the volumetric strain energy-density decreases counteracting the increase in energy seen in the isochoric component of the total strain-energy. The increases in isochoric strain-energy occured due to increased strain during the passive lengthening phase. These impacts on the energies are likely due to a greater energetic penalty associated with volume change. The isochoric components of the strain energy-density distribution (passive fibre and base material) appear nearly unaffected, which can be explained by the difference in magnitudes of the strain-energy. However, the distribution of the strain energy-densities was impacted by the choice of bulk moduli, which contributed to the energy balance in muscle and the ability to resist volume change. The total contractile force produced by the muscle during the fixed-end contraction was not strongly impacted by the bulk moduli (Table 3.2). The main effect from increasing the bulk moduli was in the decreased ability of the material to change volume.

Investigation of the strain-energy distribution in the muscle model allows for an understanding of muscle behaviour during deformation and contraction. Fig 3.7 shows that as the muscle is pulled to a traction of 1×10^5 Pa there is a strong energy dependence on the stiffness of the material. The results show that there is larger internal energy developed by the material with lower stiffness (2 % ECM), which is expected given that compliant tissue will have a larger strain. Interestingly, there are negative volumetric strain energy-densities that appear during passive lengthening and activation. This is due to the calculation of the strain energy-densities, which are calculated with respect to the initial configuration in which the energy is assumed to be zero for all the components. Therefore, negative values are expected for the balance of the energies. The increasing activation in the muscle had a relatively small impact on the passive fibre and base material energies (Fig 3.7), likely due to the constraints imposed during fixed-length activation restricting movement of the $\pm x$ faces of the geometries. Large variations occur in the volumetric and isochoric energies in Fig 3.7, and are partly due to the difference in bulk moduli of the micro-mechanical components (similarly to Fig 3.6). Although, the stiffness of the material does play a significant role in increasing the variation in energy for varying volume fractions. By investigating the effects of the strain energy-density distributions, an understanding of how the stiffness of the material, which can be altered through the homogenized model, impacts the energy lost or gained through a three dimensional muscle architecture. In this case the increase in stiffness

of the material was shown to increase the volumetric energies and hence reduce the ability of a muscle to deform or bulge during contraction. This in turn gives an understanding of how the combination of the microscopic composition and macroscopic deformation of the muscle impact the distribution of strain energy-densities, which demonstrates the critical role these material properties play in contributing to the force produced by skeletal muscle. The micro-mechanical parameters demonstrated a strong impact on muscle mechanics, while κ_{cell} had a strong effect on the model's ability to change volume, the volume fraction of the ECM, α, was particularly important in altering the strain energy-density distribution.

3.6.3 Applications

Homogenization models are used to analyze the impacts of the variation of micro-mechanical components, and have the ability to investigate the effects from many conditions such as fibrosis. Fibrosis is the increase in collagen content in the muscle as the result of diseases such as cerebral palsy or muscular dystrophies [168, 92]. This model allows for the investigation of these effects by altering the volume fraction of the ECM. Fig 3.7 shows that alterations in the volume fraction of the material have strong effects on the mechanics of the muscle, and further investigation of varying micro-mechanical properties and the impacts on the strain energy-density distribution could provide a deeper understanding of the effects from fibrosis. The stiffness parameter for ECM, s_{ECM}, allows for investigation of effects such as glycination, which is a type of biochemical linkage between a sugar and a protein or lipid. In the process of aging, glycination occurs which increases the stiffness of the ECM [67], and these effects could be further understood through an application of this model. The formulation of forces and energies in the model allows for an analysis of the contribution from each of the homogenized components to the whole muscle mechanics. This ability to analyze the impacts from individual components is not typically found in macroscopic models, but can provide insight into the mechanics of muscles under conditions of varying micro-mechanical properties.

3.7 Conclusion

In this paper we have developed a principled model for muscle base material, which has been designed to easily encorporate available micro-mechanical experimental data from the literature into a macroscopic model. The characteristics of this model were then examined through tension and activation experiments for both normal stress and shear stress experiments. The breakdown of the strain energy-densities associated with passive lengthening and activation were analyzed under the effects of micro-mechanical components, and these components were found to have an effect on the distribution of these energies. This numerical model has the potential for gaining a deeper understanding on the effects of changes to

the tissue micro-structure and composition on the three dimensional mechanics of muscle contraction.

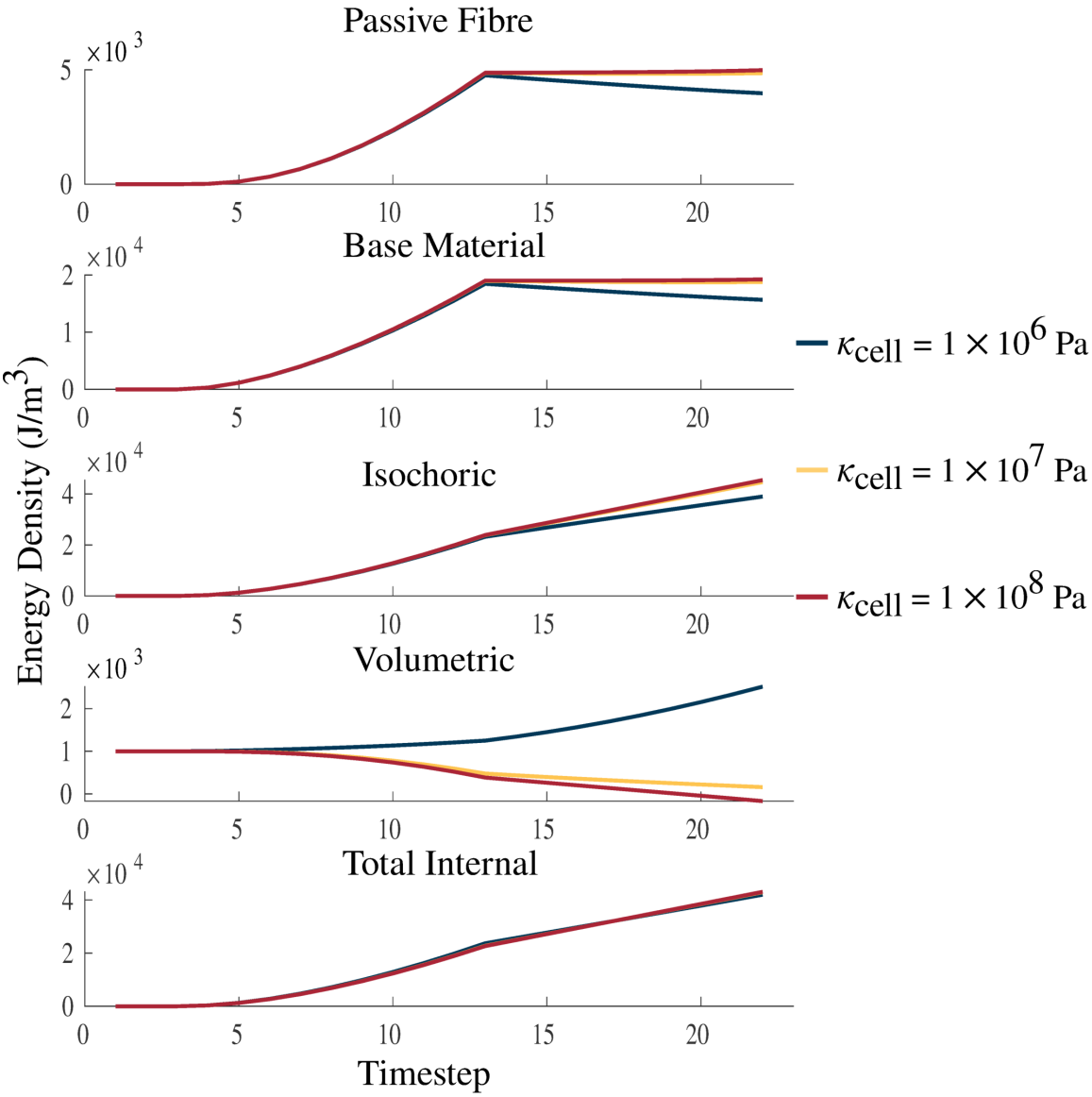

Figure 3.6: Strain energy-density with varying κ_{cell}. Plots of passive fibre, base material, isochoric, volumetric, and total internal strain energy-densities. The energies are plotted over a passive lengthening period, up to a traction of 1×10^5 Pa, from timestep 3 to 13, and a linearly increasing fixed-length activation from timestep 13 to 23. κ_{cell} is varied between values 1×10^6 Pa, 1×10^7 Pa, and 1×10^8 Pa. The larger values of κ_{cell} demonstrate increasing incompressibility and approach the bulk moduli of water (2.15×10^9 Pa [51]), which is considered to be almost completely incompressible. The total internal strain energy-density is the combination of the volumetric, isochoric, and activation (not shown in figure) energies.

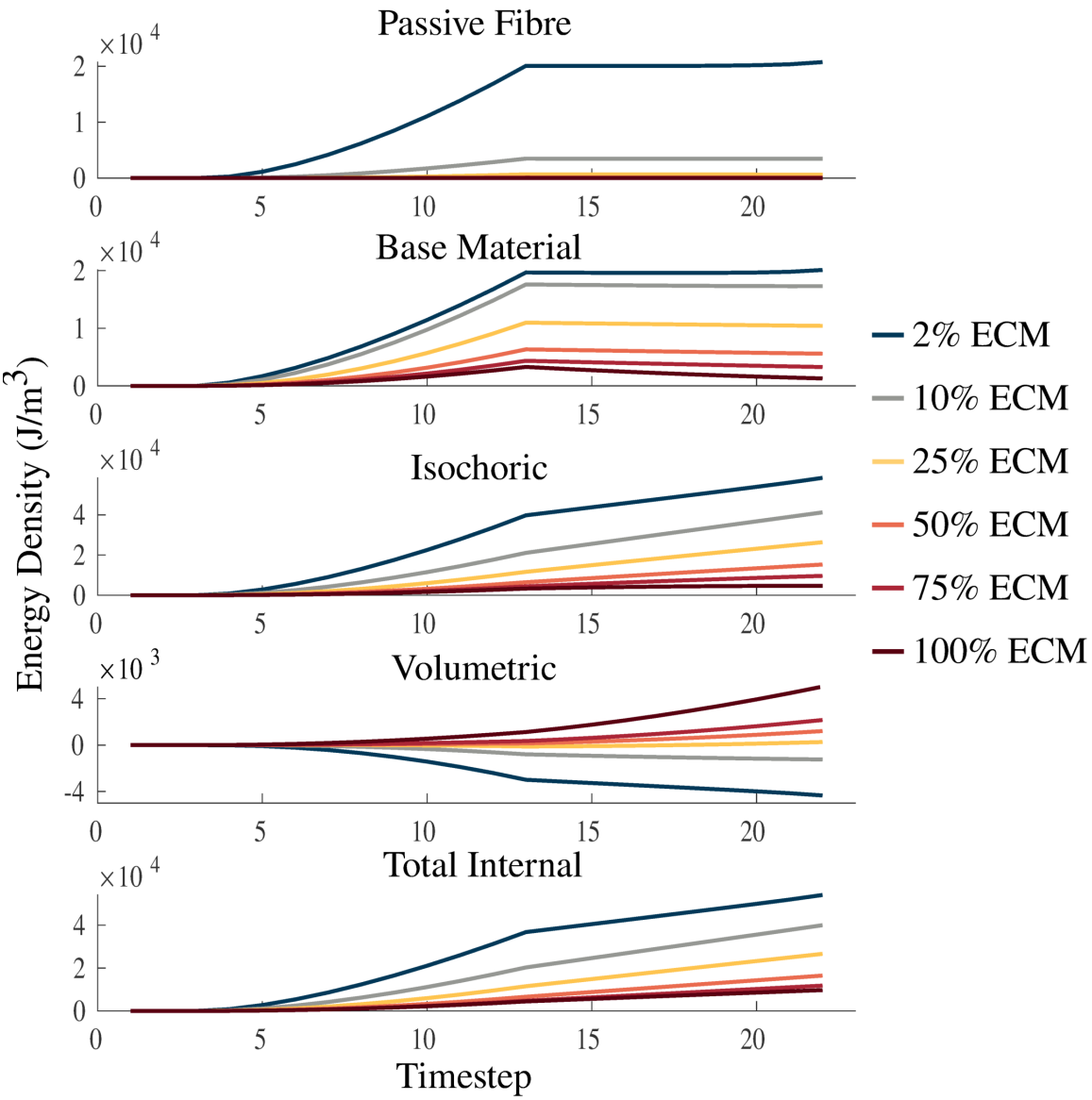

Figure 3.7: Strain energy-density with varying ECM volume fraction. Plots of passive fibre, base material, isochoric, volumetric, and total internal strain energy-densities. The energies are plotted over a passive lengthening period, up to a traction of 1×10^5 Pa, from timestep 3 to 13, and a linearly increasing fixed-length activation from timestep 13 to 23. Volume fractions of the ECM are varied between 2 %, 25 %, 50 %, 75 %, and 100 % to investigate the physics of the model.

Chapter 4

The contributions of extracellular matrix and sarcomere properties to passive muscle stiffness in cerebral palsy

4.1 Abstract

Cerebral palsy results from an upper motor neuron lesion and significantly affects skeletal muscle stiffness. The increased stiffness that occurs is partly a result of changes in the microstructural components of muscle. In particular, alterations in extracellular matrix, sarcomere length, fibre diameter, and fat content have been reported; however, experimental studies have shown wide variability in the degree of alteration. Many studies have reported changes in the extracellular matrix, while others have reported no differences. A consistent finding is increased sarcomere length in cerebral palsy affected muscle. Often many components are altered simultaneously, making it difficult to determine the individual effects on muscle stiffness. In this study, we use a three dimensional modelling approach to isolate individual effects of microstructural alterations typically occurring due to cerebral palsy on whole muscle behaviour; in particular, the effects of extracellular matrix volume fraction, stiffness, and sarcomere length. Causation between the changes to the microstructure and the overall muscle response is difficult to determine experimentally, since components of muscle cannot be manipulated individually; however, utilizing a modelling approach allows greater control over each factor. We find that extracellular matrix volume fraction has the largest effect on whole muscle stiffness and mitigates effects from sarcomere length.

4.2 Introduction

Cerebral palsy (CP) results from an upper motor neuron lesion and has a significant effect on the musculoskeletal system. It develops during early childhood and leads to muscle

alterations including contracture, which is the chronic shortening of a muscle. Contracture results in muscle that cannot be stretched through its typical range of motion due to an increase in stiffness, and this has substantial effects on the ability of muscle to generate force and reduces daily functioning. Typically, this is observed in the upper and lower limb flexor muscles. CP will affect individuals differently, and the changes that can occur will vary depending on the location of the muscle and disease severity [91, 39, 65]. This variability increases the difficulty in quantifying the amount and types of changes that occur as a result of CP. However, despite the variability, alterations in the microstructural properties of skeletal muscle are commonly observed [179], which will have a significant effect on whole muscle behaviour, including force production and movement.

There are many structural differences comparing CP muscle to typically developed (TD) muscle, including changes in fat content [114, 46], extracellular matrix (ECM) stiffness [93, 167], amount of ECM [93, 167], fascicle length [107], fibre diameter [98], fibre geometry [11], and sarcomere length [167, 98, 90]. Experimental studies have investigated CP muscle stiffness *in vivo* and have found stiffer tissue compared to TD muscle using shear wave elastography [86, 24] and through measuring joint movement [10, 184]. However, these methods are unable to capture the underlying causes of this increased stiffness.

The exact microstructural changes that alter whole muscle stiffness have yet to be fully understood, as the extent of measured changes varies between studies [91]. For example, [167] performed passive mechanical experiments on both muscle fibre bundles and single fibres extracted from CP and TD muscle. They found that CP muscle had longer *in vivo* sarcomere lengths and increased fibre bundle, but not fibre, stiffness, which suggests that the changes in muscle stiffness are due to alterations in the ECM. Another study by [98], which used a similar experimental protocol as [167], also showed increased *in vivo* sarcomere lengths. However, the authors demonstrated a difference in the single fibre stiffness and not the fibre bundles, suggesting that there is not a significant effect from the ECM, and that any alterations to passive stiffness occur on the muscle fibre level. [167] performed studies on the Gracilis and Semitendinosus muscles, whereas [98] looked at the Gastrocnemii and the Soleus muscles. [98] mention that the difference in the results is possibly due to the locations of the muscles or different mechanical properties of ECM between TD and CP muscle. Another possible explanation for the differences between the two studies is the that the TD groups in the study by [98] had a much older average age (47.7 ± 15.3) compared to [167] (15.8 ± 1.8). Other studies have reported that CP muscle has a greater accumulation of fibrotic tissue, and potentially even results in an ECM with a larger volume fraction but compromised stiffness [93]. Additionally, [22] suggested that collagen plays a role in the increased muscle stiffness that is observed in CP. However, it has been observed that fibrosis does not always alter the stiffness of muscle [165], and so there may be an effect from the stiffness and structure of the ECM. In TD muscle the ECM has been shown to be a major contributor to passive whole muscle mechanics due its composition of stiff collagen fibres

[60, 105]. In particular, work has shown that in mammalian muscle, the ECM is responsible for about half of load bearing in passive tension [105]. Sarcomere length is a commonly observed alteration in CP muscle, and has been said to have a large effect on active muscle mechanics [90, 167, 100]. While many changes have been observed in CP muscle, the changes that are most common between studies are changes in ECM volume fraction, ECM stiffness, and sarcomere length. However, the individual roles of the ECM properties and sarcomere length in passive whole muscle stiffness have yet to be fully understood.

The purpose of this study was to determine which microstructural change occurring with CP has the largest contribution to whole muscle stiffness. In particular, whether the ECM, through changes in volume fraction or stiffness, or the sarcomere, through increases in length that result in an increased passive response from the titin, will have the greatest influence on passive whole muscle behaviour. During experimental studies, it is not possible to change a component of muscle, while keeping all other components constant; therefore, causation cannot be determined. This is especially difficult in CP where many components of muscle are known to vary between individuals [91, 179]. In this study, we try not to determine the cause of changes to the microstructure, but the relationship between changes to the microstucture and the overall muscle stiffness. Using a modelling approach, we investigated the influence of the microstructural components on passive muscle stiffness. We utilized a three dimensional continuum model of skeletal muscle, developed in previous studies [192, 129, 144, 82], which can be modified to incorporate the effects of ECM and passive fibre properties on whole muscle mechanics. Here we do not explicitly model the process of contracture, but instead the resulting changes to the microstructure. Any mechanical response we observe in this study will also be relevant to muscle without clear contracture, but with similar changes to the material properties. By modifying the material properties in the muscle, we investigated changes that occur with CP to understand how each component contributes to whole muscle stiffness.

4.3 Methods

4.3.1 Computational Model

In this study, we utilized a continuum mechanical model of muscle as a fibre-reinforced composite biomaterial. The model uses a three field formulation in terms of the velocity, $\mathbf{u}$, pressure, p, and dilation, J, and the balance of strain-energy potentials based on work by [160] and [195]. In particular, we want to minimize the total strain-energy

$$E_{\text{tot}}(\mathbf{u}, p, J) = U_{\text{int}}(\mathbf{u}, p, J) - W_{\text{ext}}(\mathbf{u}), \tag{4.1}$$

where U_{int} is the internal strain-energy potential and W_{ext} is the total external work done on the muscle. We characterized the passive mechanical behaviour of muscle in terms of its

stress-strain behaviour, which is the relationship between the stress applied to the muscle and the strain experienced. Here we use the full Cauchy stress tensors, so the shear stress response is built into this tensor implicitly and has been investigated in [82]. The relationship between the stress in the material, σ, and the strain-energy potential of a material, U, is given by the constitutive law

$$\sigma = 2J^{-1}\mathbf{B}\frac{\partial U(\mathbf{B})}{\partial \mathbf{B}}, \tag{4.2}$$

where $\mathbf{B}$ is a strain tensor measuring the deformation. To capture muscle, we split the model into a three dimensional isotropic base material with one dimensional fibres running along the length of the muscle, making the composite material anisotropic. The total stress response from the muscle (σ_{muscle}) is then additive contributions from the base material (σ_{base}) and fibre (σ_{fibre}) components

$$\sigma_{\text{muscle}} = \sigma_{\text{fibre}} + \sigma_{\text{base}}. \tag{4.3}$$

Our model is a homogenized muscle material that included contributions from the fibres and base material at every element in the mesh. A more precise formulation of the model is described in the appendix of [192] and in [82]. We used a finite element method to solve the continuum model that was implemented using an open source finite element library deal.II [6].

There are two main components of our muscle model: the fibre components and the three base material. The base material encompasses effects from extracellular matrix and cellular components, including satellite cells and capillaries, while the fibre component runs along the length of the muscle and contains the passive effects from titin and active effects from the contractile elements. To investigate the role of CP on whole muscle stiffness, considering the individual effects from the ECM and cellular components is necessary. To do this, we let α be the volume fraction of the ECM, which includes effects from the collagen fibre matrix (Figure 4.1). Meanwhile, $1-\alpha$ is the volume fraction of the cellular component, which includes effects from any other material in the muscle aside from the contractile units. In particular the cellular material includes the myofibres, satellite cells, and other cellular materials. We also introduced a parameter s_{ECM} (Figure 4.1), which is a stiffness factor multiplying the stiffness of ECM. A larger s_{ECM} corresponds to a stiffer ECM, which can occur as a result of structural changes while the ECM volume fraction remains the same [59]. Meanwhile, a smaller value of s_{ECM} results in an ECM with decreased stiffness, which can occur as a result of an ECM with compromised structure [93]. The total stress response from the base material is a homogenization of the ECM and cellular components given by

$$\sigma_{\text{base}}(\mathbf{B}) = \alpha s_{\text{ECM}}\sigma_{\text{ECM}}(\mathbf{B}) + (1-\alpha)\sigma_{\text{CELL}}(\mathbf{B}). \tag{4.4}$$

$\sigma_{\text{ECM}}(\mathbf{B})$ corresponds to the stress response from the ECM, while $\sigma_{\text{CELL}}(\mathbf{B})$ is the stress response from the cellular component. To ensure the volume of the muscle remains nearly constant, the bulk modulus for the cellular component is chosen to be 1×10^7 Pa, while the bulk modulus of the ECM component was set to 1×10^6 Pa [82]. While the cellular component of the muscle contributes less to the overall stress response, it consists largely of water, so its bulk modulus is set to be larger than the ECM component. The exact form of the stress-strain response for the microstructural components are given in [82] along with more detail on the homogenized base material.

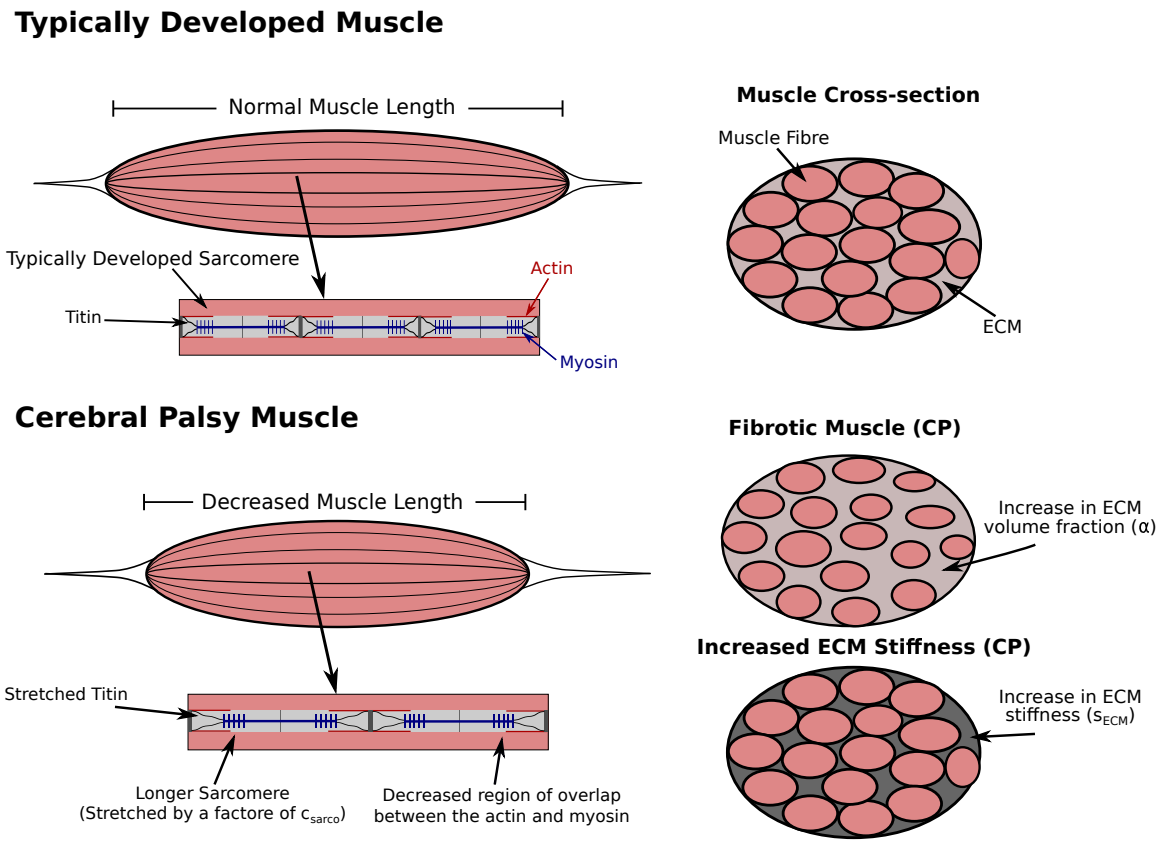

Figure 4.1: Comparison of typically developed (TD) and cerebral palsy (CP) muscle. CP results in contracture, which is the chronic shortening of muscle, decreasing muscle length relative to TD muscle (not investigated in this study). Longer sarcomere lengths relative to the rest of the muscle have also been observed compared to TD muscle [167, 100]. There is an increase in passive forces due to the increased stretch in the titin proteins. The longer sarcomeres lengths in muscle affected by CP reduces the regions of overlap of the actin and myosin filaments, which results in decreased contractile forces. Additionally, there is an increase in extracellular matrix (ECM) volume fraction, and a possible increase or decrease in ECM stiffness. Any combination of changes to the sarcomere length or ECM properties could occur with CP.

The other alteration typically observed in CP is an increase in *in vivo* sarcomere length [167, 100], which alters the passive muscle stiffness by stretching the titin protein. Experi-

mentally, the sarcomere lengths for muscles in the lower extremities were measured with 90 degrees hip and knee flexion [98, 167], and with the ankle in full dorsiflexion for the lower leg muscles [98]. Our model does not have a joint angle, and so we define the *in vivo* length of the sarcomeres to be the length of the sarcomeres when the whole muscle is at its resting length. This change in length also decreases the contractile force produced when the muscle is active by reducing the number of attached actin-myosin crossbridges (Figure 4.1). We modelled this using a dimensionless parameter, c_{sarco}, which corresponds to a shift in the passive force-length curve of the sarcomeres

$$\sigma_{\text{fibre}} = \sigma_{\text{fibre}}(\overline{\lambda}_{\text{tot}} + c_{\text{sarco}}), \tag{4.5}$$

where $\overline{\lambda}_{\text{tot}}$ is the total average stretch of the fibres over the muscle volume. This parameter acts as an additive contribution to the intrinsic stress-stretch relationship, resulting in larger stresses in the fibres at a given stretch (Figure 4.2). It is important to note that, while the fibre component of the muscle depends on c_{sarco}, the intrinsic stress response from the base material, $\sigma_{\text{base}}(\mathbf{B})$, only depends on the deformation and stretch of the muscle, and not c_{sarco}. At a value of $c_{\text{sarco}} = 0.0$, the behaviour of the sarcomere is the same as that of TD muscle. Increasing values of c_{sarco} results in longer lengths of the sarcomeres given by

$$l_{\text{sarco}} = l_0(\overline{\lambda}_{\text{tot}} + c_{\text{sarco}}), \tag{4.6}$$

where l_{sarco} is the new length of the sarcomere and we assume $l_0 = 2.2\mu$m is the optimal length of a sarcomere [27]. This will vary depending on the value of c_{sarco}. The fibres in the model are based off the one dimensional Hill type model [72, 203] and are described in [192]. It is possible the behaviour of the fibre will vary in more than a shift of its force-length curve, such as a different force-length relationship, which may be due to factors in the myofibres other than the sarcomeres. However, as this is not observed frequently and data are limited, we focus on the effects from the sarcomere length.

4.3.2 Whole Muscle Experiments

To investigate the passive effects of α, s_{ECM}, and c_{sarco} on skeletal muscle, we constructed a rectangular block of muscle with dimensions 3cm $\times$ 1cm $\times$ 1cm. These dimensions, while not the same as muscle affected by CP, sufficiently capture the behaviour of muscle on a macroscopic scale. Using a block geometry reduces the need to consider the additional effects from architecture, aponeurosis, and pennation angle, which affects muscle behaviour [192], and instead allowed us to isolate the effects due to CP independent of a specific architecture. Additionally, this geometry has been previously validated to capture the general qualitative behaviour of muscle when compared to the mechanics within a MRI derived whole muscle geometry [192] and has the benefit of computational simplicity. To compare the passive behaviour of the model to experimental data, we performed stress-strain tests. This involved

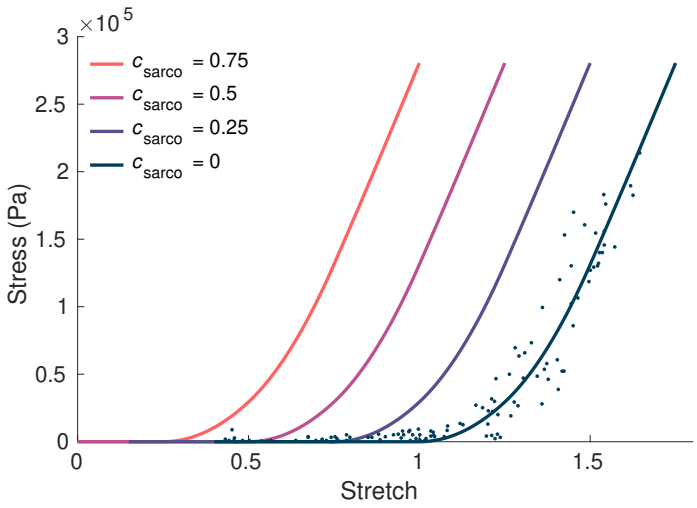

Figure 4.2: The influence of c_{sarco} on the intrinsic fibre stress-stretch relationship. Here we plot the stress from the fibre component of our model against the stretch in the fibres. The curve corresponding to typically developed muscle ($c_{\text{sarco}} = 0$) was obtained based on curves and data in [145]. This was done through trigonometric polynomial and second-order piecewise polynomial fits to experimental data from [200] (denoted by the dots).

constraining one end face of the model from movement in all directions, while a normal stress was applied to the opposite face stretching the muscle. In addition to the stress-strain tests, we investigated the stiffness of the muscle to compare with experimental studies (eg. [167, 100]). α, s_{ECM}, and c_{sarco} each have an individual contribution to the overall stiffness of muscle. To investigate the stiffness in the model, the modulus (in Pa) of the muscle material was calculated during the stress-strain experiments using the slope of the tangent line to the overall stress-stretch relationship. This was done by performing a nonlinear least-squares fit of a cubic polynomial to the overall stress-strain data in the longitudinal direction. This method for calculating the modulus is only representative of the stiffness at the given stretch value, since the stress-stretch curves are nonlinear; however, we do this to compare with experimental studies.

TD muscle has been observed to have a value for α between 0.02-0.10 [13], while larger volume fractions ($\alpha \approx 0.6$) have been observed for fibrotic tissue [93, 165]. Experimental studies have only found an increase in *in vivo* sarcomere lengths [167, 98, 90], so we varied c_{sarco} from 0 to 0.75. This corresponded to a 0-75 % increase in the sarcomeres relative to the sarcomeres in typically developed muscle, which has been observed in the literature [90, 100, 167]. Experiments are often performed on severe cases of CP, so larger sarcomere lengths have been reported ($c_{\text{sarco}} > 0.75$); however, in this study, we considered less severely stretched sarcomeres to represent less severe cases of CP. It is possible that muscle altered by CP does not always have such a substantial increase in sarcomere length, since measurements are typically taken from children with severe CP undergoing surgery

[91]. The final parameter that was manipulated in the model is s_{ECM}. While the stiffness of muscle can vary depending on the type of muscle, the properties of the base material, including the effects from the ECM, represent and have been validated for TD muscle [82], so we set $s_{\text{ECM}} = 1$ for TD muscle (this corresponds to a value of 150 in [82]). During our stress-strain tests, we then considered the possibility of the ECM component of muscle being stiffer ($s_{\text{ECM}} = 1.33$) and less stiff ($s_{\text{ECM}} = 0.66$). Note that a s_{ECM} value of 1.33 corresponds to a stiffness of 133 % compared to TD muscle, while a value 0.66 corresponds to a stiffness of 66 % relative to TD muscle. Data for the changes in stiffness of the ECM are not available experimentally, so these values of s_{ECM} were chosen to investigate the effects of altering this component. In summary, to investigate the effects of CP, our parameter ranges were $\alpha = 0.02$ to 0.6, $c_{\text{sarco}} = 0.0$ to 0.75, and $s_{\text{ECM}} = 0.66$ to 1.33, while TD muscle had parameters $\alpha = 0.05$, $c_{\text{sarco}} = 0.0$, and $s_{\text{ECM}} = 1.0$.

4.4 Results

4.4.1 Effects of c_{sarco}

For TD muscle ($c_{\text{sarco}} = 0.0$, $s_{\text{ECM}} = 1.0$, and $\alpha = 0.05$), we observed typical overall stress-stretch behaviour for passive skeletal muscle: as the stress increased, the muscle stretch and sarcomere lengths also increased (Figure 4.3). The muscle block in its resting and stretched states is shown in Figure 4.3 C and D, respectively. The shift in the intrinsic passive sarcomere stress-stretch relationship, c_{sarco}, affected the muscle behaviour in both the stress-length for the sarcomeres and overall stress-stretch for the whole muscle relationships of the model (Figure 4.3). At *in vivo* lengths, we found that there is no longer zero stress for $c_{\text{sarco}} > 0.0$ (Figure 4.3 A). This indicates that larger forces are required to stretch muscles with increased sarcomere lengths, as well as to hold it at the resting length of the muscle. We also see that there is a nonlinear relationship between the effect of c_{sarco} on the fibre component (Figure 4.2) and the overall muscle response which is influenced by the base material (Figure 3). Additionally, optimal length of the sarcomeres no longer occurred at the same resting length of the whole muscle. For the same range of stress values (0-3 $\times 10^5$ Pa), we saw a larger range of whole muscle stretches with larger c_{sarco} (Figure 4.3). This is likely due to effects from the base material and, therefore, the ECM, which acts to deform the muscle back to optimal length. At stretch values less than 1.0, the base material works to extend the muscle to optimal length, while the sarcomeres are still working to shorten the muscle for $c_{\text{sarco}} > 0.0$.

In addition to the behaviour in the along-fibre direction of the muscle, c_{sarco} also affects the behaviour transverse to the muscle fibres (Figure 4.4). We observed a similar change in concavity of the stress-stretch curves in both the stress-stretch relationships in the longitudinal (Figure 4.3 B) and transverse (Figure 4.4) directions. This demonstrates similar effects from the muscle ECM component in both directions. For stretch values in the y

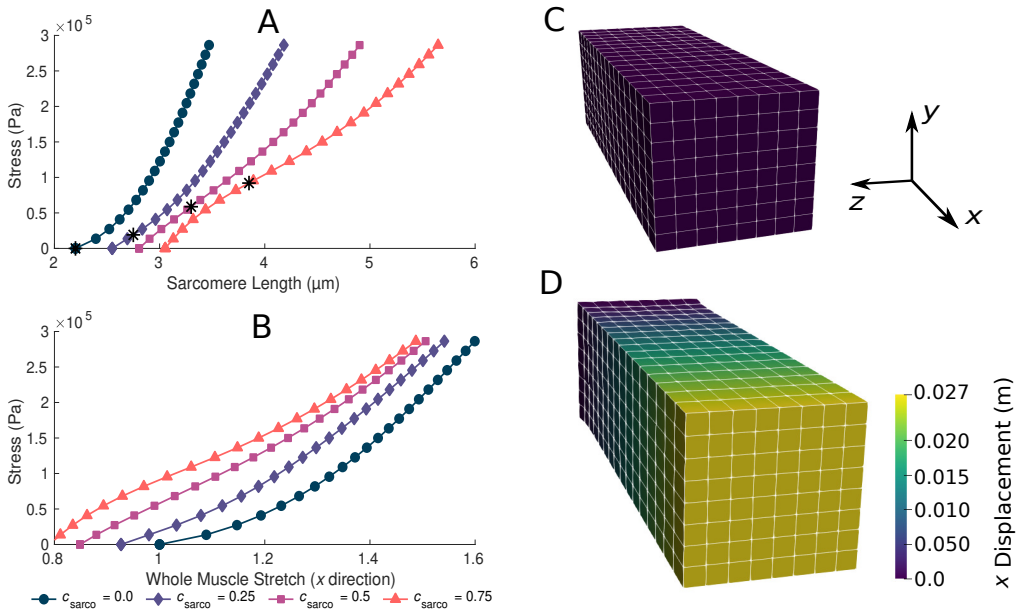

Figure 4.3: Plots of whole muscle stress in the along fibre direction against sarcomere length (A) and whole muscle stretch (B). Plots are from the computational model during passive lengthening with ECM volume fraction, α, of 0.05 and ECM stiffness factor, s_{ECM}, of 1.0. Each curve represents a shift in the sarcomere stretch by a factor of c_{sarco}. $*$ represents *in vivo* sarcomere length for corresponding c_{sarco}. C and D show the mesh at resting length and at a deformed state after the stress has been applied to the model.

direction less than 0.85, the influence of the sarcomeres on the stress-stretch relationship decreased, and there was larger influence from the ECM. For smaller normal stresses in the longitudinal directions, there were larger effects from sarcomere length relative to larger stresses (Figure 4.4). The sarcomeres, acting only in the along-fibre direction, altered three dimensional deformation, which could effect muscle force production [192].

4.4.2 Effects of α and s_{ECM}

The ECM properties also had a substantial effect on the overall stress-stretch relationships (Figure 4.5). Given the range of possible values for the ECM volume fraction, α, (0.02-0.6), it had a larger effect on the muscle stiffness compared to the ECM stiffness parameter, s_{ECM}. As s_{ECM} was increased, with fixed $\alpha = 0.05$ or 0.6, the overall stress-stretch relationship became more linear and covered a smaller range of stretch values (Figure 4.5). Increases in both α and s_{ECM} reduced the effect from the sarcomere length on the stress-stretch relationship (Figure 4.5). Due to the lack of available data for the stiffness of the ECM, the s_{ECM} was only varied between 0.66 and 1.33, which is a relatively small range compared to the volume fraction of the ECM. Similar effects were observed from changing s_{ECM} and α, but α had more effect on the overall stress-stretch behaviour. This is expected given the

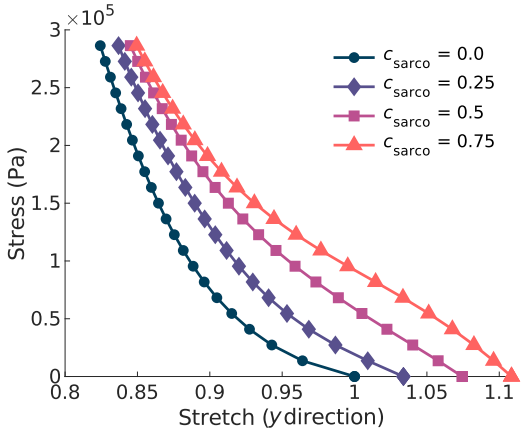

Figure 4.4: Plot of the normal stress applied in the along-fibre direction (x) against the stretch in the muscle transverse to the fibres. Given the symmetry in the muscle geometry transverse to the fibres (y), the stress-stretch response shown is the same in the z direction. Each line represents a shift in the sarcomere stretch by a factor of c_{sarco}.

change in composition of the base material; however, due to the limited data for s_{ECM}, it is possible that real muscle has a larger range of values than investigated in this study, but to ensure that we remain within realistic physiological ranges we chose this limited range. Our results showed that s_{ECM} had very little effect on the overall stress-stress relationship for smaller values of α and it has the most effect when α is large. The main effects from the s_{ECM} are in altering the influence of c_{sarco} on the overall muscle stress-stretch relationship (Figure 4.5). Varying s_{ECM} over a larger range of values would likely only influence the effect of the sarcomere length on the overall stress-stretch response.

4.4.3 Muscle Stiffness

As c_{sarco} was increased up to a value of 0.5, the modulus of the muscle in the x direction increased at optimal length of the muscle (Figure 4.6 A,B). However, after a value of 0.5, the muscle modulus decreased, and this was observed when looking at the variations in c_{sarco} with constant α and s_{ECM} (Figure 4.6 A,B). The modulus at optimal length was dominated by α. For changes in c_{sarco} and s_{ECM}, the change in modulus (at most 4×10^5 Pa) was less than the possible variation in modulus with changes in α (up to 15×10^5 Pa for highly fibrotic tissue). While holding c_{sarco} constant, we found a linear increase in the modulus when increasing α and s_{ECM} (Figure 4.6 C,D).

While holding c_{sarco} constant, there was a larger effect from volume fraction of the ECM, α, than the stiffness of the ECM, s_{ECM}, on the overall muscle stiffness (Figure 4.7 A,B). However, as α was increased, there was a greater effect of s_{ECM}. The nonlinear behaviour, which showed increasing muscle modulus with increasing α and s_{ECM} was more pronounced at larger stretches (Figure 4.7 B,D). At a stretch of 1.20 in the x direction, the stiffness appeared to be more nonlinear when moving along the lines of constant s_{ECM} and when

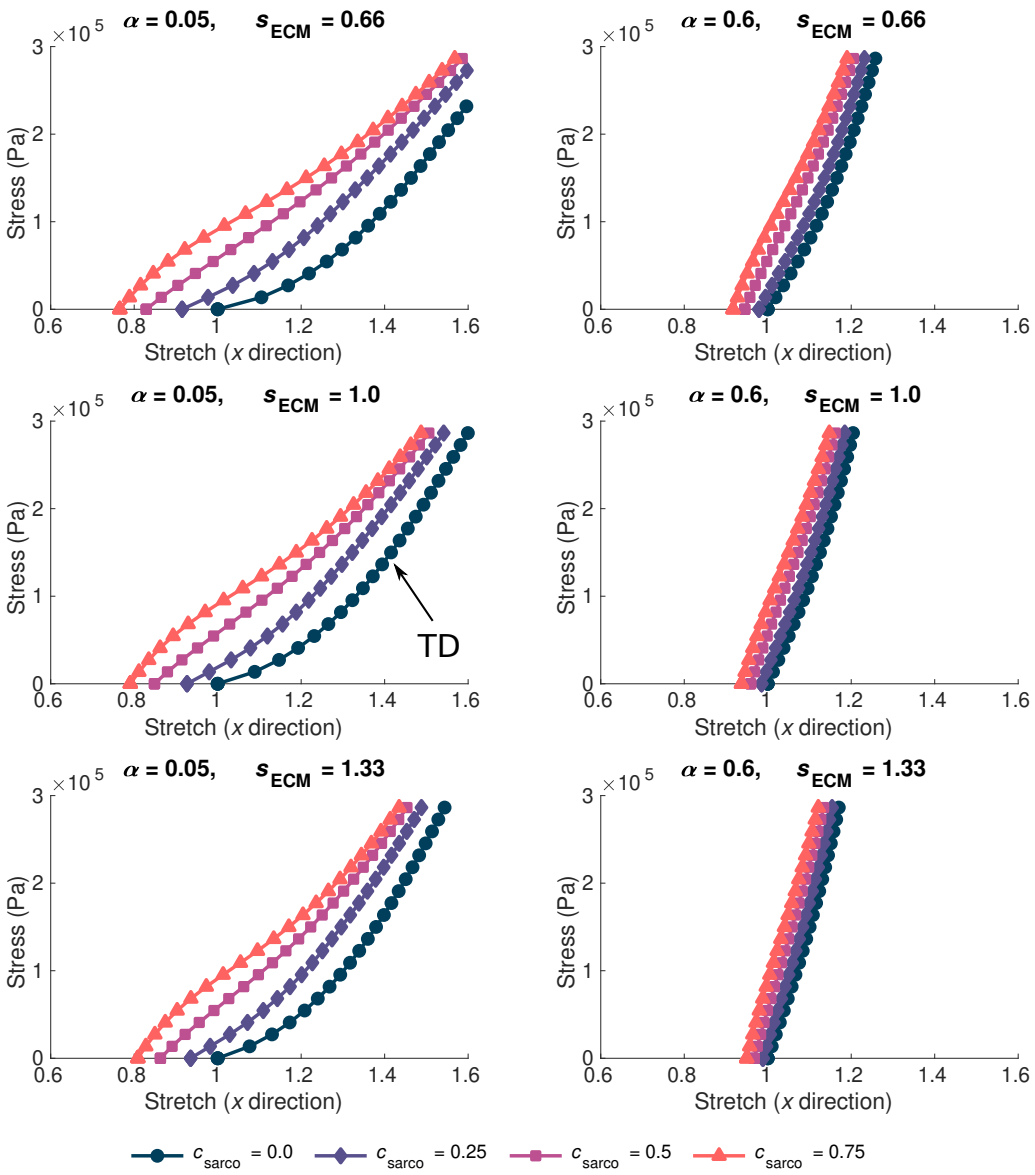

Figure 4.5: Stress-stretch plot during passive lengthening of the muscle model for various values of ECM volume fraction, α, and stiffness, s_{ECM}. The traction was linearly increased on the $+x$ face of the muscle to 3×10^5 Pa, while the $-x$ face was constrained in all directions. Individual lines on each plot represent a shift in sarcomere stretch by c_{sarco}. Typically developed (TD) muscle has values of $\alpha = 0.05$, $s_{\text{ECM}} = 1.0$, and $c_{\text{sarco}} = 0.0$, while cerebral palsy muscle could have a combination of $\alpha > 0.1$, $s_{\text{ECM}} = 0.66$ or 1.33, and $c_{\text{sarco}} > 0$.

moving along the lines of constant α for $\alpha > 0.2$ (Figure 4.7 C,D). When holding s_{ECM} constant, there was a larger effect α on the modulus of the muscle compared to c_{sarco}, particularly at larger stretch values (Figure 4.7 C,D). As the stretch increased there was an increase in modulus from the ECM parameters; however, there was a decrease in the effects

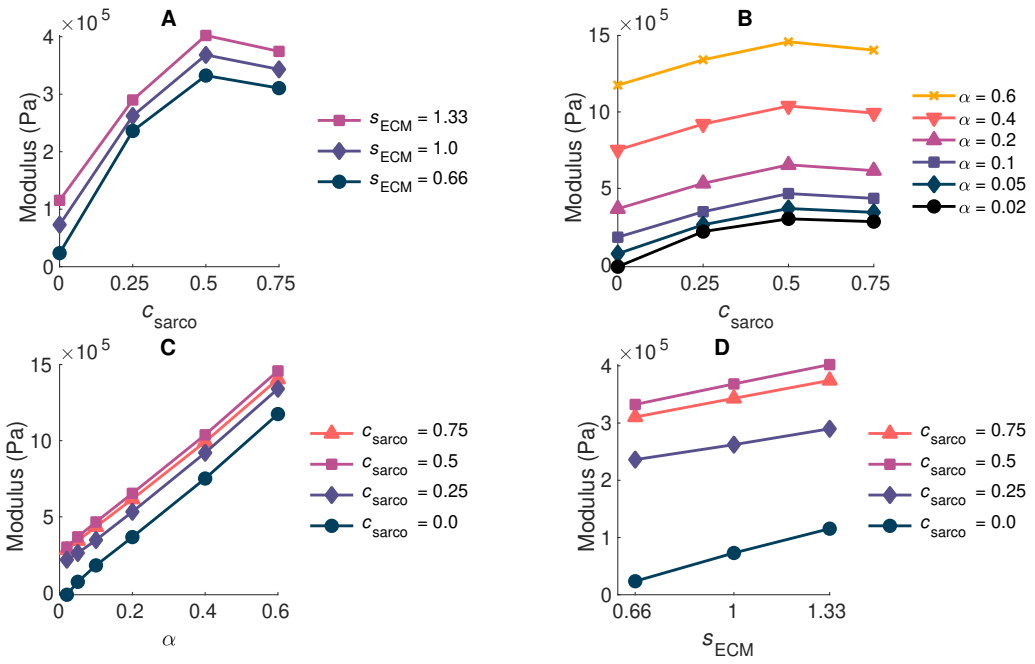

Figure 4.6: Plot of whole muscle modulus vs. c_{sarco} (A,B), α (C), and s_{ECM} (D) at optimal length ($\bar{\lambda}_{\text{tot}} = 1.0$). Where α is the ECM volume fraction, s_{ECM} is the ECM stiffness factor, and c_{sarco} is the shift in the sarcomere stretch. In plots A,D α is held constant at 0.05, and in plots B,C s_{ECM} is held constant at 1.0.

of c_{sarco} (Figure 4.7 E and F). The reduced influence of c_{sarco} was due to more pronounced behaviour from the base material at larger stretches (Figures 4.5 and 4.7).

4.5 Discussion

In CP, alterations occur on the microstructural level that can influence whole muscle stiffness and reduce function. In particular, alterations to ECM properties and sarcomere length can occur; however, their relative contributions to muscle stiffness in CP is unknown. Isolating individual effects on passive muscle stiffness is difficult to do in experimental studies as there is large variability between subjects and individual muscles [108, 28, 177]. Therefore, to determine whether the ECM properties or sarcomere lengths have more effect on the passive muscle behaviour, we used a three dimensional continuum model [129, 192, 144, 82]. This model does not actually develop joint contractures; however, it allows us to isolate the effects from individual microscopic components, and investigate the relative contributions to whole muscle function.

4.5.1 Physiological Changes to Muscle During Cerebral Palsy

The ECM is composed of a highly structured arrangement of collagen fibres and plays a substantial role in skeletal muscle mechanics [61]. In this study, we investigated the effects

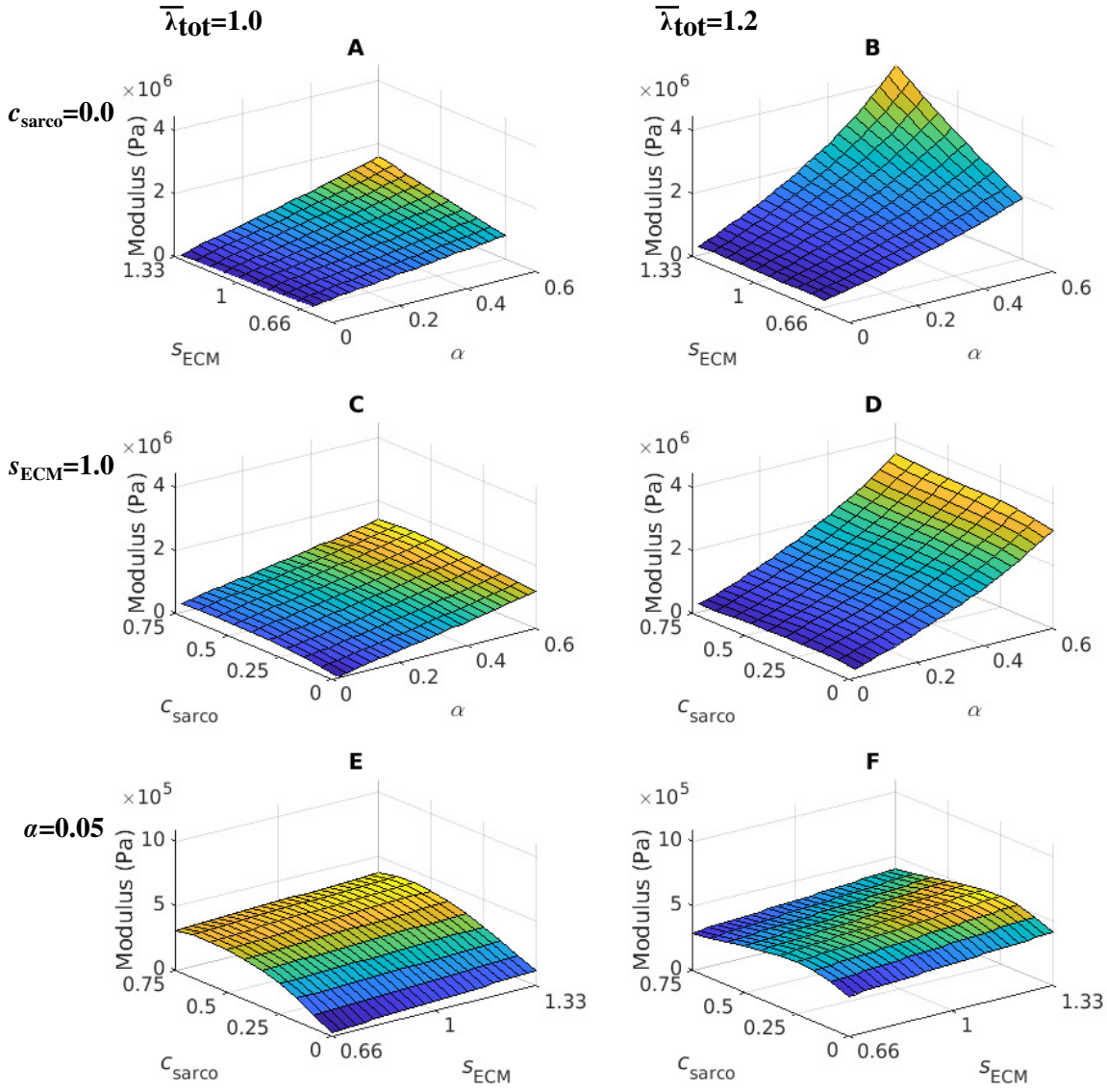

Figure 4.7: Surface plot of the whole muscle modulus at an average muscle stretch, $\overline{\lambda}_{\text{tot}}$, of 1.0 (A,C,E) and 1.2 (B,D,F). The ECM stiffness factor, s_{ECM}, was varied between values of 0.66 and 1.33; ECM volume fraction, α, from 0.02 to 0.6; and shift in sarcomere stretch, c_{sarco}, from 0.0 to 0.75. Modulus values were extracted from passive lengthening simulations with $c_{\text{sarco}} = 0.0$ in A,B; $s_{\text{ECM}} = 1.0$ in C,D; and $\alpha = 0.05$ in E,F.

of changes to ECM volume fraction and stiffness on the whole muscle stiffness. Changes in ECM volume fraction have been observed in previous studies, particularly as a result of fibrosis (eg. [167]). This corresponds to an increase in ECM material, while the contributions from the cellular components in muscle, such as the contractile fibres and other cells, decreases. In addition, fibrosis creates a physical barrier that can impact muscle regeneration [34], which will reduce the ability for muscle to grow and add sarcomeres in the

muscle fibres, further decreasing the compliance of the muscle. Additionally, it is possible that while the volume fraction stays constant, changes in the structure or composition of collagen types varies. However, studies have found that the ratio of collagen isoforms is the same in both TD and CP muscle [166], and so it is unlikely that a difference in collagen isoforms in muscle accounts for the increase in whole muscle stiffness with CP. It is possible that there are alterations in ECM structure, such as the organization of collagen fibres, that occur with CP [93], and this could increase or decrease ECM stiffness depending on the change. Therefore, both effects were considered in the model to investigate the relative contributions to stiffness on a whole muscle level.

It has also been well documented that increases in the sarcomere length occur with CP [91, 179]. Stiffness changes have been reported on the fibre level by looking at the stress-strain relationship for TD and CP muscle fibres [98]. It is possible that these effects are not only a result of increased sarcomere lengths, but due to different titin isoforms, as they could result in a different stress-strain relationship for the individual sarcomeres [123]. However, [167] found that there is no change in the composition of titin isoforms between TD and CP muscle. Therefore, changes in stiffness due to the sarcomeres are not likely due to changes in titin isoforms. While it is possible that an increased stretch of the titin is responsible for the increased passive stiffness of the fibres, this could also be a result of changes to other mechanical properties in the myofibres. More investigation is required to confirm the main cause of the increased stiffness at a fibre level.

4.5.2 Microstructural Contributions to Whole Muscle behaviour

It has been demonstrated experimentally that the ECM has a significant contribution to muscle passive stiffness [61], and that fibrosis has been observed in CP [93]. We found that the volume fraction of the ECM had a larger influence on whole muscle stiffness compared to ECM stiffness and sarcomere length. The contribution from the ECM increased as stretch increased (Figure 4.7), demonstrating a nonlinear relationship between the ECM volume fraction and muscle stretch. At larger stretch values, the ECM contributes more to the whole muscle stiffness; these nonlinear effects imply that fibrosis will substantially reduce the ability of a muscle to deform at larger stretch values. The ECM is composed of crimped collagen fibres, which likely do not contribute as much to the stress initially [61], and this is reflected in a smaller effect from the ECM volume fraction at optimal length. Currently, experimental data for the variation in stiffness of the ECM due to structural changes are not available; however, in the ranges tested in this study, the stiffness of the ECM did not alter whole muscle stiffness as much as the volume fraction. At larger volume fractions of the ECM there was a more substantial contribution from the ECM stiffness (Figure 4.7 B), and since larger volume fractions are typically seen in CP, this could play a larger role.

The contribution of the sarcomere length to whole muscle stiffness varied depending on the ECM properties. There was minimal effect of the sarcomeres on the passive stiffness in

the fibrotic tissue (Figure 4.6), which corresponds to volume fractions of ECM greater than 10 %, and this larger effect from the ECM has been observed during experiments [167]. Furthermore, the sarcomere effects are mitigated at larger stretches as the ECM begins to dominate the muscle stiffness. At whole muscle stretches near 1.0, we found a larger effect of sarcomere length (Figure 4.6), which agrees with the results from [98] for fibre bundles. The work by [98] indicates that there was no increase in the stiffness of the ECM during CP in the muscles investigated. They found that there was no difference in the stiffness of fibre bundles at larger stretches, which could be explained by the dominating behaviour of the ECM. This agrees with our findings that demonstrate that if a muscle is operating near optimal length, then there might be a noticeable effect of sarcomere length. However, if the muscle has a larger range of motion, then the ECM would likely have a larger contribution to muscle passive stiffness. It is likely that the lengthening of the sarcomeres during CP has a larger effect on the active properties of the muscle (which we have not evaluated in this study) compared to the passive properties as noted by [91].

Using this model we can obtain a deeper understanding of the three-dimensional effects that occur in muscle altered by CP. As shown in previous modelling [192, 148] and experimental studies [132], the ability of a muscle to deform both in the along and transverse fibre directions can alter muscle function. Additionally, our results agree with experimental evidence that the whole muscle response is not the same as the response from individual fibres [194]. In our model, the three-dimensional behaviour is captured in part by the base material, which works to return the muscle to its original state. At longer muscle lengths, the base material will work in the same direction as the sarcomeres, which are trying to shorten the muscle. Meanwhile, when the whole muscle stretch is less than one, the ECM will be working to return the muscle back to the original muscle length. We have observed in the model that the stiffness of the muscle decreases after sarcomere lengths greater than 3.3 μm (Figure 4.6), and this is due to the three dimensional behaviour of the model we are using. In a one dimensional model, there are no effects from the volume conserving nature of the base material or other effects transverse to the fibres. This is a nearly incompressible and nonlinear model, and so the effects from the volumetric component of the model contribute more with larger shifts in the sarcomere force-length curve. While these effects have been observed based on our assumptions for the model (see [192] and [82]), which are typical of many finite element models [15, 158, 172], these effects have not been reported experimentally. Experimentally, the decrease in muscle stiffness may not be as substantial as the changes observed in this study; however it is likely a similar trend would appear. Another important consequence of the three-dimensional behaviour is that changes occurring strictly in the along-fibre direction, such as changes in the sarcomere length, affect the stretch transverse to the fibres (Figure 4.4). In particular, the bulging and stretching in the transverse direction is decreased by increased *in vivo* sarcomere lengths, which increases the passive stiffness of the muscle fibres. Given this reduced movement in the transverse direction, it is

likely that there would be a decreased contractile force produced given the significant effect of three dimensional deformation [148]. This demonstrates that to accurately capture all of the effects from CP, investigating three dimensional behaviour is required to completely understand the mechanical behaviour of the muscle.

4.5.3 Model Parameters

Experimental studies are key to understanding the mechanical changes that occur with CP; however, many of the procedures are invasive and unable to determine the exact role each change due to CP plays in altering muscle stiffness [91, 167, 179]. Additionally, there is contradicting data as to whether fibres, ECM, or both have a substantial contribution to passive stiffness [167, 98], which likely depends on the severity of the disease [179]. There are less invasive procedures that have been developed to investigate the relationship between muscle stiffness and CP [86]; however, they are still unable to isolate the role of individual factors. For example, experimental studies have found that stiffness of CP muscle is twice as high as TD muscle [190]; however, they were not able to determine which microstructural changes led to this increase in stiffness. While this model cannot directly determine which microstructural changes will cause this experimental increase in stiffness, it can provide insight into how various changes on the microscopic level could lead to these effects on muscle stiffness. We have observed that there is approximately double the increase in stiffness when the volume fraction of ECM in our model increases from 5 % to 20 %. Another possible way to achieve this increase in muscle stiffness is through increasing the stiffness of the ECM, or some combination of the two. The possible changes that cause increased stiffness can be investigated through our modelling approach and can indicate which factors may have the most impact on muscle behaviour. It is difficult to perform experimental tests on whole muscles affected by CP, although tests have been done on mice with spasticity or fibrosis [165, 204], as muscle can only be dissected during surgery making it difficult to obtain data for an accurate comparison to similar TD muscle tissue. Muscle is a three-dimensional material, so applying a continuum model to CP muscle allows us to understand the underlying muscle mechanics. In particular, developing an understanding of the complete behaviour of muscle will give insight into the role each microstructural alteration that occurs in CP will play in whole muscle mechanical behaviour.

While the model has the ability to investigate behaviour of muscle that is difficult to examine experimentally, it relies on accurate experimental data for its intrinsic properties. Unfortunately, mechanical data for the effects of stiffness of the ECM are not available, so the value for the ECM stiffness parameter was chosen to vary by 33 % from healthy muscle. It is possible that changes in the structure of the ECM would change by more than this value; however, these values were chosen to probe the behaviour of the ECM stiffness. Given the derivation of the whole muscle stress in the model (Equation 4.4) it is likely that the volume fraction of the ECM would still have the largest contribution to

whole muscle stiffness. Both the ECM volume fraction and stiffness multiply the ECM stress response, so they have similar contributions to whole muscle behaviour for small variations in their values. However, only the ECM volume fraction decreases the contributions from the cellular components. This aspect of the model is realistic, since it is not likely changes in the structure of the ECM will decrease the contribution of the fibres to whole muscle stiffness.

4.5.4 Limitations and Future Directions

A limitation of this model is the lack of current experimental certainty on changes that occur with CP. Many changes to individual components have been observed in CP affected muscle; however, the extent to which microstructural changes occur are varied [179]. Therefore, the effectiveness of the model in providing a comparison to CP muscle will depend on the specific muscle. Additionally, there are very little data available for the changes in stiffness of the ECM, and so it is possible that this could vary more than investigated in this study. This would result in a large influence of the stiffness of the ECM component. Work by Brashear et al. [25] found that stiffness and orientation of the ECM component may have more effect than the amount of the ECM, so this lack of experimental data for ECM stiffness is a limitation of our model. Additionally, it is possible that a focalized accumulation of collagen [39, 188] could occur in contrast to the even distribution investigated in this study. This would likely influence the mechanical response of muscle; however, this was not investigated in this study. The reponse of the base material likely changes in response to compression as opposed to tension. Currently, the available data for the ECM is limited to tension, and so a different response for compression was not implemented in the model. However, we expect the effect on the output from our model would be minimal.

In the model, we have assumed for simplicity that with changes in the volume fraction of the ECM, there is no effect on the amount of force produced by the fibres. Any reduction in contribution from the muscle fibres is assumed to be included in the decrease in cellular component contribution to the base material response. In addition to changes in the microstucture, it is possible that changes occur to the geometry of the muscle in CP. The results of this study only demonstrate the effects of the changes to the material properties, and the effect of changes to the geometry could be investigated in future work. We have not investigated the active behaviour of muscle in this study, although it is fundamental in muscle function. In CP, the contractile force produced has been seen to decrease [173], so using this model to investigate the influence of ECM and sarcomere properties on active force would be valuable and would give additional insight into how the structural alterations that occur with CP individually impact muscle contraction. In this model, the properties of our TD muscle may not be representative of all muscles as the material properties vary both across and within studies [108, 28, 177]. So, while the qualitative passive behaviour is

captured in this model, the exact values could vary between muscles. However, we would expect the general trends observed during this study to hold.

4.6 Conclusion

The purpose of this study was to determine the effects of the microstructural changes that are normally observed during experimental studies of CP muscle, including variation in ECM volume fraction, stiffness, and sarcomere length, on whole muscle stiffness. To do this, a three dimensional computational model of skeletal muscle was used, and overall stress-stretch relationships and muscle stiffness were calculated by measuring the passive stress of the whole muscle. We found that the volume fraction of the ECM had a larger effect on overall muscle stiffness compared to the ECM stiffness and sarcomere length, and that the effects of the sarcomere length were mitigated at larger ECM volume fractions. Investigating these effects provides a causal relationship between changes to microstructural properties and the overall response of the muscle. Experimental research is currently unable to vary independent components of muscle, and so this work can be used to help direct future experimental research. In this study, we were able to determine the crucial role that the microstructural alterations observed in CP have on whole skeletal muscle behaviour.

Chapter 5

Active mechanics in cerebral palsy affected muscle

5.1 Introduction

In the previous chapter, we only considered the passive mechanics of skeletal muscle; however, one of the important functions of skeletal muscle is that it can activate to produce force. In this chapter, the goal will be to investigate the active mechanics of CP affected muscle. Here we still only consider the quasi-static mechanics of CP muscle. Including the dynamic effects would substantially complicate the model, and require us to include spasticity effects (see Section 1.4.1). As observed in the previous chapter, the quasi-static regime will still have interesting mechanics due to the highly nonlinear nature of model and the complex material response of skeletal muscle.

We also now consider more complex muscle geometries; up to this point, we have only considered block geometries. In CP muscle, many changes occur to the macroscopic characteristics of muscle, including the muscle volume and the PCSA [45, 66, 111]. To fully investigate these effects we need a geometry, that more realistically capture the geometry of muscle *in vivo*. While utilizing MRI derived geometries would be ideal, these are computationally expensive and difficult to control for the muscle volume and PCSA independently; however, we will demonstrate the ability to solve our model on these realistic geometries. For the majority of this chapter, we opt for a simplified pennate geometry (see Section 1.1), which has muscle fibres orientated an angle to the line of action and an aponeurosis, which the fibres insert into. In the previous chapter, we do not consider the effects from adipose tissue into the model, but in CP muscle there is an increase in volume fraction compared to TD muscle [46, 114]. Rahemi et al. [130] found that including adipose tissue is important for isometric muscle mechanics, and that the effect will vary depending on the distribution of the tissue; therefore, in this section we also consider these effects and develop a material model for adipose tissue.

The remainder of this chapter will be organized as follows. First, we investigate the material properties for the aponeurosis, and implement them into the model to understand the effects on muscle force (Section 5.2). Subsequently, we determine material properties for adipose tissue and implement them into our material model for muscle (Section 5.3. We investigate the active force-length relationships for our model and investigate the influence of volume, PCSA, and material properties in CP affected muscle (Section 5.4). Finally, in Section 5.5, we apply the model to a MRI derived subject-specific geometry to demonstrate the ability of the computational method to handle realistically shaped domains.

5.2 Aponeurosis Properties

Aponeurosis properties are difficult to determine experimentally, as it is a very thin and stiff tissue. The data used in modelling studies, such as this one, require a stress response for the material, which comes from dividing the force by the cross-sectional area; however, with the aponeurosis, accurate data is difficult to obtain as calculating the cross-sectional area is difficult. To work around this, many skeletal muscle models use properties obtained for the tendon [192, 35], which are often thought of as extensions of the aponeurosis. Aponeurosis are typically around a millimeter thick [156], which may be difficult to implement in a computational model; therefore, the exact material properties may need to be adjusted to obtain the correct muscle mechanics. The exact properties of the aponeurosis typically used in modelling vary between studies [81, 192, 35], and so we investigate the different properties previously used. In our case, the optimal properties will be those that result in the model producing a realistic approximation of the total muscle force.

5.2.1 Intrinsic properties

We consider the modelling results for the aponeurosis for three recent continuum modelling studies: Chi et al. [35], Knaus et al. [81], and Wakeling et al. [192]. These studies specifically modelled the material response of the aponeurosis. We see that the properties used by Knaus et al. [81] are much stiffer that the other properties used in our model [192] and by [35] (Figure 5.1). In most cases, the aponeuroses are modelled as a fibre reinforced composite [192, 81]; however, [35] models aponeurosis as isotropic. Both the fibre and base material are much stiffer in [81] compared to [192] (Figure 5.1) .

The material response from each of the aforementioned papers in shown in Figure 5.1. We see that at small stretches the stress for a given stretch is much larger for the material responses from [81], whereas the most compliant material properties are those from [35]. The bottom left and bottom right plots in Figure 5.1 show that the uniaxial base material response is larger from [81] compared to the [192], while at small stretches [81] has a more compliant fibre response. We also plot here the properties from [192] increased by a factor of 10, as this has been done in the past to represent a stiffer aponeurosis [129]. This still results

in a more compliant response at small stretches, but due to the nonlinear response in the base material, at larger stretches this material has a stiffer response. We include the material parameters used for each of these functions in Table 5.1. The along-fibre parameters for [81] correspond to those from an exponential power law function

$$W(\lambda) = \frac{\xi}{\alpha\beta}\left(e^{\alpha(\lambda^2-1)^\beta} - 1\right). \tag{5.1}$$

The parameters ξ, α, and β are given in Table 5.1. The along-fibre properties from Wakeling et al. [192] are given by the stress function

$$\hat{\sigma}_{\text{pass,apo}}(\lambda) = \begin{cases} 0 & 0 \leq \lambda \leq 1.0 \\ 515.882034(\lambda-1.0)^2 + 0.01(\lambda-1.0) + 0.01 & 1.0 \leq \lambda \leq 1.01 \\ 600.590242(\lambda-1.01)^2 + 0.327640(\lambda-1.01) + 0.06168820 & 1.01 \leq \lambda \leq 1.02 \\ -9.975321(\lambda-1.02)^2 + 22.3394455(\lambda-1.02) + 0.2250236 & 1.02 \leq \lambda \leq 1.15 \\ 19.7458618(\lambda-1.15) + 2.960568 & \lambda > 1.15 \end{cases} \tag{5.2}$$

which was obtained through fitting to tendon data from [42]. For this function, the coefficients are normalized to $\sigma_0 = 2 \times 10^5$ Pa.

Base Material	c_1	c_2	c_3
Knaus et al. 2022	45-55$\times 10^6$	0	0
Chi et al. 2010	30×10^4	80×10^4	800×10^4
Wakeling et al. 2020	9.379×10^5	-6.910$\times 10^5$	9.698×10^7
Fibre	ξ	α	β
Knaus et al. 2022	15-500$\times 10^6$	0	2.5

Table 5.1: Aponeurosis properties from [192, 81, 35]. Parameters c_i, $i = 1, 2, 3$ correspond to the parameters from the Yeoh model (Equation 3.11), while the fibre parameters correspond to the parameters from Equation 5.1. Only fibre properties are included for the data from [81], since [35] used an isotropic response and [192] used an piecewise function given in Equation 5.2. The properties from Knaus et al. [81] were varied depending on the aponeurosis type, anterior (AA) and posterior (PA), between the two values listed.

We note at this point the variation in the data that comes from these different models. In each of the models [35, 81, 192], the aponeurosis properties used were obtained to be within a physiologically reasonable range and to produce realistic strain mechanics. But due to the aforementioned computational constraints on the aponeurosis thickness, the properties shown here may have been adjusted to account for an increased thickness [129, 192]. If a thicker aponeurosis is utilized, then it is likely that more compliant aponeurosis material properties are required. Given this, it is possible that the material responses analyzed in this section may not be adequate for the thickness chosen in our muscle geometry. Nevertheless, we implement these properties into our model to understand the effects on force developed by

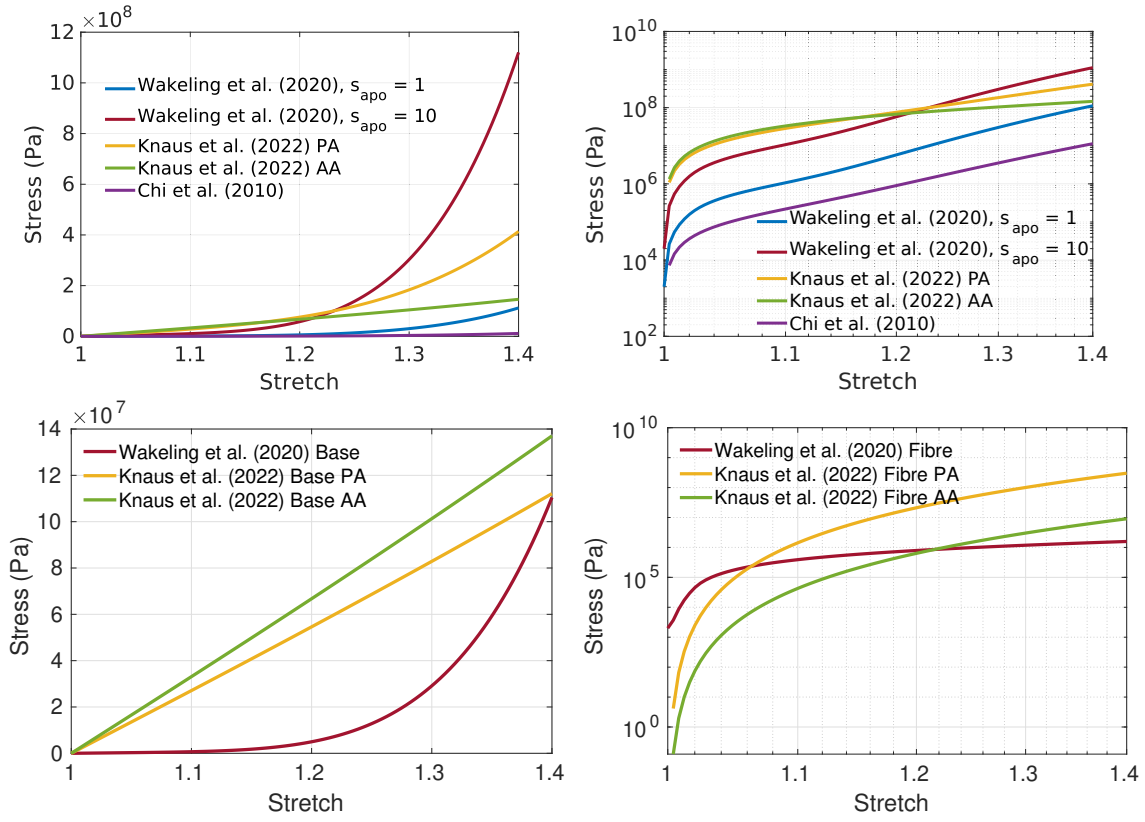

Figure 5.1: Aponeurosis properties used in [192], [35], and [81]: total (top left and right), base (bottom left), and fibre (bottom right).

the muscle; the variability in aponeurosis properties observed experimentally and difficulty in measurement means that the option that results in a reasonable force developed by the muscle is likely also physiologically reasonable.

5.2.2 Aponeurosis effect on muscle force

The material properties from the previous section were implemented into the skeletal muscle model, and the resulting mechanics were investigated. Here we use a pennate geometry with pennation angle $\theta = 25°$ (Figure 5.2). This allows us to implement and investigate the properties of the aponeurosis. The block geometry used in the previous chapters did not have an aponeurosis. With the pennate geometry, muscle fibres insert into the aponeurosis, which is 2mm thick. The dimensions of the muscle will be a width, w, of 5cm; a length, l, of 11cm; and a fibre length, l_f, of 3.8cm (Figure 5.2). These geometries were shown to approximate the medial gastronemius muscle. The PCSA is calculated to be 50 cm^2, which using a maximum isometric stress of 2×10^5Pa and assuming the relation

$$F_{tot} = PCSA \cos(\theta)\, \sigma_0 \tag{5.3}$$

gives us a maximum force of 1000N at optimal length ($\lambda = 1$). Hence, we should expect to see forces on this order of magnitude. We are interested in the active force produced by cerebral palsy affected muscle, so we compute the active force-length relationships. This involves pulling the muscle to a given length, then activating to 100% activation.

There are two main outputs that can be considered when looking at the force-length relationship: the magnitude of the force and the shape of the resulting force-stretch relationship for the whole muscle. We investigate the magnitude of the force produced by the muscle during contraction by comparing model results to the expected force calculated using Equation 5.3. The expected shape of the force-stretch relationship for whole muscle should be similar to the response observed in experimental studies [200]. From the intrinsic material properties in the model (Figure 2.2), we would expect that there will be a local maximum in the force at $\lambda = 1$, and a decrease in the force away from $\lambda = 1$, but with forces increasing at larger stretches, where the passive fibre and base material forces will dominate.

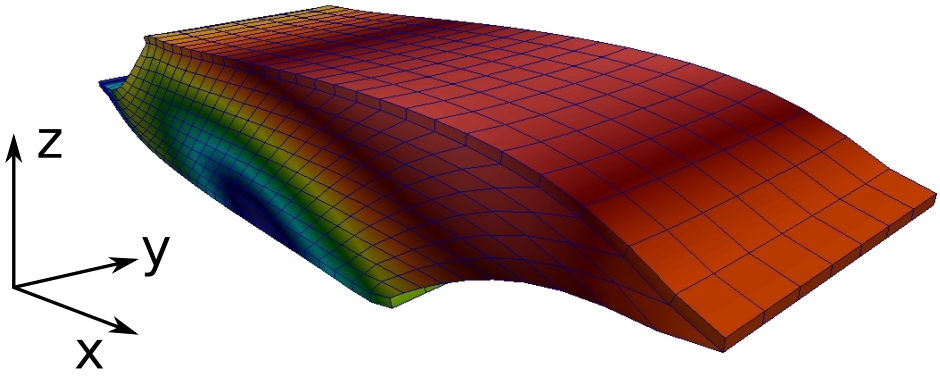

Figure 5.2: Pennate muscle geometry at 100 % activation. To compute the force-length relationships, we apply zero Dirichlet conditions in all directions on the $-x$ face, zero traction conditions on the $\pm y$ and $\pm z$ faces, while applying the displacement condition, $d(t) \neq 0$, to the $+x$ face to lengthen or shorten the muscle. Once the muscle has reached the desired length, we set $d(t) = 0$ and activate the muscle.

We find that the best response is from the aponeurosis properties, in terms of the magnitude of the force at $\lambda = 1$ is from Knaus et al. [81] (Figure 5.3). While both the posterior and anterior aponeurosis produce a good force-length relationship, the best response is from the anterior aponeurosis properties with the stiffer along-fibre properties. In addition to the larger magnitude of force, there is a more realistic shape to the force-length relationship. The more compliant aponeurosis tissue, which corresponds to those from Chi et al. [35] and Wakeling et al. [192], do not result in the expected shape of active force-length relationship nor the magnitude (Figure 5.3). The force produced by the muscle only increases as the strain increases and there is no decrease, as we would expect from experimental studies at

stretches just greater than 1. The stiffer aponeurosis properties obtained by increasing the response from [192] by a factor of 10 result in a reasonable shape to the curve, but smaller magnitude of force relative to [81]. Based on these results, it seems the best aponeurosis properties come from those by Knaus et al. [81], as they result in the largest forces and the most realistic force-length relationship; however, in the presence of the aponeurosis in a pennate geometry, it is possible that Equation 5.3 does not hold exactly, and so we aim to have forces on at least a similar order of magnitude. Due to the difficulty in measuring the aponeurosis properties themselves, it is likely that any of these options that produce the correct shape of the force-stretch relationship would be acceptable.

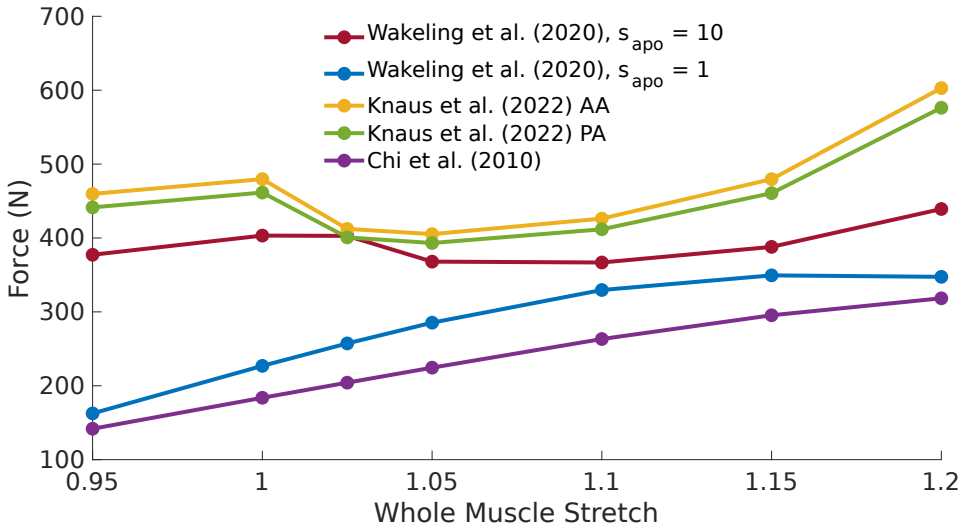

Figure 5.3: Total force-length relationship for varying aponeurosis properties from [35, 81, 192].

Comparing the aponeurosis models investigated, the optimal values are from Knaus et al. [81]; however, the force values are still 50% of those expected from Equation 5.3. It is possible that another aspect of the model is the cause of the lower forces. The ECM component of the base material is also a difficult component of muscle to obtain stress response data. Achieving this response from the ECM requires decellularizing the muscle, but this may also alter the material response of the ECM. It will certainly alter the structure and the interaction of the ECM with the muscle fibres, which may be critical to how it produces force [60]. There is also the problem of measuring the cross-sectional area of ECM (see Chapter 3), since there will be many gaps in the material from the fibres. A further investigation of the base material properties may be required to fully understand why these values are differ from the physiologically expected values.

5.3 Adipose Tissue

Another property of muscle commonly found to vary in CP muscle is the amount of adipose tissue [46, 114]. Often there is an increase in the volume fraction of the adipose tissue, which compromises the tissue structure. Additionally, the amount may vary in location throughout the muscle and with severity of the disorder [46, 114]. In this section we investigate the mechanical response of adipose tissue, determine a material model for the tissue, and implement it into our model.

5.3.1 Intrinsic Properties

There are many reasons for researching the material properties of adipose tissue including improving surgical models or understanding the effects of vehicle trauma [175]. There were many available adipose tissue studies including the ones referenced in the review by [175], although not all apply to muscle mechanics. In particular, there were studies that mainly looked at high strain rate applications, which include investigating subcutaneous adipose tissue behaviour during vehicle crashes [176]. Other studies might look at the behaviour of specific regions of adipose tissue including orbital adipose tissue (in the eye) [33] and calcaneal pad adipose tissue [106]. In many studies, the data was not available to allow us to apply it in our model [56, 151, 176]. After review the literature for mechanical studies of adipose tissue, we were left with following studies: [170, 37, 4, 178].

There are many types of adipose tissue to consider, all of which may differ from that within muscle, but the adipose tissue within muscle would be difficult to measure experimentally. The main types of adipose tissue that we consider here are subcutaneous and breast tissue, which was used by [130] to look at the distribution of adipose tissue throughout the muscle. Ideally, we would also like to have both compression and tension data that could be implemented into the model, although this is not available in most studies. The studies on live participants (eg. [178]) will only use the compression tests, since tension is not possible. It would be ideal to have an isolated response from the adipose tissue (no effects from skin or other material), although any response will not be able to completely isolated adipose tissue, as adipose tissue (like muscle fibres) is embedded in an ECM.

To compare the material responses of the adipose tissue we can look at the resulting stress-strain responses. Here we neglect considering whether the strain in the experimental data was tensile or compressive and simply look at the magnitude of the strain, so we can compare with the results used by [130]. One caveat with the data obtained by [170] is that the data only contains biaxial and triaxial tests. This means that the adipose tissue was pulled in either two or one direction simultaneously; therefore, this material may have a stiffer response compared to a uniaxial test. A comparison of the material properties is shown in Figure 5.4, where the stress-strain curves are shown. Each of the curves are obtained through digitizing the stress-strain plots from the respected studies.

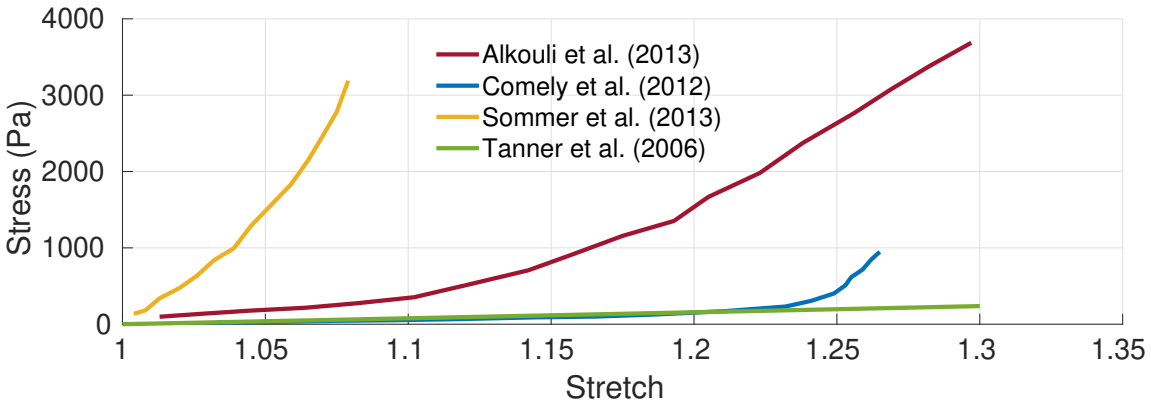

Figure 5.4: Stress-stretch response for adipose tissue obtained from [4, 37, 170, 178].

Since we want to use a tensile response for the adipose material properties, we opt to use the adipose tissue data from [4]. These data are in the middle of the range of adipose tissue data and are for subcutaneous fat. To determine the correct material model, we test both the Neo-hookean

$$W_{Neo-Hookean}(\mathbf{B}) = c_1(I_3(\mathbf{B}) - 3) \tag{5.4}$$

and Yeoh models (Equation 3.11). We find that the Yeoh produced the best results with an R^2 of 0.998. The results are shown in Table 5.2 and Figure 5.5.

	Yeoh	Neo-hookean
R^2	0.998	0.84
c_1	323.91	1570.8
c_2	5163.1	-
c_3	-3872.9	-

Table 5.2: Parameters from the model fits and R^2 values for the Neo-hookean and Yeoh models.

5.3.2 Modelling adipose tissue in skeletal muscle

There are a few possible options for modelling the adipose tissue infiltration in skeletal muscle. In the study by Rahemi et al. [130], they outlined a number of different implementations of adipose material properties in the model. The first option would be to treat adipose tissue as a completely different material from muscle, in a similar way to modelling the aponeurosis. This would result in each element in the mesh having either adipose tissue or muscle properties. This approach would not allow for us to consider adipose tissue fractions, which can be obtained using MRI data; hence, to make our model more usable with MRI data, we opt to homogenize the muscle material with adipose tissue, so that we can prescribe a muscle volume fraction and a adipose tissue volume fraction in each element.

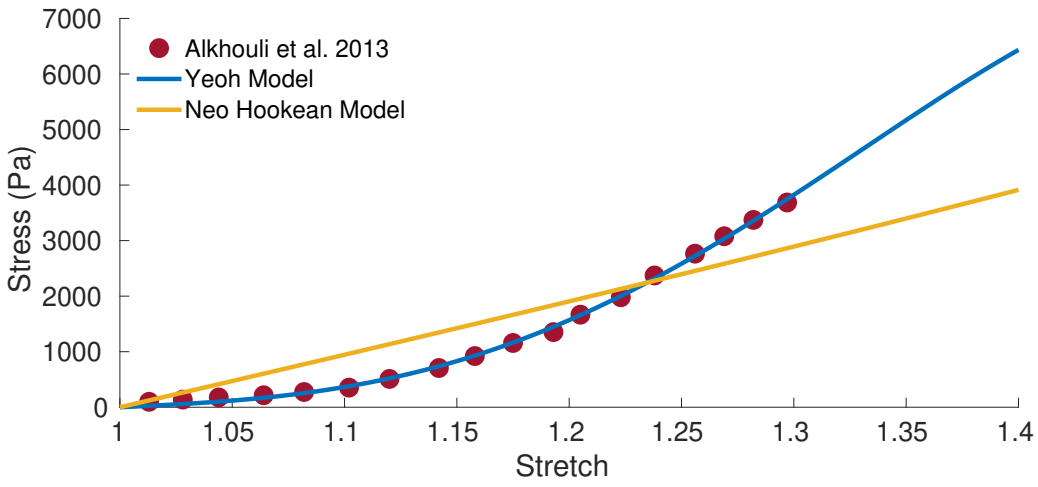

Figure 5.5: Fit of the Yeoh and Neo-hookean models to the adipose tissue data from Alkhouli et al. [4].

The next choice is whether adipose tissue is homogenized as part of the base material or as a seperate material. We opt to use a similar formulation to M4 in [130], where both the base material and fibre material are affected by the fraction of adipose tissue. Physiologically, this can be though of intracellular adipose tissue, which leaves less room for active contributions of muscle. The whole strain-energy potential for muscle will be given by

$$W_{\text{muscle}}(\mathbf{B}) = (1-\beta)\left\{\alpha W_{\text{ECM}}(\mathbf{B}) + (1-\alpha)\left[W_{\text{fibre}}(\mathbf{B}) + W_{\text{CELL}}(\mathbf{B})\right]\right\} + \beta W_{\text{adipose}}(\mathbf{B}). \tag{5.5}$$

Here β represents the volume fraction of adipose tissue. This option also slight alters the previous homogenization model derived in Chapter 3, as the contribution from the ECM volume fraction now alters the fibre component of the model.

Now that we have determined the material properties for the aponeurosis and adipose tissue, in the next section we look into active mechanics of CP affected skeletal muscle. To do this, we vary the volume and PCSA, as well as the material properties.

5.4 Active mechanics: the effects of cerebral palsy

In this section, we investigate the active mechanics of CP affected muscle. For these simulations we will consider the pennate geometry, previously described in Figure 5.2. This allows us to consider effects from CP that we have not investigated previously, such as changes to the muscle geometry. In CP affected muscle, muscle shape is altered in addition to the morphological changes occurring to the ECM, adipose tissue, and sarcomeres [46, 11, 66]. The main changes that occur are decreased volume and PCSA; however, it is difficult to understand how each change independently alters the force produced by the muscle. It is

likely given Equation 5.3 that the force produced by the muscle is largely influenced by the PCSA, but this effect could change in the presence of a pennate geometry and different muscle material properties. To achieve a better understanding of the architectural effects, as well as the CP material properties, we utilize our model to vary each of the muscle properties individually.

5.4.1 Methods

For these tests, we use the same experimental setup with pennate geometry as in Section 5.2. To investigate the effects of the muscle architecture, we vary the dimensions, so that we either maintain a constant volume or PCSA. Using the results from MRI and ultrasound studies on changes to the morphology of skeletal muscle [45, 111, 66], we find that the volume and PCSA typically decrease in CP muscle by about 30%. While the values differ between studies, 30% is a reasonable value and changing both parameters by 30% allows for us to compare the two effects; experimentally, a decrease of approximately 35% volume and approximately 29% PCSA has been observed [45]. To change the volume by maintaining a constant PCSA, we vary the fibre length, while keeping the other parameters fixed. To change the PCSA, while maintaining a constant volume, the fibre length is decreased while the muscle width is increased. In both cases we maintain a fixed pennation angle. A summary of the changes that are made to investigate the effects of muscle architecture are included in Table 5.3. In addition to varying the geometry, we also look at the effects of varying the material properties. For TD material properties, we us $\alpha = 0.02$, $\beta = 0.1$, and $c_{\text{sarco}} = 0$, while for CP material properties we use $\alpha = 0.2$, $\beta = 0.2$, $c_{\text{sarco}} = 0.25$. For these tests, we opt to use the same properties for the aponeurosis as previously used in Wakeling et al. [192], but with increased stiffness by a factor of 10 as described in Section 5.2. The numerical experiments will involve computing the active force-stretch relationship, as in Section 5.2.2.

	-	-30% volume	-30% PCSA
l_f	3.8	2.66	5.4
w	5	5	3.5

Table 5.3: Geometries used in each of the tests. Note that aponeurosis thickness was fixed at 0.2cm, the length one aponeurosis was fixed at 11cm, and the pennation angle was fixed at 25 degrees. The geometries with a decrease in volume had fixed PCSA, and vice versa. l_f is the fibre length and w is the width of the muscle. Values in table are given in cm.

5.4.2 Results

Effects of geometry on whole muscle force

We find that the PCSA has a larger influence than the volume on the total force produced by muscle near optimal length (Figure 5.6). The resulting force-stretch relationship with decreased PCSA appears to have a larger range of stretches where the muscle is producing

the same force as optimal length; meanwhile, there is a shorter range of stretches when looking at the effects of the decreased muscle volume. We also note that the decreased volume curve has a larger force produced at larger stretches, which is due to the difference in fibre stretches in the geometries. Plotting the total force output from the model against the average stretch throughout the muscle, as opposed to the total stretch of the muscle from end to end, we see that there is little effect from the volume (Figure 5.7).

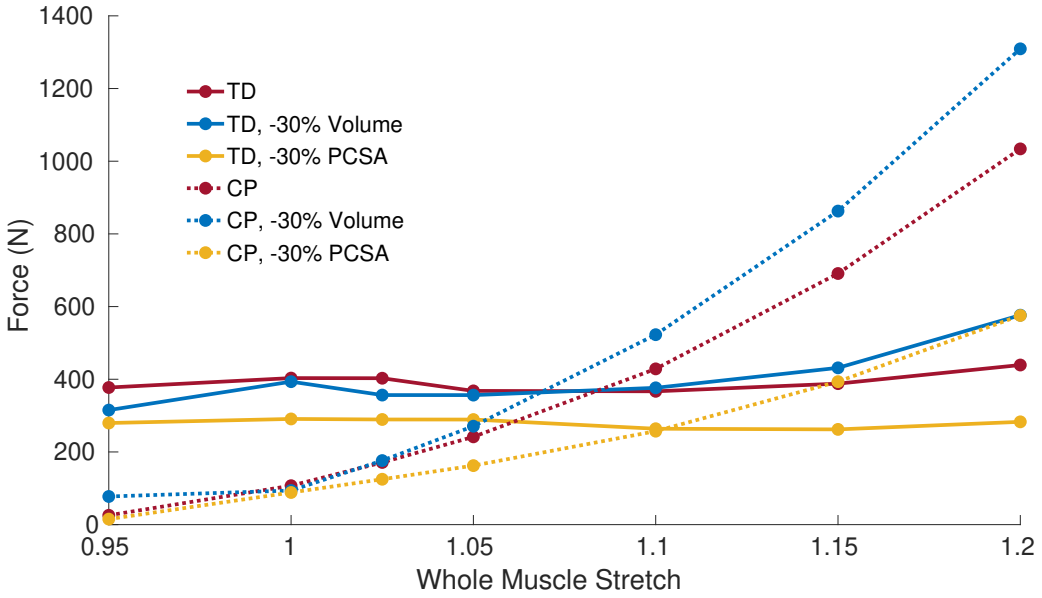

Figure 5.6: Total force-length results for the block geometry with TD and CP muscle material properties. The geometries were varied from the typical muscle by a decrease in 30% volume or 30% $PCSA$.

The force at optimal length is reduced by 29% with a 30% decrease in the $PCSA$ (Table 5.4), which is similar to the value predicted by Equation 5.3. This indicates that our model generally follows the properties expected from experimental studies; however, looking at the absolute values of the total force, we see that they are significantly lower than the expected 900N when accounting for the $PCSA$, adipose tissue, and ECM effects. This is the same as described in Section 5.2. It is possible that this is due to the base material response or the shape of the muscle geometry. The muscle geometry used here may not be close enough to the real muscle shape and may not allow for the correct bulging and deformation.

	-	-30% Vol	-30% PCSA
TD	403.2	399.4	290.8
CP	107.1	93.82	88.44

Table 5.4: Force (N) produced at optimal length for a given experimental setup. TD muscle corresponds to $\alpha = 0.02$, $\beta = 0.1$, and $c_{\text{sarco}} = 0$. CP muscle corresponds to $\alpha = 0.2$, $\beta = 0.1$, and $c_{\text{sarco}} = 0.25$.

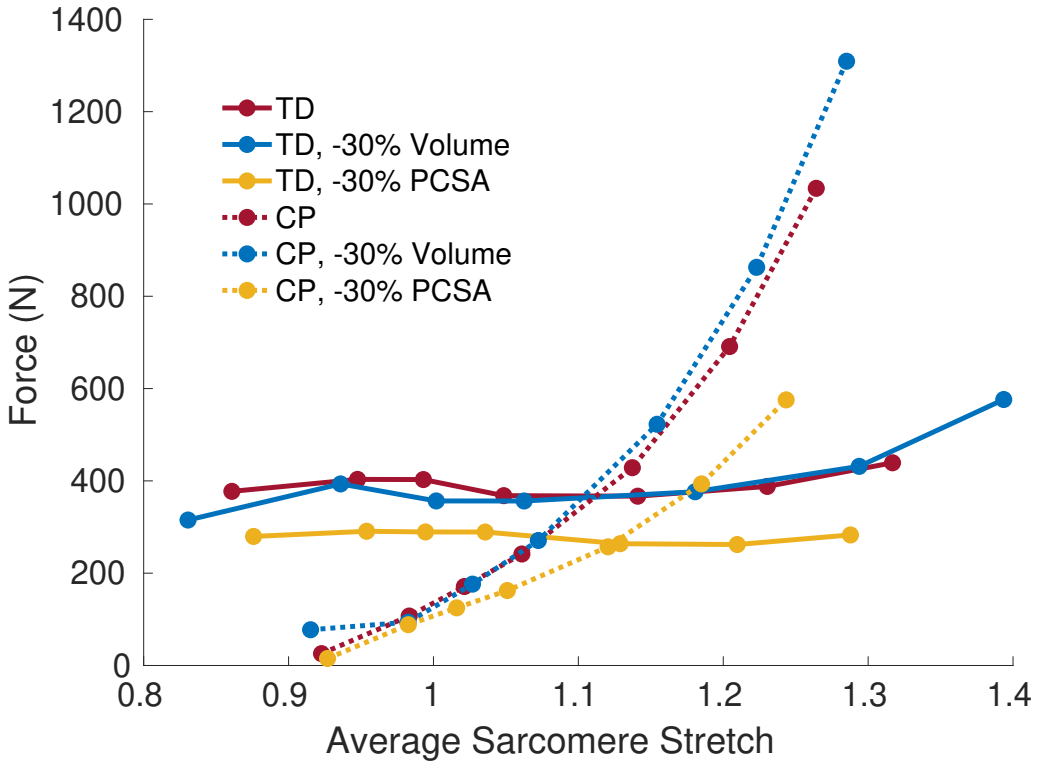

Figure 5.7: Whole muscle force against the average sarcomere stretch throughout the muscle.

The force output was substantially affected by the material composition. We see that the CP muscle had a reduced force relative to the TD muscle near optimal length (Figure 5.6. However, as the stretch is increased, the force produced at larger stretches is more compared to the TD muscle. This is likely due to the high stiffness and nonlinear response of the ECM component of the material and the larger sarcomere stretches ($c_{\text{sarco}} = 0.25$). Again, similarly to the TD muscle, there is a larger effect from the PCSA on the force produced; however, the reduced force is only 18%, which is less than estimated by Equation 5.3. This is possibly due to the change in the sarcomere length during CP. At non-optimal fibre lengths that this relation may no longer hold. Similarly to TD muscle, the effect of the volume decrease is larger at $\lambda \neq 1$. This may be emphasized with the CP material due to the greater stiffness of the base material.

Effects of CP on average stretch throughout the muscle

The stretch throughout the muscle is directly related to the force output from the muscle, since the active force-length relationship depends on the stretch at a given point. It is then useful to investigate the average stretch ($\bar{\lambda}_{tot}$) over the muscle before and after activation. We find, at optimal length, that the average stretch decreases for the TD muscle during activation, but with the CP material properties there is less of a decrease (Figure 5.8). For

TD muscle the decrease in stretch during activation is true at all lengths, but in CP muscle, there is substantially less decrease at larger stretches.

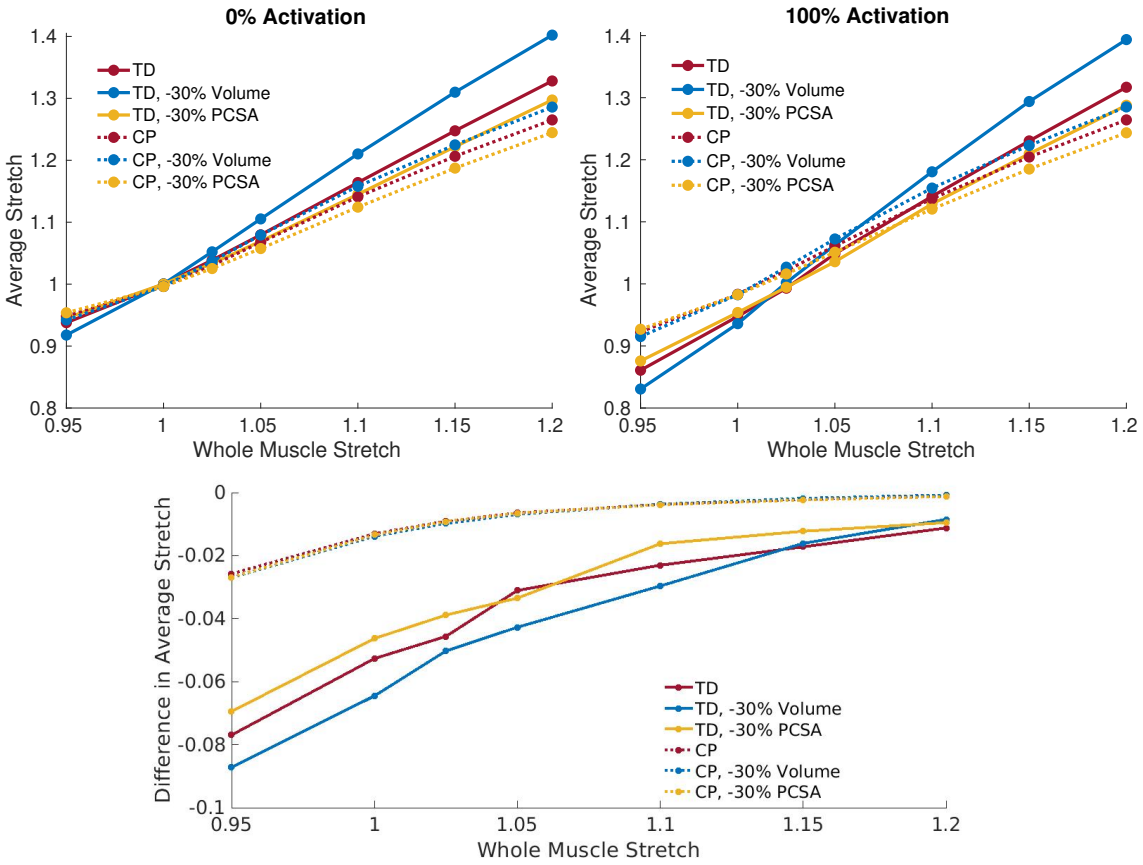

Figure 5.8: Plots of the average stretch at 0% (top left) and 100% (top right) activation against the whole muscle stretch. The bottom plot shows the difference in the average stretch throughout the muscle during activation.

Comparing the average the stretch in the muscle to the whole muscle stretch can be used to explain the volume effects in Figure 5.6. In Figure 5.6, there was a larger effect from the decreased muscle volume at larger whole muscle stretches, and this effect disappears when looking at the force-stretch relation calculated using the average stretch. Comparing the average stretch in the muscle with whole muscle stretch, we see that the decreased volume of the muscle results in there being more dependence of the average stretch on the whole muscle stretch for TD muscle material properties (Figure 5.8). The reason for this is the shorter fibre lengths used to decrease the muscle volume (see Table 5.3). Additionally, this means that larger passive forces will be developed and smaller active forces at a given whole muscle stretch, which explains the effects observed in Figure 5.6. When adding the CP muscle properties, a similar effect is observed (Figure 5.6), but there is effect from volume on the average stretch of the muscle at a given whole muscle stretch (Figure 5.8). This is likely a result of the shift in the intrinsic passive fibre force-stretch relationship and the

increased base material stiffness; the muscle material will be less compliant, and so the local stretches in the muscle will be reduced.

5.5 Subject-specific geometries

We can utilize a realistic MRI-derived geometry with our model to account for subject-specific data (Figure 5.9), which were obtained by D'Souza et al. [45]. Using these data allows us to account for variations in the structure of muscle that may vary between subjects. Key changes during CP are the changes to muscle thickness, length, and volume [45, 66, 112, 111], which all have an effect on the $PCSA$ and mechanics of skeletal muscle [89, 192]. The amount to which each of these properties vary will depend on the subject [45, 66, 112, 111], and so using our model we can better understand the muscle mechanics for specific subjects. In addition to modelling the subject specific effects of CP, we are also able to better capture the fibre orientations and adipose tissue distributions, which are not uniform throughout the muscle.

Here we demonstrate the implementation of the model on an MRI derived geometry as a proof of concept. Further work is required to accurately tune the model to account for correct aponeurosis dimensions and reduce the run time of these simulations. Along with the MRI derived geometry, we also account for adipose tissue distributions and fibre orientations obtained through diffusion tensor imaging (for details see eg. [21]). Figure 5.9 shows a simulation where the muscle was stretched in the x direction to a whole muscle stretch of 1.1, and subsequently activated to 100% activation at a fixed length. The $+z$ and $-z$ faces have a portion of the surface covered by an aponeurosis, which the muscle fibres insert into.

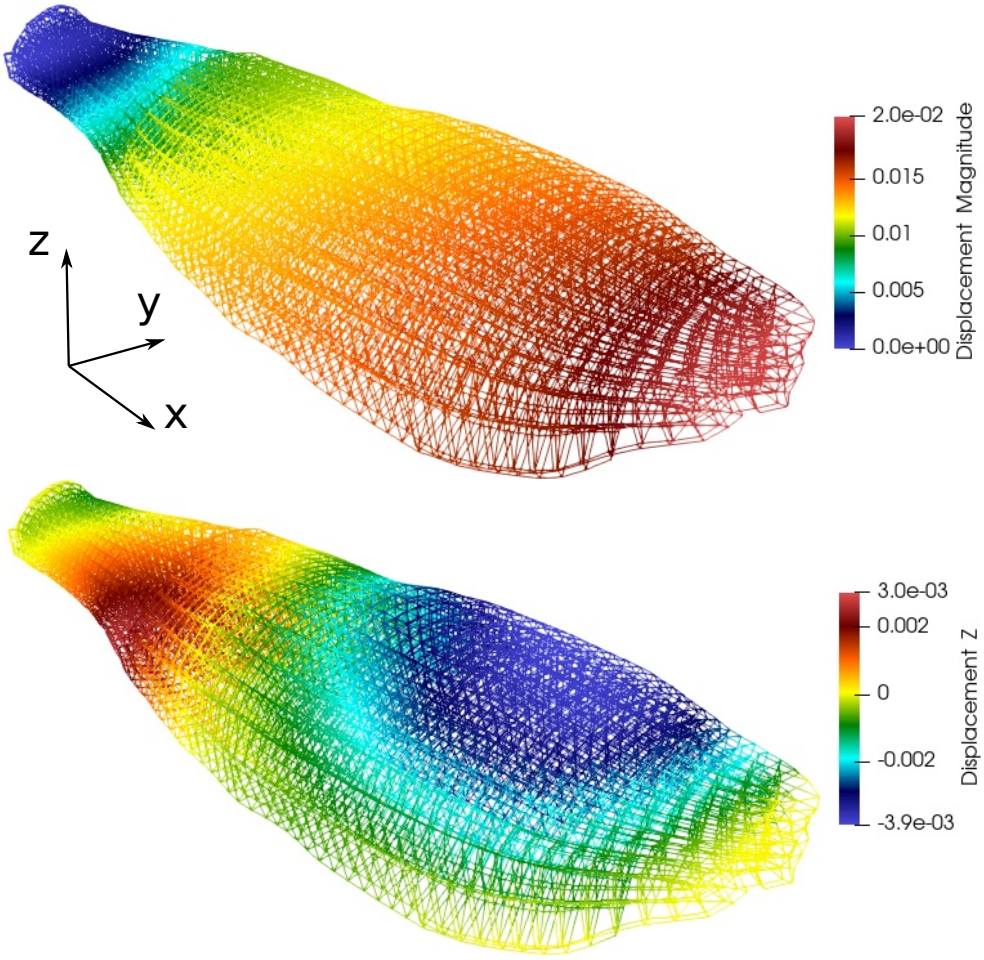

Figure 5.9: Magnitude of displacement (Top) and z direction displacement at 100% activation on a TD subject specific MRI-derived geometry.

Chapter 6

Conclusion

This thesis describes the development of a mathematical model to investigate the effects of cerebral palsy on skeletal muscle mechanics. This section summarizes the significant contributions of this work and describes future directions.

6.1 Summary of the thesis

Chapter 2 describes the development of a mathematical model for skeletal muscle using the theory of finite-strain elasticity. This was based on previous work and uses a quasi-static formulation of the model [192]. The model can be derived using a strain-energy formulation, and the resulting model equations can be found using a minimization of potential energy. The resulting system is highly nonlinear, and so we linearize using a Newton method, and solve the linearized system using a Conjugate-Gradient method. We also demonstrate convergence in some of the relevant outcomes.

Chapter 3 describes a principled approach to muscle mechanics. Here the base material portion of the muscle is broken down into the contributions from the ECM and the cellular material. The ECM material response is obtained through data from a decellularized muscle [61], while the cellular material is obtained from brain grey matter [79]. The response from these two materials is then homogenized into the base material response. This is done using a representative volume element and a Voigt approximation. This results in an aggregate material that captures the response from the ECM and cellular material on a macroscopic scale. Modelling the individual heterogeneities on the macroscopic scale is not computationally feasible, so this homogenization is required. The remainder of the chapter involves the implementation into the skeletal muscle model described in Chapter 2, and performing simulations of muscle contraction. We find that there are significant volume effects, and the three dimensional implementation is required to fully understand the material behaviour of skeletal muscle.

Subsequently, in Chapter 4 we apply the homogenized base material model to skeletal muscle affected by CP. CP muscle suffers from many morphological changes that cause sub-

stantial alterations to the deformation of skeletal muscle. Some commonly observed changes are the ECM, which varies in volume fraction and structure, and the sarcomere length, which is typically longer in CP muscle. This results in a muscle that is much stiffer than typically developed muscle. To investigate the relative effects from the ECM and sarcomere length, we passively lengthened the muscle to determine the stress-stretch relationship for a combination of material parameters. The main findings of these tests are that during CP, ECM has a larger contribution to the muscle stiffness. Another important finding was that due to the substantial nonlinear stress-stretch relationship in the ECM, the ECM effects were larger at larger stretches and the sarcomere effects were mitigated at larger stretches. This work points to the fact that there is relatively small influence from the sarcomeres in passive mechanics, but there may be a larger effect in active mechanics.

In Chapter 5, the effect of CP on the active mechanics of muscle is investigated. This includes implementing the muscle model on a more complex pennate geometry and including the effects of an aponeurosis. To understand the influence of the aponeurosis on muscle mechanics, we compare aponeurosis models from previous modelling studies, and investigate the effects on muscle force. In addition to the aponeurosis, we also include the effects from adipose tissue into the model. The results of CP muscle tissue, as well as the effects of changes to the muscle architecture are investigated, and effects are characterized by determining the active force-length relationship. From this, we are able to determine the effect of CP material properties and geometry on muscle behaviour. We find that the CP material properties altered the shape of the total force-length relationship and altered the effect of changes to the muscle volume. The ability to model subject-specific changes is also important for muscle affected by CP, since the exact changes to muscle often vary between subjects; hence, we demonstrate the ability to model the active mechanics of CP skeletal muscle on MRI derived geometries and adipose tissue distributions.

6.2 Future directions

Future directions for this modelling work could involve probing the basic mechanics of skeletal muscle, as well as the application of the model to more complicated effects from CP. From a mathematical and physical perspective, there are a number of changes that could be made to the model to more accurately capture the correct mechanics of muscle. One change that could be made to improve the response of the muscle in compression is to implement a tension-compression asymmetry. Muscle has been shown to have a different response in response to compression opposed to tension [108, 28, 62]. While this is partly explained by the along-fibre properties in the model, this asymmetry has also been shown transverse to the muscle fibres [108]. Implementing these effects may help to more accurately capture the force produced by muscle and the bulging that occurs in muscle mechanics.

Another direction for this work is a more accurate model for the ECM response, in which the structure and orientation of the collagen fibres within the matrix is considered. This has been done in other homogenization models [172, 14] as well as in smaller scale models [62]. Implementing this aspect of the model would help to develop a more accurate model of the muscle base material. This comes at the disadvantage of making the model more computationally costly, and so may not be desirable if implementing the model on more complex geometries such as an MRI derived mesh.

To further investigate the mechanics of CP affected muscle, directions could involve a more detailed application of the model to subject-specific data, further study on the effects of sarcomere length on active force production, and the effects of ECM stiffness. The accurate modelling of subject-specific data would provide more detail on how CP affects individual subjects and could allow us to understand the influence of realistic muscle geometries influence the force produced by muscle. Investigating the influence of muscle geometries could be done using statistical shape modelling (see eg. [30]), where the average CP geometries could be compared to average TD muscle geometries. Additionally, the effect of sarcomere length could be further investigated in the active force produced by muscle. It was found in Chapter 4 that the sarcomere length was not as important in passive mechanics, but determining the relative effects of sarcomere length to ECM in active mechanics could be valuable in clinical treatments for the CP. The structure of the ECM has been investigated in spastic muscle, and its possible that the structure varies independently of the volume fraction [93, 25]. This could be investigated using our model to understand the relative effect of a compromised ECM on the overall muscle mechanics. A more detailed approach would be to implement the collagen architecture, as described above, and investigate the influence of changes to muscle behaviour. CP has a complex effect on skeletal muscle, resulting in many changes to its structure, and determining the relative effects on the mechanics of muscle can be investigated using this model.

Bibliography

[1] B.C. Abbott and R.J. Baskin. Volume changes in frog muscle during contraction. *J. Physiol.*, 161(3):379–391, 1962.

[2] T. Ahamed, M. B. Rubin, B. A. Trimmer, and L. Dorfmann. Time-dependent behavior of passive skeletal muscle. *Continuum Mechanics and Thermodynamics*, 28(1-2):561–577, 2016.

[3] R. M.N. Alexander, A. S. Jayes, G. M.O. Maloiy, and E. M. Wathuta. Allometry of the leg muscles of mammals. *Journal of Zoology*, 194(4):539–552, 1981.

[4] N. Alkhouli, J. Mansfield, E. Green, J. Bel, B. Knight, N. Liversedge, J. C. Tham, R. Welbourn, A. C. Shore, K. Kos, and C. P. Winlove. The mechanical properties of human adipose tissues and their relationships to the structure and composition of the extracellular matrix. *American Journal of Physiology - Endocrinology and Metabolism*, 305(12):1427–1435, 2013.

[5] C. J. Arellano, N. J. Gidmark, N. Konow, E. Azizi, and T. J. Roberts. Determinants of aponeurosis shape change during muscle contraction. *J. Biomech.*, 49(9):1812–1817, 2016.

[6] D. Arndt, W. Bangerth, D. Davydov, T. Heister, L. Heltai, M. Kronbichler, M. Maier, J. P. Pelteret, B. Turcksin, and D. Wells. The deal.II Library, Version 8.5. *J. Numer. Math.*, 25:137–146, 2017.

[7] E. Azizi and T. J. Roberts. Biaxial strain and variable stiffness in aponeuroses. *Journal of Physiology*, 587(17):4309–4318, 2009.

[8] L. Bar-On, E. Aertbeliën, G. Molenaers, and K. Desloovere. Muscle activation patterns when passively stretching spastic lower limb muscles of children with cerebral palsy. *PLoS ONE*, 9(3), 2014.

[9] M. Bárány. ATPase activity of myosin correlated with speed of muscle shortening. *The Journal of general physiology*, 50(6), 1967.

[10] L. Barber, R. Barrett, and G. Lichtwark. Passive muscle mechanical properties of the medial gastrocnemius in young adults with spastic cerebral palsy. *J. Biomech.*, 44(13):2496–2500, 2011.

[11] R. S. Barrett and G. A. Lichtwark. Gross muscle morphology and structure in spastic cerebral palsy: a systematic review. *Dev. Med. Child Neurol.*, 52(9):794–804, 2010.

[12] R. J. Baskin and P. J. Paolini. Volume change and pressure development in muscle during contraction. *The American journal of physiology*, 213(4):1025–1030, 1967.

[13] B.I. Binder-Markey, N.M. Broda, and R.L. Lieber. Intramuscular anatomy drives collagen content variation within and between muscles. *Front. Physiol.*, 11:293, 2020.

[14] C. Bleiler, P. Ponte Castañeda, and O. Röhrle. A microstructurally-based, multi-scale, continuum-mechanical model for the passive behaviour of skeletal muscle tissue. *J. Mech. Behav. Biomed.*, 97:171–186, 2019.

[15] S. S. Blemker and S. L. Delp. Three-Dimensional Representation of Complex Muscle Architectures and Geometries. *Ann. Biomed. Eng.*, 33(5):661–673, 2005.

[16] R. W. Bohannon and M. B. Smith. Interrater reliability of a modified Ashworth scale of muscle spasticity. *Physical Therapy*, 67(2):206–207, 1987.

[17] M. Böl, R. Iyer, J. Dittmann, M. Garcés-Schröder, and A. Dietzel. Investigating the passive mechanical behaviour of skeletal muscle fibres: Micromechanical experiments and Bayesian hierarchical modelling. *Acta Biomater.*, 92:277–289, 2019.

[18] M. Böl and S. Reese. Micromechanical modelling of skeletal muscles based on the finite element method. *Comput. Method Biomech.*, 11(5):489–504, 2008.

[19] M. Böl, M. Sturmat, C. Weichert, and C. Kober. A new approach for the validation of skeletal muscle modeling using MRI data. *Computational Mechanics*, 47(5):591–601, 2011.

[20] B. Bolsterlee, A. D'Souza, S.C. Gandevia, and R.D. Herbert. How does passive lengthening change the architecture of the human medial gastrocnemius muscle? *J. Appl. Physiol.*, 122(4):727–738, 2017.

[21] B. Bolsterlee, A. D'Souza, and R. D. Herbert. Reliability and robustness of muscle architecture measurements obtained using diffusion tensor imaging with anatomically constrained tractography. *Journal of Biomechanics*, 86:71–78, 2019.

[22] C. M. Booth, M. J. F. Cortina-Borja, and T. N. Theologis. Collagen accumulation in muscles of children with cerebral palsy and correlation with severity of spasticity. *Dev. Med. Child Neurol.*, 43(5):314–320, 2001.

[23] S. M. Brændvik, A. K.G. Elvrum, B. Vereijken, and K. Roeleveld. Involuntary and voluntary muscle activation in children with unilateral cerebral palsy-Relationship to upper limb activity. *European Journal of Paediatric Neurology*, 17(3):274–279, 2013.

[24] J. E. Brandenburg, S. F. Eby, P. Song, S. Kingsley-Berg, W. Bamlet, G. C. Sieck, and K.N. An. Quantifying passive muscle stiffness in children with and without cerebral palsy using ultrasound shear wave elastography. *Dev. Med. Child Neurol.*, 58(12):1288–1294, 2016.

[25] S. E. Brashear, R. P. Wohlgemuth, G. Gonzalez, and L. R. Smith. Passive stiffness of fibrotic skeletal muscle in mdx mice relates to collagen architecture. *J. Physiol.*, 599(3):943–962, 2021.

[26] S. Budday, G. Sommer, C. Birkl, C. Langkammer, J. Haybaeck, J. Kohnert, M. Bauer, F. Paulsen, P. Steinmann, E. Kuhl, and G. A. Holzapfel. Mechanical characterization of human brain tissue. *Acta Biomater.*, 48:319–340, 2017.

[27] T. J. Burkholder and R. L. Lieber. Sarcomere length operating range of vertebrate muscles during movement. *J. Exp. Biol.*, 204(9):1529–1536, 2001.

[28] B. Calvo, A. Ramírez, A. Alonso, J. Grasa, F. Soteras, R. Osta, and M. J. Muñoz. Passive nonlinear elastic behaviour of skeletal muscle: Experimental results and model formulation. *J. Biomech.*, 43(2):318–325, 2010.

[29] M. E. Castle, T. A. Reyman, and M. Schneider. Pathology of spastic muscle in cerebral palsy. *Clinical orthopaedics and related research*, 142(142):223–233, 1979.

[30] J. Cates, S. Elhabian, and R. Whitaker. Shapeworks: particle-based shape correspondence and visualization software. In *Statistical Shape and Deformation Analysis*, pages 257–298. Elsevier, 2017.

[31] K. K. Ceelen, C. W.J. Oomens, and F. P.T. Baaijens. Microstructural analysis of deformation-induced hypoxic damage in skeletal muscle. *Biomech. Model. Mechanobiol.*, 7(4):277–284, 2008.

[32] G. Chagnon, M. Rebouah, and D. Favier. Hyperelastic Energy Densities for Soft Biological Tissues: A Review. *J. Elast.*, 120(2):129–160, 2015.

[33] K. Chen and J. D. Weiland. Mechanical properties of orbital fat and its encapsulating connective tissue. *Journal of Biomechanical Engineering*, 133(6):1–3, 2011.

[34] X. Chen and Y. Li. Role of matrix metalloproteinases in skeletal muscle. *Cell. Adh. Mig.*, 3(4):337–341, 2009. PMID: 19667757.

[35] S. W. Chi, J. Hodgson, J.-S. Chen, V. Reggie Edgerton, D. D. Shin, R. A. Roiz, and S. Sinha. Finite element modeling reveals complex strain mechanics in the aponeuroses of contracting skeletal muscle. *J. Biomech.*, 43(7):1243–1250, 2010.

[36] C. Chui, E. Kobayashi, X. Chen, T. Hisada, and I. Sakuma. Combined compression and elongation experiments and non-linear modelling of liver tissue for surgical simulation. *Med. Biol. Eng. Comput.*, 42(6):787–798, 2004.

[37] K. Comley and N. Fleck. The compressive response of porcine adipose tissue from low to high strain rate. *International Journal of Impact Engineering*, 46:1–10, 2012.

[38] M. De Bruin, M. J. Smeulders, M. Kreulen, P. A. Huijing, and R. T. Jaspers. Intramuscular connective tissue differences in spastic and control muscle: A mechanical and histological study. *PLoS ONE*, 9(6), 2014.

[39] M. de Bruin, M. J. Smeulders, M. Kreulen, P. A. Huijing, and R. T. Jaspers. Intramuscular connective tissue differences in spastic and control muscle: A mechanical and histological study. *PLoS ONE*, 9(6):e101038, 2014.

[40] S. L. Delp, F. C. Anderson, A. S. Arnold, P. Loan, A. Habib, C. T. John, E. Guendelman, and D. G. Thelen. OpenSim: Open-source software to create and analyze dynamic simulations of movement. *IEEE Transactions on Biomedical Engineering*, 54(11):1940–1950, 2007.

[41] T. J.M. Dick, A. A. Biewener, and J. M. Wakeling. Comparison of human gastrocnemius forces predicted by Hill-type muscle models and estimated from ultrasound images. *Journal of Experimental Biology*, 220(9):1643–1653, 2017.

[42] T. J.M. Dick and C. J. Clemente. How to build your dragon: Scaling of muscle architecture from the world's smallest to the world's largest monitor lizard. *Frontiers in Zoology*, 13(1):1–17, 2016.

[43] M.H. Dickinson, C.T. Farley, R.J. Full, M.A.R. Koehl, R. Kram, and S. Lehman. How animals move: An integrative view. *Science*, 288(5463):100–106, 2000.

[44] S. Dominguez. *From eigenbeauty to large-deformation horror*. PhD thesis, Simon Fraser University, 2020.

[45] A. D'Souza, B. Bolsterlee, A. Lancaster, and R. D. Herbert. Muscle architecture in children with cerebral palsy and ankle contractures: an investigation using diffusion tensor imaging. *Clinical Biomechanics*, 68:205–211, 2019.

[46] A. D'Souza, B. Bolsterlee, A. Lancaster, and R. D. Herbert. Intramuscular fat in children with unilateral cerebral palsy. *Clin. Biomech.*, 80:105183, 2020.

[47] G. C.B. Elder, G. Stewart, K. Cook, D. Weir, A. Marshall, and L. Leahey. Contributing factors to muscle weakness in children with cerebral palsy. *Developmental Medicine and Child Neurology*, 45(8):542–550, 2003.

[48] C. M. Eng, L. H. Smallwood, M. P. Rainiero, M. Lahey, S. R. Ward, and R. L. Lieber. Scaling of muscle architecture and fiber types in the rat hindlimb. *Journal of Experimental Biology*, 211(14):2336–2345, 2008.

[49] J. M.N. Enslin, U. K. Rohlwink, and A. Figaji. Management of Spasticity After Traumatic Brain Injury in Children, 2020.

[50] J. W. Fee and R. A. Foulds. Neuromuscular Modeling of Spasticity in Cerebral Palsy. *IEEE Transactions on Neural Systems and Rehabilitation Engineering*, 12(1):55–64, 2004.

[51] R.A. Fine and F.J. Millero. Compressibility of water as a function of temperature and pressure. *J. Chem. Phys.*, 59(10):5529–5536, 1973.

[52] E. G. Fowler, A. I. Nwigwe, and T. W. Ho. Sensitivity of the pendulum test for assessing spasticity in persons with cerebral palsy. *Developmental Medicine and Child Neurology*, 42(3):182–189, 2000.

[53] T. Fukunaga, Y. Ichinose, M. Ito, Y. Kawakami, and S. Fukashiro. Determination of fascicle length and pennation in a contracting human muscle in vivo. *Journal of Applied Physiology*, 82(1):354–358, 1997.

[54] Y. Gao, T. Y. Kostrominova, J. A. Faulkner, and A. S. Wineman. Age-related changes in the mechanical properties of the epimysium in skeletal muscles of rats. *Journal of Biomechanics*, 41(2):465–469, 2008.

[55] J. C. Gardiner and J. A. Weiss. Simple shear testing of parallel-fibered planar soft tissues. *J. Biomech. Eng.*, 123(2):170–175, 2001.

[56] A. Gefen and E. Haberman. Viscoelastic properties of ovine adipose tissue covering the gluteus muscles. *Journal of Biomechanical Engineering*, 129(6):924–930, 2007.

[57] M. H. Gfrerer and B. Simeon. Fiber-based modeling and simulation of skeletal muscles. *Multibody System Dynamics*, 52(1):1–30, 2021.

[58] G. Giantesio, A. Musesti, and D. Riccobelli. A Comparison Between Active Strain and Active Stress in Transversely Isotropic Hyperelastic Materials. *Journal of Elasticity*, 137(1):63–82, 2019.

[59] A. R. Gillies, M. A. Chapman, E. A. Bushong, T. J. Deerinck, M. H. Ellisman, and R. L. Lieber. High resolution three-dimensional reconstruction of fibrotic skeletal muscle extracellular matrix. *J. Physiol.*, 595(4):1159–1171, 2016.

[60] A. R. Gillies and R. L. Lieber. Structure and function of the skeletal muscle extracellular matrix. *Muscle Nerve*, 44(3):318–331, 2011.

[61] A. R. Gillies, L. R. Smith, R. L. Lieber, and S. Varghese. Method for decellularizing skeletal muscle without detergents or proteolytic enzymes. *Tissue Eng. Part C Methods*, 17(4):383–389, 2011.

[62] J. Gindre, M. Takaza, K. M. Moerman, and C. K. Simms. A structural model of passive skeletal muscle shows two reinforcement processes in resisting deformation. *J. Mech. Behav. Biomed. Mat.*, 22:84–94, 2013.

[63] A. M. Gordon, A. F. Huxley, and F. J. Julian. The variation in isometric tension with sarcomere length in vertebrate muscle fibres. *The Journal of Physiology*, 184(1):170–192, 1966.

[64] J. M. Gracies, A. Brashear, R. Jech, P. McAllister, M. Banach, P. Valkovic, H. Walker, C. Marciniak, T. Deltombe, A. Skoromets, S. Khatkova, S. Edgley, F. Gul, F. Catus, B. B. De Fer, C. Vilain, P. Picaut, Z. Ayyoub, D. Bensmail, A. R Bentivoglio, F. Boyer, A. Csanyi, Z. Denes, P. Hedera, S. Isaacson, M. E. Isner-Horobeti, A. Kaminska, S. Kocer, T. Lejeune, P. Marque, M. O'Dell, O. Remy-Neris, B. Rubin, M. Rudzinska, D. Simpson, S. L. Timerbaeva, M. Vecchio, and M. Wimmer. Safety and efficacy of abobotulinumtoxinA for hemiparesis in adults with upper limb spasticity after stroke or traumatic brain injury: A double-blind randomised controlled trial. *The Lancet Neurology*, 14(10):992–1001, 2015.

[65] G.G. Handsfield, C.H. Meyer, M.F. Abel, and S.S. Blemker. Heterogeneity of muscle sizes in the lower limbs of children with cerebral palsy: Cp muscle size heterogeneity. *Muscle Nerve*, 53(6):933–945, 2016.

[66] B. Hanssen, N. Peeters, I. Vandekerckhove, N. De Beukelaer, L. Bar-On, G. Molenaers, A. Van Campenhout, M. Degelaen, C. Van den Broeck, P. Calders, and K. Desloovere. The Contribution of Decreased Muscle Size to Muscle Weakness in Children With Spastic Cerebral Palsy. *Frontiers in Neurology*, 12:1156, 2021.

[67] J. M. Haus, J. A. Carrithers, S. W. Trappe, and T. A. Trappe. Collagen, cross-linking, and advanced glycation end products in aging human skeletal muscle. *J. Appl. Physiol.*, 103(6):2068–2076, 2007.

[68] B. Hernández-Gascón, J. Grasa, B. Calvo, and J. F. Rodríguez. A 3D electro-mechanical continuum model for simulating skeletal muscle contraction. *J. Theor. Biol.*, 335:108–118, 2013.

[69] W. Herzog. Mechanisms of enhanced force production in lengthening (eccentric) muscle contractions. *Journal of applied physiology (1985)*, 116(11):1407–1417, 2014.

[70] W. Herzog. The multiple roles of titin in muscle contraction and force production. *Biophysical Reviews*, 10(4):1187–1199, 2018.

[71] W. Herzog and T. R. Leonard. Force enhancement following stretching of skeletal muscle: A new mechanism. *Journal of Experimental Biology*, 205(9):1275–1283, 2002.

[72] A. V. Hill. The Heat of Shortening and the Dynamic Constants of Muscle. *Proc. R. Soc. B.*, 126(843):136–195, 1938.

[73] J. J. Howard and W. Herzog. Skeletal Muscle in Cerebral Palsy: From Belly to Myofibril. *Frontiers in Neurology*, 12:1–15, 2021.

[74] A. F. Huxley. Mechanics and models of the myosin motor. *Philosophical Transactions of the Royal Society of London. Series B: Biological Sciences*, 355(1396):433–440, 2000.

[75] A.F. Huxley. Muscle structure and theories of contraction. *Prog. Biophys. Mol. Biol.*, 7:255–318, 1957.

[76] H. E. Huxley. Past, present and future experiments on muscle. *Philosophical Transactions of the Royal Society of London. Series B: Biological Sciences*, 355(1396):539–543, 2000.

[77] J. Ito, A. Araki, H. Tanaka, T. Tasaki, K. Cho, and R. Yamazaki. Muscle histopathology in spastic cerebral palsy. *Brain Dev.*, 18(4):299–303, 1996.

[78] B.C. Jayne and G.V. Lauder. How swimming fish use slow and fast muscle fibers: implications for models of vertebrate muscle recruitment. *Journal of Comparative Physiology A*, 175(1):123–131, 1994.

[79] X. Jin, F. Zhu, H. Mao, M. Shen, and K.H. Yang. A comprehensive experimental study on material properties of human brain tissue. *J. Biomech.*, 46(16):2795–2801, 2013.

[80] A. Karimi and A. Shojaei. An Experimental Study to Measure the Mechanical Properties of the Human Liver. *Digest. Dis.*, 36(2):150–155, 2018.

[81] K. R. Knaus, G. G. Handsfield, and S. S. Blemker. A 3D model of the soleus reveals effects of aponeuroses morphology and material properties on complex muscle fascicle behavior. *Journal of Biomechanics*, 130:110877, 2022.

[82] R. N. Konno, N. Nigam, and J. M. Wakeling. Modelling extracellular matrix and cellular contributions to whole muscle mechanics. *PloS ONE*, 16(4):e0249601, 2021.

[83] R. N. Konno, N. Nigam, J. M. Wakeling, and S. A. Ross. The Contributions of Extracellular Matrix and Sarcomere Properties to Passive Muscle Stiffness in Cerebral Palsy. *Frontiers in Physiology*, 12(January):1–13, 2022.

[84] D. R. Kwon, G. Y. Park, S. U. Lee, and I. Chung. Spastic cerebral palsy in children: Dynamic sonoelastographic findings of medial gastrocnemius. *Radiology*, 263(3):794–801, 2012.

[85] M. K. Lebiedowska and J. R. Fisk. Knee resistance during passive stretch in patients with hypertonia. *Journal of Neuroscience Methods*, 179(2):323–330, 2009.

[86] S. S.M. Lee, D. Gaebler-Spira, L.-Q. Zhang, W. Z. Rymer, and K. M. Steele. Use of shear wave ultrasound elastography to quantify muscle properties in cerebral palsy. *Clin. Biomech.*, 31:20–28, 2016.

[87] T. R. Leonard and W. Herzog. Regulation of muscle force in the absence of actin-myosin-based cross-bridge interaction. *American Journal of Physiology - Cell Physiology*, 299(1):14–20, 2010.

[88] G. A. Lichtwark and A. M. Wilson. Interactions between the human gastrocnemius muscle and the Achilles tendon during incline, level and decline locomotion. *Journal of Experimental Biology*, 209(21):4379–4388, 2006.

[89] R. L. Lieber and J. Fridén. Functional and Clinical Significance of Skeletal Muscle Architecture. *Muscle Nerve*, 23:1647–1666, 2000.

[90] R. L. Lieber and J. Fridén. Spasticity causes a fundamental rearrangement of muscle-joint interaction. *Muscle Nerve*, 25(2):265–270, 2002.

[91] R. L. Lieber and J. Fridén. Muscle contracture and passive mechanics in cerebral palsy. *J. Appl. Physiol.*, 126(5):1492–1501, 2019.

[92] R. L. Lieber and S. R. Ward. Cellular mechanisms of tissue fibrosis. 4. structural and functional consequences of skeletal muscle fibrosis. *Am. J. Physiol. Cell Physiol.*, 305(3), 2013.

[93] R.L. Lieber, E. Runesson, F. Einarsson, and J. Fridén. Inferior mechanical properties of spastic muscle bundles due to hypertrophic but compromised extracellular matrix material. *Muscle Nerve*, 28(4):464–471, 2003.

[94] C. N. Maganaris, V. Baltzopoulos, and A. J. Sargeant. In vivo measurements of the triceps surae complex architecture in man: Implications for muscle function. *Journal of Physiology*, 512(2):603–614, 1998.

[95] C.N. Maganaris. Force-length characteristics of in vivo human skeletal muscle. *Acta. Physiol. Scand.*, 172(4):279–285, 2001.

[96] R. Malaiya, A. E. McNee, N. R. Fry, L. C. Eve, M. Gough, and A. P. Shortland. The morphology of the medial gastrocnemius in typically developing children and children with spastic hemiplegic cerebral palsy. *Journal of electromyography and kinesiology*, 17(6):657–663, 2007.

[97] K. Maruyama. Connectin, an Elastic Protein from Myofibrils. *Journal of biochemistry (Tokyo)*, 80(2):405–407, 1976.

[98] M. A. Mathewson, H. G. Chambers, P. J. Girard, M. Tenenhaus, A. K. Schwartz, and R. L. Lieber. Stiff muscle fibers in calf muscles of patients with cerebral palsy lead to high passive muscle stiffness. *J. Orthop. Res.*, 32(12):1667–1674, 2014.

[99] M. A. Mathewson and R. L. Lieber. Pathophysiology of muscle contractures in cerebral palsy. *Phys. Med. Rehabil. Clin. N. Am.*, 26(1):57–67, 2015.

[100] M. A. Mathewson, S. R. Ward, H. G. Chambers, and R. L. Lieber. High resolution muscle measurements provide insights into equinus contractures in patients with cerebral palsy. *J. Orth. Res.*, 33(1):33–39, 2014.

[101] S. Matthiasdottir, M. Hahn, M. Yaraskavitch, and W. Herzog. Muscle and fascicle excursion in children with cerebral palsy. *Clinical Biomechanics*, 29(4):458–462, 2014.

[102] R. Mayne and R.D. Sanderson. The Extracellular Matrix of Skeletal Muscle. *Top. Catal.*, 5(5):449–468, 1985.

[103] C. A. McGibbon, A. Sexton, M. Jones, and C. O'Connell. Elbow spasticity during passive stretch-reflex: Clinical evaluation using a wearable sensor system. *Journal of NeuroEngineering and Rehabilitation*, 10(1), 2013.

[104] M. McMahon, D. Pruitt, and J. Vargus-Adams. Cerebral palsy. In M. A. Alexander, D. J. Matthews, and K. P. Murphy, editors, *Pediatric Rehabilitation*, pages 336–372. Springer Publishing Company, New York, 2015.

[105] G. Meyer and R. L. Lieber. Muscle fibers bear a larger fraction of passive muscle tension in frogs compared with mice. *J. Exp. Biol.*, 221(22), 2018.

[106] J. E. Miller-Young, N. A. Duncan, and G. Baroud. Material properties of the human calcaneal fat pad in compression: Experiment and theory. *Journal of Biomechanics*, 35(12):1523–1531, 2002.

[107] A. A. Mohagheghi, T. Khan, T. H. Meadows, K. Giannikas, V. Baltzopoulos, and C. N. Maganaris. In vivogastrocnemius muscle fascicle length in children with and without diplegic cerebral palsy. *Dev. Med. Child Neurol.*, 50(1):44–50, 2008.

[108] M. Mohammadkhah, P. Murphy, and C. K. Simms. The in vitro passive elastic response of chicken pectoralis muscle to applied tensile and compressive deformation. *J. Mech. Behav. Biomed.*, 62:468–480, 2016.

[109] K. C. Nishikawa, J. A. Monroy, T. E. Uyeno, S. H. Yeo, D. K. Pai, and S. L. Lindstedt. Is titin a 'winding filament'? A new twist on muscle contraction. *Proceedings of the Royal Society B: Biological Sciences*, 279(1730):981–990, 2012.

[110] J. J. Noble, G. D. Charles-Edwards, S. F. Keevil, A. P. Lewis, M. Gough, and A. P. Shortland. Intramuscular fat in ambulant young adults with bilateral spastic cerebral palsy. *BMC Musculoskeletal Disorders*, 15(1), 2014.

[111] J. J. Noble, N. R. Fry, A. P. Lewis, S. F. Keevil, M. Gough, and A. P. Shortland. Lower limb muscle volumes in bilateral spastic cerebral palsy. *Brain and Development*, 36(4):294–300, 2014.

[112] K. Oberhofer, N. S. Stott, K. Mithraratne, and I. A. Anderson. Subject-specific modelling of lower limb muscles in children with cerebral palsy. *Clinical Biomechanics*, 25(1):88–94, 2010.

[113] R. W. Ogden. *Non-linear elastic deformations*. Dover Publications, 1984.

[114] K. Ohata, T. Tsuboyama, T. Haruta, N. Ichihashi, and T. Nakamura. Longitudinal change in muscle and fat thickness in children and adolescents with cerebral palsy. *Dev. Med. Child Neurol.*, 51(12):943–948, 2009.

[115] C. W.J. Oomens, M. Maenhout, C. H. Van Oijen, M. R. Drost, and F. P. Baaijens. Finite element modelling of contracting skeletal muscle. *Philos. Trans. R. Soc. Lond., B, Biol. Sci.*, 358(1437):1453–1460, 2003.

[116] M. Ounjian, R. R. Roy, E. Eldred, A. Garfinkel, J. R. Payne, A. Armstrong, A. W. Toga, and V. R. Edgerton. Physiological and developmental implications of motor unit anatomy. *Journal of neurobiology*, 22(5):547–559, 1991.

[117] J.-P. Pelteret and A. McBride. The deal.ii tutorial step-44: Three-field formulation for non-linear solid mechanics, 2012.

[118] S. L. Peterson and G. M. Rayan. Shoulder and Upper Arm Muscle Architecture. *The Journal of Hand Surgery*, 36(5):881–889, 2011.

[119] D. Pette, M. E. Smith, H. W. Staudte, and G. Vrbová. Effects of long-term electrical stimulation on some contractile and metabolic characteristics of fast rabbit muscles. *Pflügers Archiv*, 338(3):257–272, 1973.

[120] D. Pette and R. S. Staron. The molecular diversity of mammalian muscle fibers. *Physiology (Bethesda, Md.)*, 8(4):153–157, 1993.

[121] B. Pierrat, J.G. Murphy, D.B. MacManus, and M.D. Gilchrist. Finite element implementation of a new model of slight compressibility for transversely isotropic materials. *Comput. Method Biomech.*, 19(7):745–758, 2016.

[122] D. M.Y. Poon and C. W.Y. Hui-Chan. Hyperactive stretch reflexes, co-contraction, and muscle weakness in children with cerebral palsy. *Developmental Medicine & Child Neurology*, 51(2):128–135, 2009.

[123] L. G. Prado, I. Makarenko, C. Andresen, M. Krüger, C. A. Opitz, and W. A. Linke. Isoform diversity of giant proteins in relation to passive and active contractile properties of rabbit skeletal muscles. *J. Gen. Physiol.*, 126(5):461–480, 2005.

[124] M. T. Prange and S. S. Margulies. Regional, directional, and age-dependent properties of the brain undergoing large deformation. *J. Biomech. Eng.*, 124(2):244–252, 2002.

[125] P. P. Purslow. The structure and functional significance of variations in the connective tissue within muscle. *Comp. Biochem. Physiol. Part A Mol. Integr. Physiol.*, 133(4):947–966, 2002.

[126] P. P. Purslow. Muscle fascia and force transmission. *J. Bodyw. Mov. Ther.*, 14(4):411–417, 2010.

[127] P. P. Purslow and J. A. Trotter. The morphology and mechanical properties of endomysium in series-fibred muscles: variations with muscle length. *Journal of Muscle Research & Cell Motility*, 15(3):299–308, 1994.

[128] P.P. Purslow. Strain-induced reorientation of an intramuscular connective tissue network: Implications for passive muscle elasticity. *J. Biomech.*, 22(1):21–31, 1989.

[129] H. Rahemi, N. Nigam, and J. M. Wakeling. Regionalizing muscle activity causes changes to the magnitude and direction of the force from whole muscles-a modeling study. *Front. Physiol.*, 5 AUG(August):1–10, 2014.

[130] H. Rahemi, N. Nigam, and J. M. Wakeling. The effect of intramuscular fat on skeletal muscle mechanics: Implications for the elderly and obese. *J. R. Soc. Interface*, 12(109), 2015.

[131] R. W. Ramsey and S. F. Street. The isometric length-tension diagram of isolated skeletal muscle fibers of the frog. *Journal of Cellular and Comparative Physiology*, 15:11–34, 1940.

[132] A. Randhawa and J. M. Wakeling. Transverse anisotropy in the deformation of the muscle during dynamic contractions. *J. Exp. Biol.*, 221(15):jeb175794, 2018.

[133] A. Randhawa and J.M. Wakeling. Multidimensional models for predicting muscle structure and fascicle pennation. *J. Theor. Biol.*, 382:57–63, 2015.

[134] T. J. Roberts and E. Azizi. The series-elastic shock absorber: Tendons attenuate muscle power during eccentric actions. *Journal of Applied Physiology*, 109(2):396–404, 2010.

[135] T. J. Roberts and E. Azizi. Flexible mechanisms: The diverse roles of biological springs in vertebrate movement. *Journal of Experimental Biology*, 214(3):353–361, 2011.

[136] T.J. Roberts, C.M. Eng, D.A. Sleboda, N.C. Holt, E.L. Brainerd, K.K. Stover, R.L. Marsh, and E. Azizi. The multi-scale, three-dimensional nature of skeletal muscle contraction. *Physiology*, 34(6):402–408, 2019.

[137] T.J. Roberts, R.L. Marsh, P.G. Weyand, and C.R. Taylor. Muscular force in running turkeys: the economy of minimizing work. *Science*, 275(5303):1113–1115, 1997.

[138] O. Röhrle. Simulating the electro-mechanical behavior of skeletal muscles. *Computing in Science and Engineering*, 12(6):48–57, 2010.

[139] O. Röhrle, J. B. Davidson, and A. J. Pullan. Bridging Scales: A Three-Dimensional Electromechanical Finite Element Model of Skeletal Muscle. *SIAM J. Sci. Comp.*, 30(6):2882–2904, 2008.

[140] O. Röhrle, J.B. Davidson, and A.J. Pullan. A physiologically based, multi-scale model of skeletal muscle structure and function. *Front. Physiol.*, 3 SEP(September):1–14, 2012.

[141] L.C. Rome, R.P. Funke, R.M. Alexander, G. Lutz, H. Aldridge, F. Scott, and M. Freadman. Why animals have different muscle fibre types. *Nature 1988 335:6193*, 335(6193):824–827, 1988.

[142] P. Rosenbaum, N. Paneth, A. Leviton, M. Goldstein, and M. Bax. A report: The definition and classification of cerebral palsy April 2006, 2007.

[143] S. A. Ross, S. Domínguez, N. Nigam, and J. M. Wakeling. The energy of muscle contraction. iii. kinetic energy during cyclic contractions. *Frontiers in Physiology*, 12:306, 2021.

[144] S. A. Ross, N. Nigam, and J. M. Wakeling. A modelling approach for exploring muscle dynamics during cyclic contractions. *PLoS Comput. Biol.*, 14(4):1–18, 2018.

[145] S. A. Ross, N. Nigam, and J. M. Wakeling. A modelling approach for exploring muscle dynamics during cyclic contractions. *PLoS Comp. Biol.*, 14(4):1–18, 2018.

[146] S. A. Ross, D. S. Ryan, S. Dominguez, N. Nigam, and J. M. Wakeling. Size, history-dependent, activation and three-dimensional effects on the work and power produced during cyclic muscle contractions. *Integr. Comp. Biol.*, 58(2):232–250, 2018.

[147] S.A. Ross and J.M. Wakeling. Muscle shortening velocity depends on tissue inertia and level of activation during submaximal contractions. *Biol. Lett.*, 12(6):2016–2019, 2016.

[148] D. S. Ryan, S. Domínguez, S. A. Ross, N. Nigam, and J. M. Wakeling. The energy of muscle contraction. II. transverse compression and work. *Front. Physiol.*, 11, 2020.

[149] D.S. Ryan, N. Stutzig, T. Siebert, and J.M. Wakeling. Passive and dynamic muscle architecture during transverse loading for gastrocnemius medialis in man. *J. Biomech.*, 86:160–166, 2019.

[150] S. Salmons and F. A. Sréter. Significance of impulse activity in the transformation of skeletal muscle type. *Nature 1976 263:5572*, 263(5572):30–34, 1976.

[151] A. Samani, J. Zubovits, and D. Plewes. Elastic moduli of normal and pathological human breast tissues: An inversion-technique-based investigation of 169 samples. *Physics in Medicine and Biology*, 52(6):1565–1576, 2007.

[152] G. S. Sawicki and N. S. Khan. A Simple Model to Estimate Plantarflexor Muscle-Tendon Mechanics and Energetics During Walking With Elastic Ankle Exoskeletons. *IEEE Transactions on Biomedical Engineering*, 63(5):914–923, 2016.

[153] N. Scherbakov, S. von Haehling, S. D. Anker, U. Dirnagl, and W. Doehner. Stroke induced sarcopenia: Muscle wasting and disability after stroke. *International Journal of Cardiology*, 170(2):89–94, 2013.

[154] S. H. Scott and G. E. Loeb. Mechanical properties of aponeurosis and tendon of the cat soleus muscle during whole-muscle isometric contractions. *Journal of Morphology*, 224(1):73–86, 1995.

[155] R.E. Shadwick, J.F. Steffensen, S.L. Katz, and T. Knower. Muscle dynamics in fish during steady swimming. *American zoologist*, 38(4):755–770, 1998.

[156] X. Shan, S. Otsuka, T. Yakura, M. Naito, T. Nakano, and Y. Kawakami. Morphological and mechanical properties of the human triceps surae aponeuroses taken from elderly cadavers: Implications for muscle-tendon interactions. *PLOS ONE*, 14(2):e0211485, 2019.

[157] B. Sharafi and S. S. Blemker. A micromechanical model of skeletal muscle to explore the effects of fiber and fascicle geometry. *J. Biomech.*, 43(16):3207–3213, 2010.

[158] B. Sharafi and S.S. Blemker. A mathematical model of force transmission from intrafascicularly terminating muscle fibers. *J. Biomech.*, 44(11):2031–2039, 2011.

[159] J.C. Simo and C. Miehe. Associative coupled thermoplasticity at finite strains: Formulation, numerical analysis and implementation. *Comput. Method. Appl. M.*, 98(1):41–104, 1992.

[160] J.C. Simo and R.L. Taylor. Quasi-incompressible finite elasticity in principal stretches. continuum basis and numerical algorithms. *Comput. Method. Appl. M.*, 85(3):273–310, 1991.

[161] D. A. Sleboda and T. J. Roberts. Incompressible fluid plays a mechanical role in the development of passive muscle tension. *Biology Letters*, 13(1), 2017.

[162] D.A. Sleboda and T.J. Roberts. Internal fluid pressure influences muscle contractile force. *Proc. Natl. Acad. Sci. U.S.A.*, 117(3):1772–1778, 2019.

[163] D.A. Sleboda, K.K. Stover, and T.J. Roberts. Diversity of extracellular matrix morphology in vertebrate skeletal muscle. *J. Morphol.*, 281(2):160–169, 2020.

[164] D.A. Sleboda, E.S. Wold, and T.J. Roberts. Passive muscle tension increases in proportion to intramuscular fluid volume. *J. Exp. Biol.*, 222(21):jeb209668, 2019.

[165] L. R. Smith and E. R. Barton. Collagen content does not alter the passive mechanical properties of fibrotic skeletal muscle inmdxmice. *Am. J. Physiol. Cell Physiol.*, 306(10):C889–C898, 2014.

[166] L. R. Smith, R. Pichika, R. C. Meza, A. R. Gillies, M. N. Baliki, H. G. Chambers, and R. L. Lieber. Contribution of extracellular matrix components to the stiffness of skeletal muscle contractures in patients with cerebral palsy. *Connect. Tissue Res.*, pages 1–12, 2019.

[167] L.R. Smith, K.S. Lee, S.R. Ward, H.G. Chambers, and R.L. Lieber. Hamstring contractures in children with spastic cerebral palsy result from a stiffer extracellular matrix and increased in vivo sarcomere length. *J. Physiol.*, 589(10):2625–2639, 2011.

[168] L.R. Smith, K.S. Lee, S.R. Ward, H.G. Chambers, and R.L. Lieber. Hamstring contractures in children with spastic cerebral palsy result from a stiffer extracellular matrix and increased in vivo sarcomere length. *J. Physiol.*, 589(10):2625–2639, 2011.

[169] M. D. Smyth and W. J. Peacock. The surgical treatment of spasticity, 2000.

[170] G. Sommer, M. Eder, L. Kovacs, H. Pathak, L. Bonitz, C. Mueller, P. Regitnig, and G. A. Holzapfel. Multiaxial mechanical properties and constitutive modeling of human adipose tissue: A basis for preoperative simulations in plastic and reconstructive surgery. *Acta Biomaterialia*, 9(11):9036–9048, 2013.

[171] L. A. Spyrou, S. Brisard, and K. Danas. Multiscale modeling of skeletal muscle tissues based on analytical and numerical homogenization. *J. Mech. Behav. Biomed.*, 92:97–117, 2019.

[172] L. A.A. Spyrou, M. Agoras, and K. Danas. A homogenization model of the Voigt type for skeletal muscle. *J. Theor. Biol.*, 414:50–61, 2017.

[173] S. K. Stackhouse, S. A. Binder-Macleod, and S. C. K. Lee. Voluntary muscle activation, contractile properties, and fatigability in children with and without cerebral palsy. *Muscle Nerve*, 31(5):594–601, 2005.

[174] M. Stefanati, C. Villa, Y. Torrente, and J. F. Rodriguez Matas. A mathematical model of healthy and dystrophic skeletal muscle biomechanics. *Journal of the Mechanics and Physics of Solids*, 134, 2020.

[175] Z. Sun, B. D. Gepner, P. S. Cottler, S. H. Lee, and J. R. Kerrigan. In vitro mechanical characterization and modeling of subcutaneous adipose tissue: A comprehensive review. *Journal of Biomechanical Engineering*, 143(7):1–9, 2021.

[176] Z. Sun, B. D. Gepner, S. H. Lee, J. Rigby, P. S. Cottler, J. J. Hallman, and J. R. Kerrigan. Multidirectional mechanical properties and constitutive modeling of human adipose tissue under dynamic loading. *Acta Biomaterialia*, 129:188–198, 2021.

[177] M. Takaza, K.M. Moerman, J. Gindre, G. Lyons, and C.K. Simms. The anisotropic mechanical behaviour of passive skeletal muscle tissue subjected to large tensile strain. *J. Mech. Behav. Biomed.*, 17:209–220, 2013.

[178] C. Tanner, J. A. Schnabel, D. L.G. Hill, D. J. Hawkes, M. O. Leach, and D. R. Hose. Factors influencing the accuracy of biomechanical breast models. *Medical Physics*, 33(6):1758–1769, 2006.

[179] A. L. Tisha, A. A. Armstrong, A. W.J., and C. López-Ortiz. Skeletal muscle adaptations and passive muscle stiffness in cerebral palsy: A literature review and conceptual model. *J. Appl. Biomech.*, 35(1):68–79, 2019.

[180] J. A. Trotter and P. P. Purslow. Functional morphology of the endomysium in series fibered muscles. *Journal of morphology*, 212(2):109–122, 1992.

[181] J. A. Trotter, F. J. Richmond, and P. P. Purslow. Functional morphology and motor control of series-fibered muscles. *Exerc. Sport Sci. Rev.*, 23:167–213, 1995.

[182] M. S. Tu and M. H. Dickinson. Modulation of negative work output from a steering muscle of the blowfly Calliphora vicina. *Journal of Experimental Biology*, 192:207–224, 1994.

[183] A. Turrina, M. A. Martínez-González, and C. Stecco. The muscular force transmission system: Role of the intramuscular connective tissue. *J. Bodyw. Mov. Ther.*, 17(1):95–102, 2013.

[184] M. M. van der Krogt, L. Bar-On, T. Kindt, K. Desloovere, and J. Harlaar. Neuromusculoskeletal simulation of instrumented contracture and spasticity assessment in children with cerebral palsy. *J. NeuroEng. Rehabil.*, 13(1), 2016.

[185] M. Van Loocke, C. K. Simms, and C. G. Lyons. Viscoelastic properties of passive skeletal muscle in compression-cyclic behaviour. *J. Biomech.*, 42(8):1038–48, 2009.

[186] K. M. Virgilio, K. S. Martin, S. M. Peirce, and S. S. Blemker. Multiscale models of skeletal muscle reveal the complex effects of muscular dystrophy on tissue mechanics and damage susceptibility. *Interface Focus*, 5(2), 2015.

[187] S. Vogel. *Comparative biomechanics: Life's physical world*. Princeton University Press, Princeton, 2 edition, 2011.

[188] F. Von Walden, S. Gantelius, C. Liu, H. Borgström, L. Björk, O. Gremark, P. St**A**l, G. A. Nader, and E. PontéN. Muscle contractures in patients with cerebral palsy and acquired brain injury are associated with extracellular matrix expansion, pro-inflammatory gene expression, and reduced rRNA synthesis. *Muscle and Nerve*, 58(2):277–285, 2018.

[189] F. Von Walden, K. Jalaleddini, B. Evertsson, J. Friberg, F. J. Valero-Cuevas, and E. Pontén. Forearm flexor muscles in children with cerebral palsy are weak, thin and stiff. *Frontiers in Computational Neuroscience*, 11(April):1–8, 2017.

[190] F. von Walden, K. Jalaleddini, B. Evertsson, J. Friberg, F. J. Valero-Cuevas, and E. Pontén. Forearm flexor muscles in children with cerebral palsy are weak, thin and stiff. *Front. Comp. Neurosci.*, 11, 2017.

[191] J. M. Wakeling, M. Jackman, and A. I. Namburete. The effect of external compression on the mechanics of muscle contraction. *Journal of Applied Biomechanics*, 29(3):360–364, 2013.

[192] J. M. Wakeling, S. A. Ross, D. S. Ryan, B. Bolsterlee, R. Konno, S. Domínguez, and N. Nigam. The energy of muscle contraction. i. tissue force and deformation during fixed-end contractions. *Front. Physiol.*, 11, 2020.

[193] J.M. Wakeling, O.M. Blake, I. Wong, M. Rana, and S.S.M. Lee. Movement mechanics as a determinate of muscle structure, recruitment and coordination. *Philosophical Transactions of the Royal Society B: Biological Sciences*, 366(1570):1554–1564, 2011.

[194] S. R. Ward, T. M. Winters, S. M. O'Connor, and R. L. Lieber. Non-linear scaling of passive mechanical properties in fibers, bundles, fascicles and whole rabbit muscles. *Frontiers in Physiology*, 11:211, 2020.

[195] J. A. Weiss, B. N. Maker, and S. Govindjee. Finite element implementation of incompressible, transversely isotropic hyperelasticity. *Comput. Method. Appl. M.*, 135(1-2):107–128, 1996.

[196] B. B. Wheatley, R. B. Pietsch, T. L. Haut Donahue, and L. N. Williams. Fully non-linear hyper-viscoelastic modeling of skeletal muscle in compression. *Computer Methods in Biomechanics and Biomedical Engineering*, 19(11):1181–1189, 2016.

[197] T. L. Wickiewicz, R. R. Roy, P. L. Powell, and V. R. Edgerton. Muscle architecture of the human lower limb. *Clinical orthopaedics and related research*, 179:275–283, 1983.

[198] L. G. Wiedemann, V. R. Jayaneththi, J. Kimpton, A. Chan, M. A. Müller, A. Hogan, E. Lim, N. C. Wilson, and A. J. McDaid. Neuromuscular characterisation in Cerebral Palsy using hybrid Hill-type models on isometric contractions. *Computers in Biology and Medicine*, 103:269–276, 2018.

[199] S. Willwacher, D.A. Sleboda, D. Mählich, G.P. Brüggemann, T.J. Roberts, and G. Bratke. The time course of calf muscle fluid volume during prolonged running. *Physiol. Rep.*, 8(9), 2020.

[200] T.M. Winters, M. Takahashi, R.L. Lieber, and S.R. Ward. Whole muscle length-tension relationships are accurately modeled as scaled sarcomeres in rabbit hindlimb muscles. *J. Biomech.*, 44(1):109–115, 2011.

[201] O. H. Yeoh. Some forms of the strain energy function for rubber. *Rubber Chemistry and Technology*, 66(5):754–771, 1993.

[202] C. A. Yucesoy, B. H.F.J.M. Koopman, P. A. Huijing, and H. J. Grootenboer. Three-dimensional finite element modeling of skeletal muscle using a two-domain approach: linked fiber-matrix mesh model. *J. Biomech.*, 35(9):1253–1262, 2002.

[203] F. E. Zajac. Muscle and Tendon: Properties, Models, Scaling, and Application to Biomechanics and Motor Control. *Crit. Rev. Biomed. Eng.*, 17(14):358–410, 1989.

[204] I. Ziv, N. Blackburn, M. Rang, and J. Koreska. Muscle growth in normal and spastic mice. *Dev. Med. Child Neurol.*, 26(1):94–99, 1984.

[205] C. J. Zuurbier, A. J. Everard, P. van der Wees, and P. A. Huijing. Length-force characteristics of the aponeurosis in the passive and active muscle condition and in the isolated condition. *Journal of Biomechanics*, 27(4):445–453, 1994.